ISOSPIN-SYMMETRY VIOLATION IN LIGHT NUCLEI

By

William Erich Ormand

A DISSERTATION

Submitted to

Michigan State University

in partial fullfillment of the requirements

for the degree of

DOCTOR OF PHILOSOPHY

Department of Physics and Astronomy

1985

ACKNOWLEDGMENTS

In this work, as in all others, there are many people who have helped to make it possible. Therefore, I would like to take this space to acknowledge these people. First and foremost, I wish to thank my advisor Dr. Alex Brown for his guidance and friendship during the two years that I have worked with him, as both of these were indispensable. Second, I wish to thank the remaining members of my guidance committee: Professors Jerry Nolen, George Bertsch, Wayne Repko, Gary Crawley, and David Scott. I would especially like to thank my first academic advisor, Professor Jerry Nolen, for his guidance early in my graduate career and the freedom he gave me to pursue my academic interests. In addition, I would like to thank both Professors Wayne Repko and George Bretsch. The former for his excellent teaching skills, and the latter for his guidance and advice during the later stages of this dissertation. I also wish to thank Professor Olaf Scholten for the deep friendship we shared. I regret his departure for the Netherlands, as I will miss him, and I wish him nothing but happiness in both his professional and personal life. In addition, I wish to thank Shari Conroy for her invaluable assistance and friendship over the past two years. To my fellow graduate students and the remaining members of the Nuclear Theory group (both past and present) I extend my eternal gratitude for the friendship and the intellectual stimulation I received. To Silvana Angius I am greatly

indebted, for her love, understanding, and support, and her critical reading of the manuscript.

Finally, I wish to thank some other people who are not at Michigan State University. First, I wish to acknowledge Dr. Thomas Myers for the friendship we shared as undergraduates at North Carolina State University. To Professor Richard Mowat at North Carolina State University I extend my gratitude for getting me started in the world of academic research. Lastly, I wish to thank my parents for their support and encouragement throughout my entire life.

TABLE OF CONTENTS

LIST OF TABLES

TABLE PAGE

TABLE PAGE

LIST OF FIGURES

FIGURE PAGE

FIGURE PAGE

FIGURE PAGE

Chapter One

1.1 Prospectus

Shortly after the discovery of the neutron, Heisenberg [Hei 32] proposed the existence of an intrinsic quantum number, similar to intrinsic spin, which expressed a symmetry between protons and neutrons. This concept was based on several similarities between the two nucleons. Both are spin 1/2 particles with approximately the same mass (the neutron is only 0.14% heavier) and are the essential building blocks of nuclear matter. In fact, the principal difference between the proton and neutron is their electric charge; protons have a charge e (e=1.6019 $\times$ 10^{-19} Coulombs), while the neutron is electrically neutral.

Heisenberg's hypothesis was to regard protons and neutrons as different charge states of the same particle. That is, they form a charge doublet of essentially identical particles. This property can be described by introducing a new spin, say $\vec{t}$, whose quantized z-component is related to the electric charge. Recall that the multiplicity of states with angular momentum j is 2j+1. The nucleon doublet, therefore, has the following new "spin" quantum numbers: t=1/2, and t_Z= $\pm$1/2. The choice as to whether the z-component of the isospin for the proton is plus or minus one-half is arbitrary, and in this work it is taken to be positive. With this convention the nucleon charge is then q = (1/2 + t_Z)e.

An essential feature of this new spin is to introduce a mechanism for labeling nuclear states of a particular symmetry. If indeed protons and neutrons are identical particles (that is, the nuclear Hamiltonian is charge independent), the energy spectrum of a system containing A

nucleons with A/2+n protons and A/2-n neutrons (for even A, n = 1, 2, 3,...; and for odd A, n = 1/2, 3/2, 5/2, ...) should be identical to that for the system containing A/2-n protons and A/2+n neutrons. A typical example of this behavior is shown in Figure 1.1, where it is seen that the $T_Z = \pm n$ nuclei ($T_Z = \sum_i^A t_Z(i)$) are essentially mirror images of one another. The small differences in the excitation energies are due to a violation of pure charge-independence, primarily due to the Coulomb force between protons.

In addition to mirror symmetry, we also expect to find analogs of states in $T_Z = \pm n$ nuclei to be present in nuclei with $|T_Z| < n$. These states have also been observed experimentally, and examples are also shown in Figure 1.1.

This new "spin" quantum number can then be used to label states of a given symmetry in isospin space for various isotopes, and was, therefore, originally referred to as isotopic spin. The idea of isotopic spin, however, had to be expanded after the discovery of other charged multiplets of essentially identical particles (π-mesons, Δ-isobars, Λ-particles, and etc.). In fact, this new "spin" was found to be a general property of all strongly interacting particles (hadrons) and is now referred to as isospin. The relation between the electric charge and the z-component of the isospin is now given by $q = (\frac{B + S}{2} + t_Z)e$, where B is the baryon number and S the strangeness quantum number. For nucleons B=1 and S=0.

It is useful at this point to introduce some of the basic principles of isospin operators. In a manner completely analogous to angular momentum [Edm 60], it is possible to build up states with

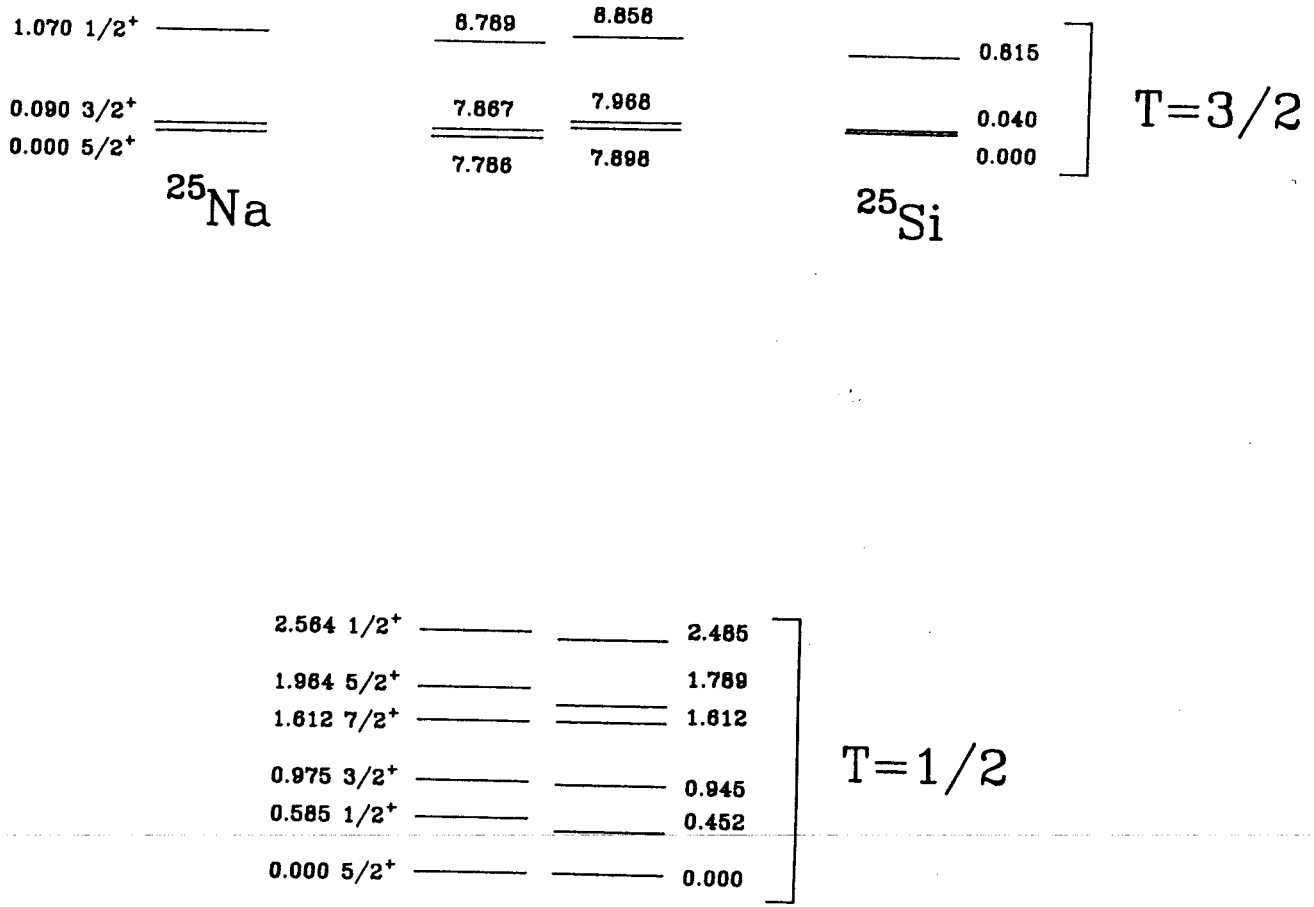

Figure 1.1: Level diagram of excitation energies in A=25 nuclei with $|T_z| \leq 3/2$. The differences in the binding energies of the ground states is suppressed in order to illustrate the mirror and analog symmetry.

definite isospin. The total isospin vector for a system containing A nucleons is given by

$$\vec{T} = \sum_{i}^{A} \vec{t}(i) \qquad (1.1.1)$$

and the z-component is

$$T_Z = \sum_{i}^{A} t_Z(i) = \frac{1}{2}(Z - N). \qquad (1.1.2)$$

Here the quantities Z and N are the total number of protons and neutrons present, respectively. In addition, we define the raising and lowering operators T_+ and T_- by

$$T_+ = \sum_{i}^{A} t_+(i) \qquad (1.1.3a)$$

$$T_- = \sum_{i}^{A} t_-(i). \qquad (1.1.3b)$$

where

$$t_+(i) = t_X(i) + it_Y(i)$$

$$t_-(i) = t_X(i) - it_Y(i).$$

Analog states are then found by operating with the raising and lowering operators on states with a given T_Z. For example the state $|T, T_Z=T-1\rangle$ is obtained by

$$|T, T_Z=T-1\rangle = \left[(T-T_Z)(T+T_Z+1)\right]^{-1/2} T_- \, |T, T_Z=T\rangle \qquad (1.1.4a)$$

or

$$|T, T_Z=T-1\rangle = \left[(T+T_Z)(T-T_Z+1)\right]^{-1/2} T_+ \, |T, T_Z=T-2\rangle. \qquad (1.1.4b)$$

The principal difference between isospin and angular momentum is that the z-component of the isospin vector distinguishes between members of an isobaric multiplet, rather than a specified orientation in space. This is because the space spanned by isospin vectors is not a physical space, but rather, a fictitious space in which proton and neutron symmetry properties can be distinguished.

The concept of an isospin quantum number used to label nuclear states is useful only if isospin is a conserved quantity, or failing that, is very nearly conserved. Any quantum mechanical operator, say A, will have values (eigenvalues) associated with it which are conserved if it commutes with the Hamiltonian H, i.e. $[A,H] = 0$. Assuming only two body interactions between nucleons, the Hamiltonian for a nucleus consisting of A nucleons is

$$H = \sum_{i}^{A} \frac{p^2(i)}{2m} + \frac{1}{2} \sum_{i \neq j}^{A} v_{ij}. \qquad (1.1.5)$$

The first term in eq.(1.1.5) is simply the sum of kinetic energy (here m_p is taken to be equal to m_n), while the second is the sum of the potential energy, which can be rewritten as

$$\sum_{i\neq j}^{A} v_{ij} = \{ \sum_{i\neq j}^{Z} v_{ij}^{(pp)} + \sum_{i\neq j}^{N} v_{ij}^{(nn)} + 2 \sum_{i=1}^{Z} \sum_{j=1}^{N} v_{ij}^{(pn)} \} +$$

$$\sum_{i\neq j}^{Z} \frac{e^2}{r_{ij}}. \qquad (1.1.6)$$

The sums inside the brackets in eq.(1.1.6) are due to the strong interaction between nucleons (proton-proton (pp), neutron-neutron (nn), and proton-neutron (pn)), while the last term is due to the Coulomb interaction between protons. Introducing isospin formalism, the sums in eq.(1.1.6) can be extended to include all particles, and the two-body interaction v_{ij} can be written as

$$v_{ij} = \{(\frac{1}{4} - \vec{t}(i)\cdot\vec{t}(j))\, v_{ij}^{(pn)} + \qquad (1.1.7a)$$

$$(\frac{3}{4} + \vec{t}(i)\cdot\vec{t}(j))\, v_{ij}^{(0)} + \qquad (1.1.7b)$$

$$\frac{1}{2}(t_z(i) + t_z(j))\, v_{ij}^{(1)} + \qquad (1.1.7c)$$

$$[t_z(i)t_z(j) - \frac{\vec{t}(i)\cdot\vec{t}(j)}{3}]\, v_{ij}^{(2)}\} \qquad (1.1.7d)$$

where

$$v_{ij}^{(0)} = \frac{1}{3}\left(v_{ij}^{(pp)} + v_{ij}^{(nn)} + v_{ij}^{(pn)} + \frac{e^2}{r_{ij}} \right) \qquad (1.1.8a)$$

$$v_{ij}^{(1)} = \left(v_{ij}^{(pp)} - v_{ij}^{(nn)} + \frac{e^2}{r_{ij}} \right) \qquad (1.1.8b)$$

$$v_{ij}^{(2)} = \left(v_{ij}^{(pp)} + v_{ij}^{(nn)} - 2v_{ij}^{(pn)} + \frac{e^2}{r_{ij}} \right). \qquad (1.1.8c)$$

Before proceeding with a discussion about isospin-symmetry violation, it is perhaps useful to describe briefly the procedure in which the many-nucleon wave functions are obtained from eq.(1.1.5). Since the total Hamiltonian is a sum of one-body and two-body operators, the total matrix element of eq.(1.1.5) can be written as sum of one-body and two-body matrix elements. In practice, this is done by adding and subtracting an appropriate single-particle potential U(i) to eq.(1.1.5), and thus obtaining the states $\psi_{n\ell j}(\vec{r}) = R_{n\ell j}(r)\,[Y^{\ell}(\hat{r}) \times \vec{s}]^{j}$, which are eigenstates of the single-particle Hamiltonian

$$H_{sp} = \sum_i \left[\frac{p^2(i)}{2m} + U(i)\right].$$

Then, the two-body matrix elements can, at least in principle, be evaluated with these single-particle wave functions by constructing the antisymmeterized two-particle states $|\rho,\rho';J,T\rangle$, where ρ represents the single-particle orbit quantum numbers $n\ell j$, J is the total angular momentum of the two-nucleon system, and T is the total isospin (T=0, or 1). Using these two-nucleon wave functions we evaluate the matrix elements $\langle \rho_i \rho_j;JT|\ v_{ij}\ |\rho_i' \rho_j';JT'\rangle$. By examining the structure of the operators in eq.(1.1.7), we find that eq.(1.1.7a) contributes only when T=T'=0, and that eqs.(1.17b), (1.1.7c), and (1.17d) contribute when T=T'=1. In addition to these components of the two-body potential, there

are also those which give nonzero matrix elements between T=0 and T'=1 systems [Hen 79]. However, these are thought to be small and are neglected in the present work.

The total many-body wave functions are then found by first constructing basis states, each with angular momentum J_{tot}, from the many-body Slater determinants. Using the expectation values $\langle\rho|\ p^2(i)/2m + U(i)\ |\rho\rangle$ and $\langle\rho,\rho';J,T|\ v_{ij}\ |\rho,\rho';J,T'\rangle$, we evaluate the matrix element H_{ik} between the i^{th} and k^{th} basis state, and by diagonalizing the resulting matrix H_{ik} obtain the eigenstates of the Hamiltonian.

The importance of writing v_{ij} in terms of equation (1.1.6) is that the isospin-space transformation properties are readily apparent. The terms (1.1.7a) and (1.1.7b) are scalars, while (1.1.7c) and (1.1.7d) transform like a vector and a tensor of rank 2 in isospin space, respectively. The quantities $v_{ij}^{(0)}$, $v_{ij}^{(1)}$, and $v_{ij}^{(2)}$ are referred to as the isoscalar, isovector, and isotensor parts of the T=1 components of the interaction. Note that any two-body interaction between nucleons can at most be isotensor because the maximum isospin of two nucleons is T=1, which can then couple to at most T=2 to give back T=1. In addition, $v^{(pp)} - v^{(nn)}$ and $v^{(pp)} + v^{(nn)} - 2v^{(pn)}$ are referred to as the charge-asymmetric ($v^{(A)}$) and charge-dependent ($v^{(CD)}$) nuclear interactions, respectively.

To determine whether isospin is a conserved quantity in nuclear systems we evaluate the commutator of the m^{th} component of $\vec{T}$ (the labels X, Y, and Z are equivalent to m = 1, 2, and 3, respectively) with the Hamiltonian, giving

$$[T_m,H] = i\hbar\,\varepsilon_{m3\ell}\sum_{i\neq j}^{A}\{[t_\ell(i)+t_\ell(j)]\,v_{ij}^{(1)} + [t_\ell(i)t_3(j)+t_3(i)t_\ell(j)]\,v_{ij}^{(2)}\} \quad (1.1.9)$$

where ε_{ijk} is the antisymmetric Levi-Civita tensor (note that $[T_i,T_j] = i\varepsilon_{ijk}T_k$). Clearly T_Z commutes with H, indicating conservation of electric charge. The components T_X and T_Y, however, commute with H only if $v^{(1)}$ and $v^{(2)}$ are zero. Note, however, that even if the nucleon-nucleon interaction is charge independent, the presence of the Coulomb interaction is enough to break pure isospin symmetry.

The objective of this work is a theoretical study of isospin-symmetry violation (isospin-mixing) caused by the isospin-nonconserving components of the nuclear Hamiltonian, V_{INC}. The strategy applied is to determine V_{INC} empirically and then to evaluate the effects of isospin-mixing on:

(1) corrections to the Fermi matrix element in superallowed β-decay,

(2) isospin-forbidden Fermi transitions, and

(3) decay of T=3/2 states in A=4n+1 nuclei ($21 \leq A \leq 37$) by isospin-forbidden proton and neutron emission.

This dissertation is organized in the following manner. First, a description of each problem under consideration here is given in the remaining part of the first chapter. In the second chapter, isospin-nonconserving interactions used throughout this work are determined

empirically by requiring that they reproduce experimentally determined isotopic mass shifts. Corrections to the Fermi matrix element for superallowed β-decays are presented in Chapter Three, while results obtained for isospin-forbidden β-decay are given in Chapter Four. In the fifth chapter, the decay of T=3/2 states via isospin-forbidden proton and neutron emission is discussed. Since the last three chapters are independent, a discussion of the results presented is given in each chapter, and a summary of results and further concluding remarks will be presented in Chapter Six.

1.2 Isotopic Mass Shifts

Perhaps the strongest effect due to the isospin-nonconserving part of the nuclear Hamiltonian is the mass difference between members of the same isobaric multiplet. From eq.(1.1.7) we see that the Hamiltonian exhibits a T_Z dependence, and therefore the eigenenergies $E(\alpha,T,T_Z)$, should also exhibit this dependence. In fact, the energies $E(\alpha,T,T_Z)$ can be parameterized [Wig 57] in terms of the isobaric mass multiplet equation (IMME) as

$$E(\alpha,T,T_Z) = a(\alpha,T) + b(\alpha,T)\ T_Z + c(\alpha,T)\ T_Z^2 \qquad (1.2.1)$$

where the $a(\alpha,T)$ is due to both the isoscalar and isotensor Hamiltonians, and $b(\alpha,T)$ and $c(\alpha,T)$ are due only to the isovector and isotensor components, respectively (the derivation of the IMME is given in Chapter Two, section 1).

The IMME was first verified by the measurement of the ground state and excitation energies of the four members of the T=3/2 quartet in the

A=9 system by Cerny [Cer 64]. The masses and excitation energies of thirteen other isobaric quartets have also been measured and were found to be in excellent agreement with the IMME [Ben 79].

The source of the mass splittings among the members of an isobaric multiplet is of course the isovector and isotensor parts of the Hamiltonian, given by eqs.(1.1.8b) and (1.1.8c), respectively. The precise form of these interactions, however, is still unknown. It has been shown [Nol 69] that the Coulomb force alone cannot account for the observed mass splittings in T=1/2 mirror nuclei. This discrepancy between experimental and calculated Coulomb mass splittings is known as the Nolen-Schiffer anomaly. Many explanations for this anomaly have been suggested (a review of these is given by Auerbach [Aue 83]), but at present, calculations of the mass splittings are still consistently three to six percent smaller than experiment [Aue 83]. Therefore, in the present work, an explicit form for the isovector and isotensor interactions is postulated. The parameters of these potentials are then determined empirically by performing a least-squares fit to experimental b- and c-coefficients (defined in eq.(1.2.1)).

With the isospin-nonconserving potential determined empirically, we then make predictions as to the extent of isospin-symmetry violation, and compare with experimental observations.

1.3 Corrections to the Fermi Matrix Element

As can be seen from eq.(1.2.1), one member of an isotopic multiplet has the highest binding energy, and therefore it is not unreasonable to expect the other members of this multiplet to decay in some fashion to this nucleus. This decay, however, involves a change in the total

charge, which is not permitted by the nuclear Hamiltonian (see eq.(1.1.9)). The weak interaction, however, allows this transition to occur through the processes

$$n \rightarrow p + e^- + \bar{\nu}_e$$

$$p \rightarrow n + e^+ + \nu_e .$$

Note that free protons cannot decay because of energy conservation, and that only through interactions with the nuclear medium is this transition permitted. The weak interaction has two components, vector and axial-vector, which allow two types of nuclear transitions. These are Fermi (vector) and Gamow-Teller (axial-vector), and are mediated by the operators $\tau_\pm$ and $\vec{\sigma}\tau_\pm$, respectively. The selection rules for these decays are:

(1) Fermi: $\Delta J = 0$, no change in parity; $\Delta T = 0$

(2) Gamow-Teller: $\Delta J = 0, 1$ ($0 \rightarrow 0$ forbidden), no change in parity; $\Delta T = 0, 1$.

The general form for the transition rate for nuclear β-decay is

$$t_{1/2}/BR = \frac{K}{f_V G_V^2 \left|M_F\right|^2 + f_A G_A^2 \left|M_{GT}\right|^2} \qquad (1.3.1)$$

where $K = 2\pi^3 \ln 2 \hbar^7 c^6/(mc^2)^5$, $t_{1/2}$ is the half-life, BR is the branching ratio for the decay ($t = t_{1/2}/BR$ is the partial half-life), f_V

and f_A are the statistical rate functions for the Fermi and Gamow-Teller transitions, respectively, G_V and G_A are the effective vector and axial-vector coupling constants for single nucleon β-decay, and M_F and M_{GT} are the matrix elements of the Fermi and Gamow-Teller operators. In this work, the conventional value of 1.251±0.009 is taken for the ratio G_A/G_V [Wil 73]. (This is consistent with the more recent value of 1.2606±0.0075 reported by Wilkinson [Wil 82].)

Fermi transitions between $J^\pi=0^+$, T=1 analog states have been the subject of much study [Bli 67, Hal 68, Bli 69, Dam 69, Bli 70, Tow 73, Har 75, Tow 77, Wil 77 and Tow 78] over the past years. An important feature of these transitions is that, since they are purely vector, their ft values are given by

$$f_R t = \frac{K}{G_V^2 |M_F|^2}, \qquad (1.3.1)$$

where the statistical rate function f is evaluated by solving the Dirac equation for the lepton in the static Coulomb potential of the residual nucleus, and is corrected with the nucleus-dependent "outer" radiative correction δ_R of Sirlin [Sir 67], i.e. $f_R = f(1 + \delta_R)$. Once all nucleus-dependent corrections have been evaluated, it is possible to extract from eq.(1.3.1) empirical values of G_V. This is important because the effective vector coupling constants for nucleon and muon β-decay are related by

$$G_V^2 = G_\mu^2 \cos^2\theta_C(1 + \Delta_\beta - \Delta_\mu),$$

where θ_C is the Cabibbo angle, and Δ_β and Δ_μ are the nucleus-independent "inner" radiative corrections to nucleon and muon β-decay, respectively. With G_V/G_μ and θ_C determined from experimental quantities, it is then possible to test current theoretical estimates for $\Delta_\beta - \Delta_\mu$.

At present, the most uncertain nucleus dependent correction to eq.(1.3.1) is that for the Fermi matrix element M_F. If the initial and final nuclear states have definite isospin, then the Fermi matrix element is model independent and given by

$$M_{F0}^2 = \left[T(T+1) - T_{Zi}T_{zf}\right] \delta_{if} \qquad (1.3.2)$$

where the Kronecker delta insures that only transitions between analog states, defined by eq.(1.1.4), are allowed. Values for G_V could then be extracted from measured ft values with eq.(1.3.1). The most accurately determined f_Rt values [Kos 85], however, are not constant within experimental uncertainty as eq.(1.3.1) would indicate, and are shown in Figure 1.2. This suggests the possibility of the breaking of analog symmetry between the initial and final nuclei due to the presence of isospin-nonconserving interactions.

The extent to which analog symmetry is broken is embodied in the correction factor δ_C defined by

$$|M_F|^2 = |M_{F0}|^2 \, (\, 1 - \delta_C). \qquad (1.3.3)$$

From experimental f_Rt values relative estimates of δ_C can be obtained. Koslowsky [Kos 83] has determined the relative corrections $\delta_C(Z) - \delta_C(^{14}O)$ from the quantity $(f_Rt(Z) - f_Rt(^{14}O))/f_Rt(^{14}O)$, and are shown in

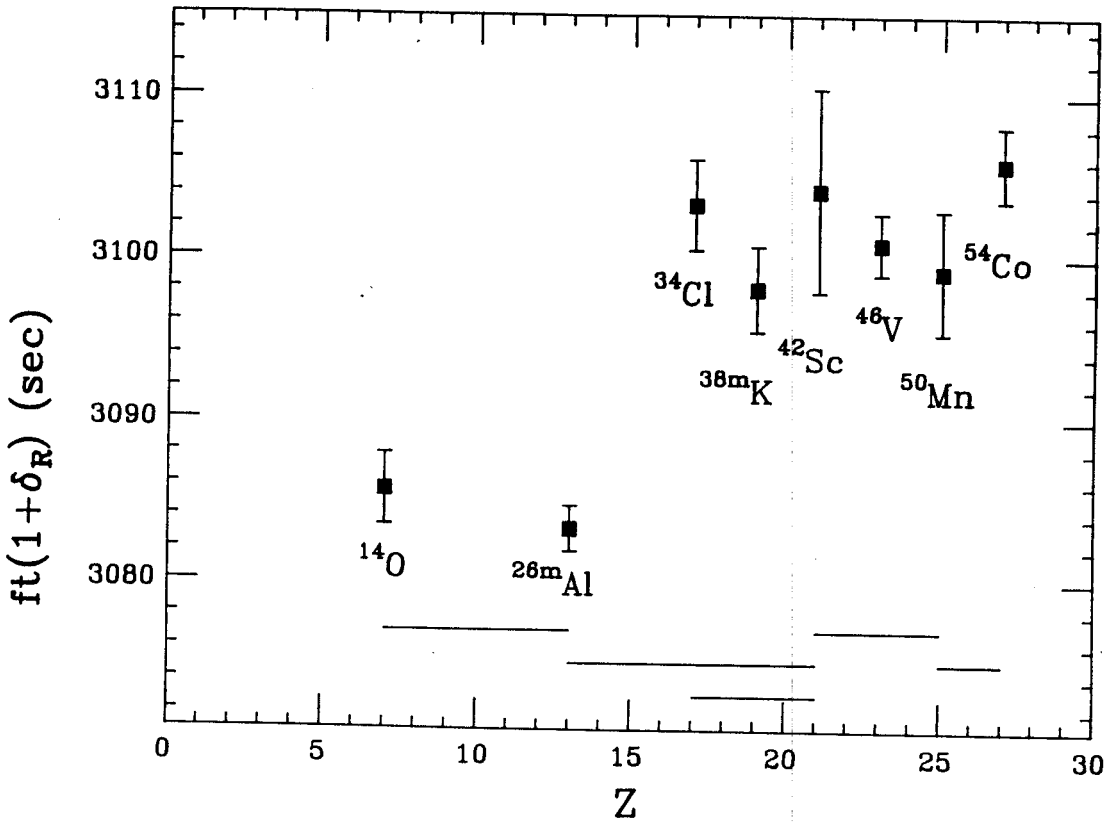

Figure 1.2: Plot of experimental ft values (including the "outer" radiative correction δ_R) for the eight most accurately measured superallowed transitions. The bars indicate pairs of nuclei whose ground state masses have been measured relative to one another.

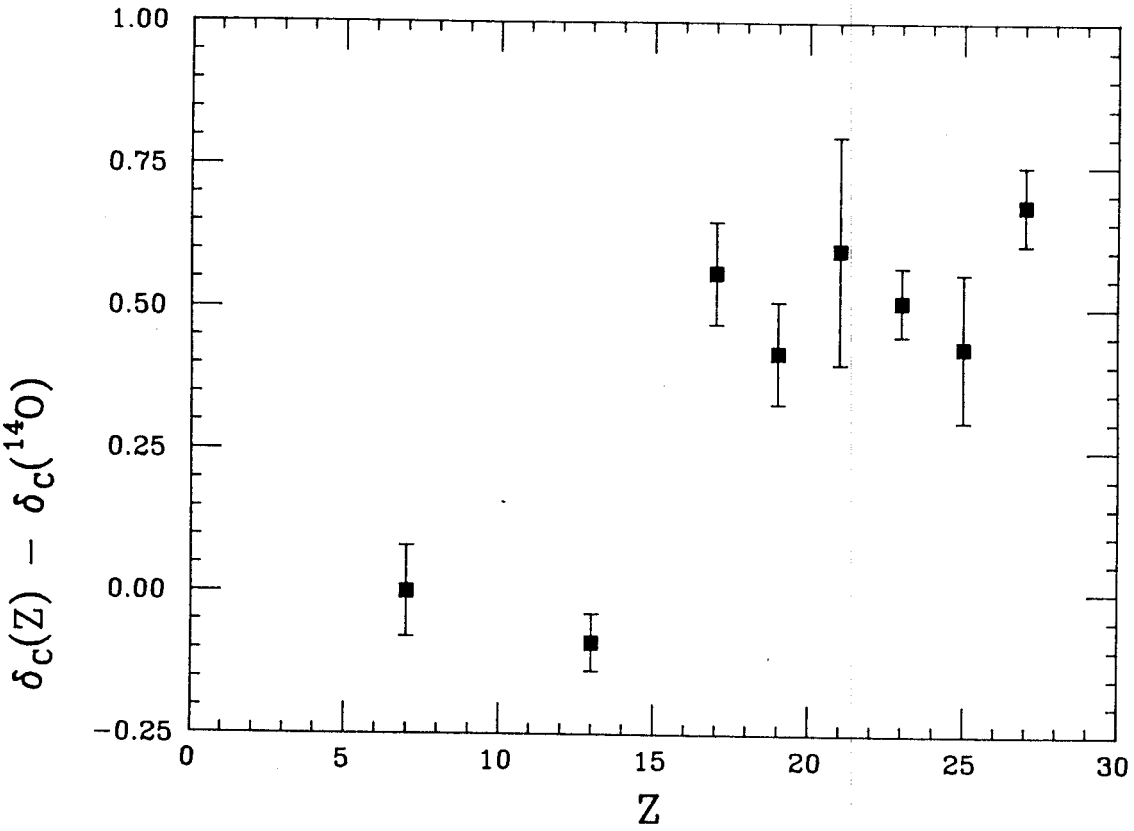

Figure 1.3: Relative values of δ_C extracted from experimental ft values.

Figure 1.3. Here it is seen that in order for the $f_R t$ values to be constant, it is necessary that an additional correction, on the order of 0.5% for higher Z values, be applied to the experimental data.

Theoretical estimates of δ_C can be determined either empirically [Wil 77], or by performing a microscopic calculation [Tow 73, Har 75, Wil 76 and Tow 77]. The first approach is based on the Behrends-Sirlin-Ademollo-Gatto (BSAG) theorem [Beh 60 and Ade 64], which states that corrections to the denominator of eq.(1.3.1) within an isospin multiplet are proportional to the square of the mass splittings due to symmetry breaking no matter what the origin of the symmetry breaking may be. For nuclei, these mass splittings go roughly as Z. Wilkinson and Alburger [Wil 76a] have found that the square of the mass splittings for the superallowed transitions under investigations are proportional to $Z^{1.86}$. The microscopic approach makes use of a model which describes the many-body nuclear wave functions as well as the single-particle radial wave functions. By performing a fit to the proportionality constant, and comparing with the results of a microscopic calculation [Wil 76], Wilkinson [Wil 77] concluded that the empirical approach was superior. Towner and Hardy [Tow 78], on the other hand, concluded that the data showed no preference for either approach, and that in particular, they saw no reason to reject microscopic calculations. Since the nuclei in question are relatively light, ranging from ^{14}O to ^{54}Co, it is not unreasonable to expect shell effects to play a significant role in δ_C.

The basis for microscopic calculations of δ_C in this work, and for those in the past [Tow 73, Har 75, Wil 76 and Tow 77], is the nuclear shell model. Shell-model wave functions consist of many-body Slater determinants obtained within the spherical single-particle basis

$|\psi_{n\ell j}(\vec{r})\rangle = R_{n\ell j}(r)[Y^{\ell}(\hat{r}) \times s]^{j}$, in which (A - C) nucleons occupy n valence orbits outside a spherically closed core of C nucleons. Due to the truncation of the shell-model space (i.e. limitations on the number of active valence orbits) it is necessary to consider the effects of isospin mixing due to the INC interaction between states which are contained in the model space as well as with those outside. Isospin mixing within the shell-model configuration space is accounted for by adding the INC interaction onto the isoscalar Hamiltonian in proton-neutron formalism. Then, by diagonalizing the resultant matrix, one obtains states of mixed isospin. Mixing with those states which lie outside the configuration space is accounted for by realizing that the effect of these states is to alter the radial wave functions. The repulsive nature of the Coulomb potential tends to push proton radial wave functions out relative to neutrons, and therefore, breaks analog symmetry. These two corrections can be factored [Tow 73 and Chapter Three, section 1] to give

$$\delta_C = \delta_{IM} + \delta_{RO} \tag{1.3.4}$$

where δ_{IM} is due to mixing between states contained in the configuration space, and δ_{RO} is the correction due to the difference between the proton and neutron radial wave functions.

A simple estimate for δ_{RO} can be obtained using harmonic oscillator wave functions [Dam 69, Lan 73, Fay 71, and Tow 77]. The change in the proton radial wave function can be described with first-order perturbation theory by the admixture of a state with one more radial node, i.e.

$$\psi_{n\ell} = \psi_{n\ell} + \alpha\psi_{n+1\ell}, \qquad (1.3.5)$$

where

$$\alpha = \frac{\langle\psi_{n+1\ell}|\ V_C\ |\psi_{n\ell}\rangle}{\Delta E},$$

$$\Delta E = E_{n+1\ell} - E_{n\ell} \approx 2\hbar\omega.$$

The two-body Coulomb potential can be replaced with the effective one-body potential of a uniformly charge sphere of radius R_C,

$$V_C = \frac{Ze^2}{2R_C}\left(3 - \frac{r^2}{R_C}\right),$$

giving

$$\delta_{RO} = \alpha^2 = \frac{Z^2}{(\hbar\omega)^4 R_C^6}(n+1)(n+\ell+3/2)\frac{e^4\hbar^4}{16m^2}. \qquad (1.3.6)$$

If we assume $\hbar\omega = 41A^{1/3}$ MeV and $R_C = 1.2A^{1/3}$ fm, eq.(1.3.6) exhibits the behavior $\delta_{RO} \propto Z^{4/3}$ with some shell structure superimposed by the orbital quantum numbers n and ℓ. Given in Table 1.1 are the values obtained by Lane and Meckjian [Lan 73] where R_C was taken to be $\frac{5}{3}\langle r_{ch}^2\rangle$ where $\langle r_{ch}^2\rangle$ is the mean square radius of the proton charge distribution determined from experimental electron scattering data.

A better approach to evaluating δ_{RO} is to obtain the radial wave-functions from a realistic nuclear single-particle potential, and to

Table 1.1

Radial-overlap (RO) and isospin-mixing (IM) corrections to the Fermi matrix element

Decaying Nucleus	δ_{RO}(%) HO	δ_{RO}(%) WS	δ_{IM}(%)	δ_C(%)
^{14}O	0.04	0.28	0.05	0.18
^{26}Al	0.11	0.27	0.07	0.34
^{34}Cl	0.18	0.62	0.23	0.85
^{38}K	-	0.54	0.16	0.70
^{42}Sc	0.25	0.35	0.13	0.48
^{46}V	0.29	0.36	0.04	0.40
^{50}Mn	0.33	0.40	0.03	0.43
^{54}Co	0.38	0.56	0.04	0.60

include effects due to structure of both the parent and daughter nuclei. This approach was taken by Towner, Hardy, and Harvey [Tow 77], in which they used wave functions obtained from a Woods-Saxon parameterization of the single-particle potential. These values are given in Table 1.1, and are compared with those obtained with harmonic oscillator wave functions. The principal effect of this method is to increase δ_{RO} relative to the harmonic oscillator values.

As mentioned above, the correction δ_{IM} can be evaluated using isospin-mixed wave functions obtained by adding the INC interaction onto the isoscalar interaction and diagonalizing the resulting Hamiltonian. δ_{IM} is then determined by evaluating M_F with the isospin-mixed wave functions, and is simply

$$\delta_{IM} = 1 - M_F/2. \qquad (1.3.7)$$

This procedure was used by Towner and Hardy [Tow 73]. They accounted for the INC interaction by : (1) adding Coulomb matrix elements to the proton-proton two-body matrix elements, (2) increasing the T = 1 part of the proton-neutron matrix elements by 2%, and (3) using isovector single-particle energies determined from the energy difference between the closed-shell-plus-proton and -neutron systems. Values of δ_{IM} obtained by Towner and Hardy are also given in Table 1.1, where it is seen that δ_{RO} dominates the total. The contribution due to δ_{IM}, however, is not insignificant, and improvements in the values of δ_C can only be expected by making improvements to both δ_{RO} and δ_{IM}.

With the corrections δ_{RO} and δ_{IM}, it is possible to extract values of G_V from eq.(1.3.1). Shown in Figure 1.4 are values of G_V/G_μ obtained

for the $f_R t$ values shown in Figure 1.2 using the value G_μ determined from muon β-decay [PDG 84 and Gio 84] and the values of δ_C of Towner and Hardy. Far from being nucleus independent, these values exhibit a discrepancy between low- and high-Z values. There appear to be two consistent values, one for $Z < 21$, and another for $Z \geq 21$.

There are at least three sources which can cause the discrepancy between low- and high-Z values of G_V/G_μ. These are: faulty experimental ft values, incorrectly accounting for the "outer" radiative correction δ_R, and uncertainty in the corrections to the Fermi matrix element. At first, it might be tempting to suspect the first source, as ft values require the accurate measurement of the mass of the parent and daughter nuclei, the half-life, and the branching ratio of the decay. These measurements are indeed difficult, and in the past the ft values shown in Figure 1.2 have changed outside the limits of experimental uncertainty due to improved experimental techniques. Recently, however, a concerted effort has been made to measure these quantities as accurately as possible [Kos 85]. In fact, these masses have been measured relative to one another, and the measured pairs are indicated by the bars in Figure 1.2. By measuring the masses in this fashion, it is hoped that random errors, which can cause fluctuations as a function of Z in the ft values, are reduced. The remaining uncertainties are then expected to be due to errors in the lifetime and branching-ratio measurements and the mass of ^{14}O. This last error, however, is systematic in all ft values, and will therefore leave the relative Z-dependence unaltered.

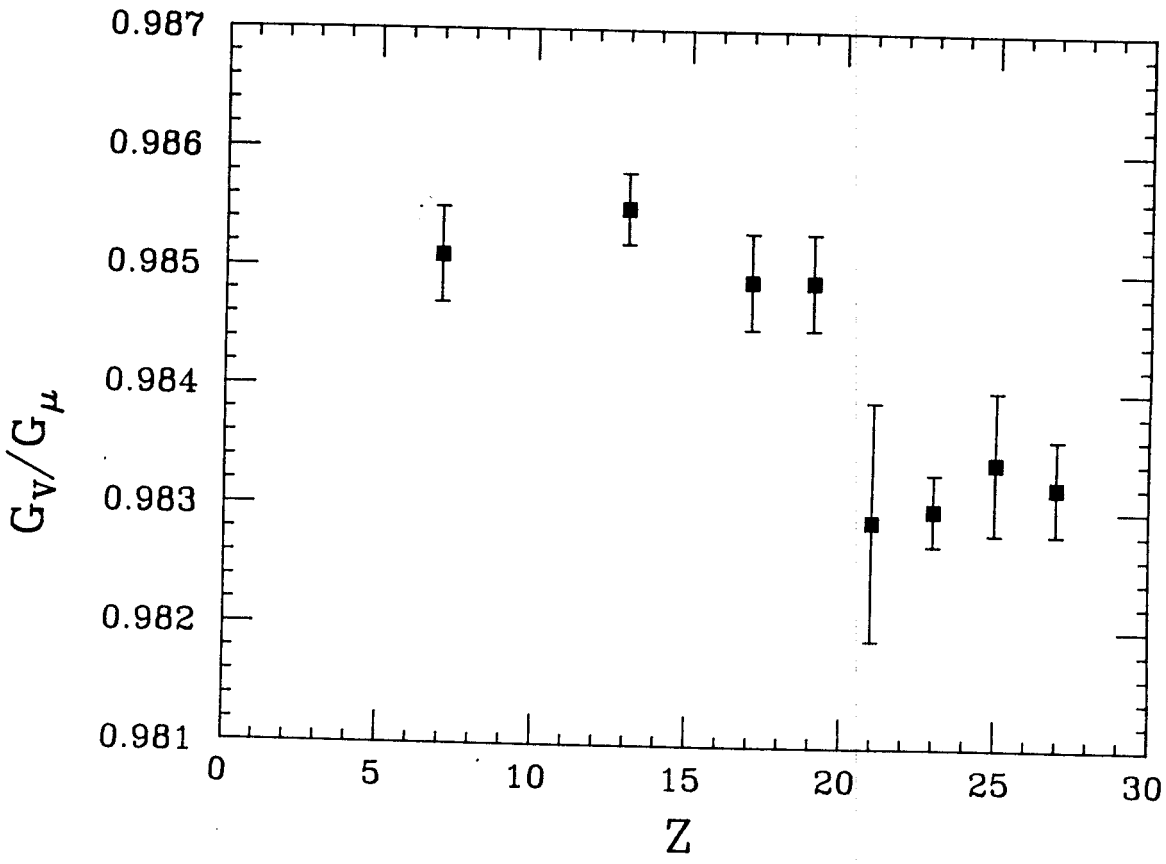

Figure 1.4: Values of the ratio of the effective vector coupling constants for nucleon and muon β-decay determined from experimental ft values and the corrections δ_C of Towner, Hardy, and Harvey.

Similarly, the correction δ_R to the statistical rate function has been under extensive study [Sir 67, Beg 69, Dic 70, Jau 70, Jau 72, Sir 74, and Sir 78]. δ_R is independent of both strong and weak interaction models to within 0.03% [Sir 67], and may be expressed as a perturbation series in $Z\alpha$, with all terms $Z^m\alpha^n$ ($m \leq n$) being present [Beg 69] (α is the fine structure constant, $\alpha \approx 1/137$). At present, δ_R has been evaluated to order $Z^2\alpha^3$, and is incorporated in the ft values shown in Figure 1.2. Higher order corrections are expected to contribute less than 0.05%, while the deviation in G_V^2/G_μ^2 is of the order 0.4%.

Corrections to the Fermi matrix element, however, are sensitive to explicit nuclear models. With this in mind, it is prudent to reinvestigate the corrections δ_{IM} and δ_{RO}, making use of recent advances in our understanding of nuclear structure, before turning to the two previously mentioned possibilities as a source of the high- and low-Z discrepancy.

In this work, the correction δ_{RO} is evaluated using radial wave functions obtained from a self-consistent Hartree-Fock calculation using a Skyrme-type interaction. The advantage of this procedure over the Woods-Saxon parameterization is that it includes an isovector single-particle potential which is induced by Coulomb repulsion. In the Hartree-Fock procedure, the effective single-particle potential is dependent on the proton and neutron densities. As the Coulomb force pushes the proton densities out, an isovector potential is thereby induced, countering the effects of Coulomb repulsion, and therefore, reducing the extent of analog symmetry breaking. With this in mind, we expect the correction δ_{RO} to be reduced relative to previous estimates.

The isospin-mixing correction δ_{IM} is calculated using the same procedure as Towner and Hardy, with the exception that the INC interaction is determined using the fitting procedure outlined in section 1.2. In addition, improved isoscalar Hamiltonians have been developed recently (for example, the mass-dependent sd-shell Hamiltonian of Wildenthal [Wil 84]), and have been used in this work. These changes in the method of evaluating δ_{IM} are important because, as will be shown in Chapter Three, δ_{IM} is sensitive to both the isoscalar Hamiltonian and the isovector single-particle energies.

With these improvements in the procedure in determining δ_C, it is hoped that the low- and high-Z discrepancy in G_V/G_μ can be resolved, or alternatively, that some indication as to where the solution might lie can be given.

1.4 Isospin-forbidden Fermi β-decay

As was shown in eq.(1.3.2), Fermi transitions between states which are analogs of one another are forbidden in first order. For such a decay to take place, it is necessary that the parent and/or daughter state contain admixtures of the analog of the daughter and/or parent states, respectively. This is possible only under the influence of isospin-nonconserving interactions. A schematic view of these types of transitions are shown in Figure 1.5. There are two classes of β-decays in which isospin-forbidden Fermi transitions can occur. The first is a purely Fermi (vector; $0^+ \rightarrow 0^+$) transition, and is greatly suppressed relative to the allowed decay. In this case the mere observation of the decay is evidence of isospin mixing. The second class includes mixed Fermi, Gamow-Teller (axial-vector: $\Delta J = 0, 1$ and $\Delta T = 0$,

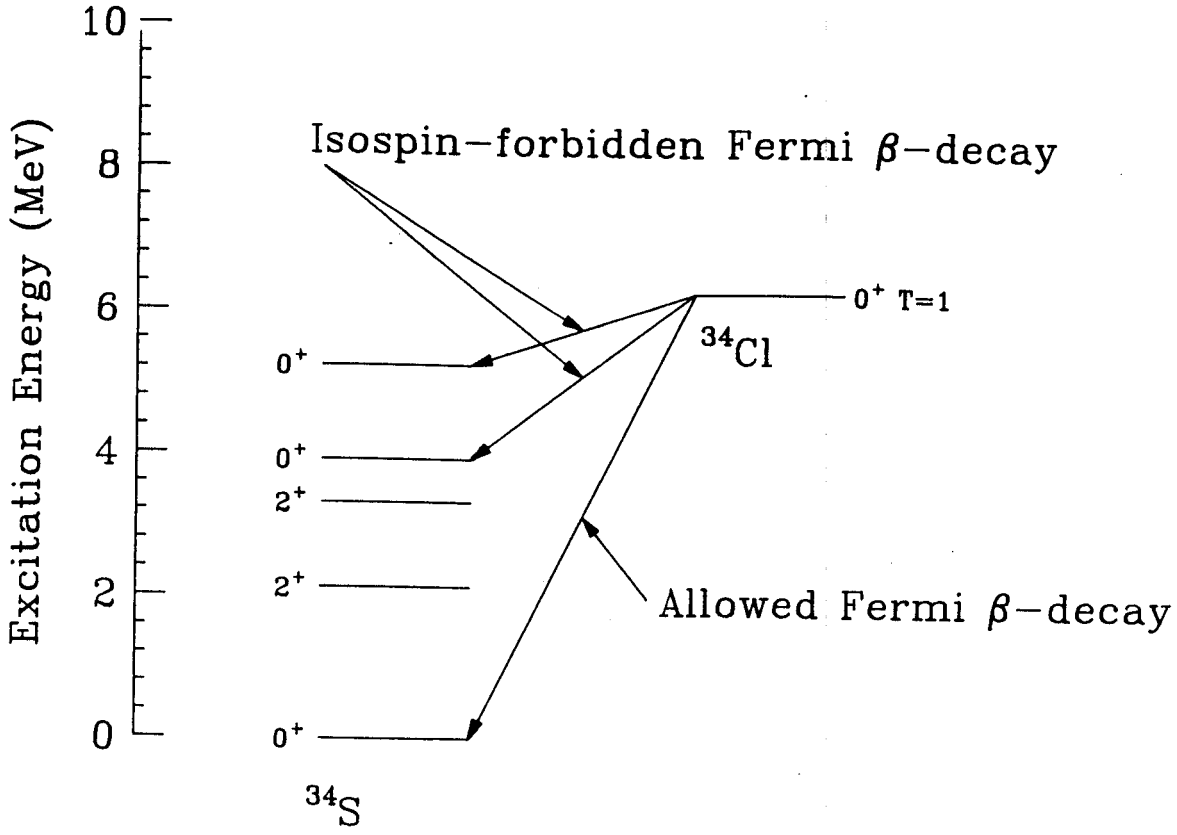

Figure 1.5: Schematic energy level diagram which illustrates a typical isospin-forbidden Fermi transition.

1; $0^+ \rightarrow 0^+$ forbidden) transitions. Since the Gamow-Teller operator is free to connect states which are not analogs, these decays are not necessarily suppressed relative to that to the analog state. Here more subtle techniques must be used to distinguish between the allowed Gamow-Teller and the forbidden Fermi components of the decay.

The first class of transitions has been observed in the decay of ^{42}Sc [Ing 77, Del 78, San 80, and Dae 85] and ^{28}Mg [Alb 79]. The matrix elements for these transitions were found to be $(9.4 \pm 1.6) \times 10^{-4}$ and $(6.7 \pm 0.8) \times 10^{-4}$, respectively. In this work, results for the isospin-forbidden β-decay of ^{28}Mg, ^{34}Ar, ^{34}Cl, and ^{42}Sc will be presented.

For the second class of decays, the ft value is given by

$$ft = \frac{K}{G_V^2|M_F|^2 + G_A^2|M_{GT}|^2}, \qquad (1.4.1)$$

where we have assumed $f_A = f_V$ (which is valid to within 0.5% [Wil 74]). Since the Fermi (vector) and Gamow-Teller (axial-vector) matrix elements do not interfere, it is clear that the transition rate will not in general provide unambiguous information about the small isospin-forbidden Fermi matrix element. Therefore, it is more useful to measure pseudoscalar quantities, such as the β-γ circular polarization correlation, which are sensitive to vector, axial-vector interference. This type of experiment has been performed for many nuclei. The decay of ^{24}Al, however, is of particular interest because this transition has the largest isospin-mixing matrix element yet observed in β-decay. A comparison between experiment and the results of a shell-model

calculation which utilizes the fitted INC interaction determined in Chapter Two is presented in Chapter Four.

1.5 Isospin-forbidden proton and neutron emission of T=3/2 states

Another clear indication of isospin mixing in light nuclei is the decay of T=3/2 states in A=4n+1 nuclei to T=0 states in A=4n nuclei by proton or neutron emission [Wei 76, Hin 81, Hin 84, McD 69, Adl 72, Iko 76, and Wil 83]. Previous conclusions [McD 78 and Wil 83] based on experimental data were that the spectroscopic amplitudes, $\Theta^{p(n)}_{INC}$, for these isospin-nonconserving decays systematically increase with mass A; have an oscillation with period $\Delta A=8$ superimposed on the proton amplitudes; are generally greater for neutron emission; generally do not increase as a function of excitation energy.

Perhaps the most striking feature of the experimental data is the oscillation as a function of A. Shown in Figure 1.6 are the spectroscopic amplitudes for the lowest T=3/2 state in each nucleus. The data show a gradual increase as a function of A, and a clear oscillation with a period $\Delta A=8$ superimposed on this increase (the experimental errors are typically less than 10% and are suppressed from the figure). The cause of this oscillation is not understood at present, and is of considerable interest [McD 78 and Wil 83].

As is the case for the corrections to the Fermi matrix element, there are two principal sources of isospin impurities which are responsible for these decays. The first is the mixing between the T=3/2 parent state and those states which lie outside the shell-model basis. This is commonly referred to as mixing with giant isovector monopole, and is also responsible for the correction δ_{RO} to Fermi matrix element.

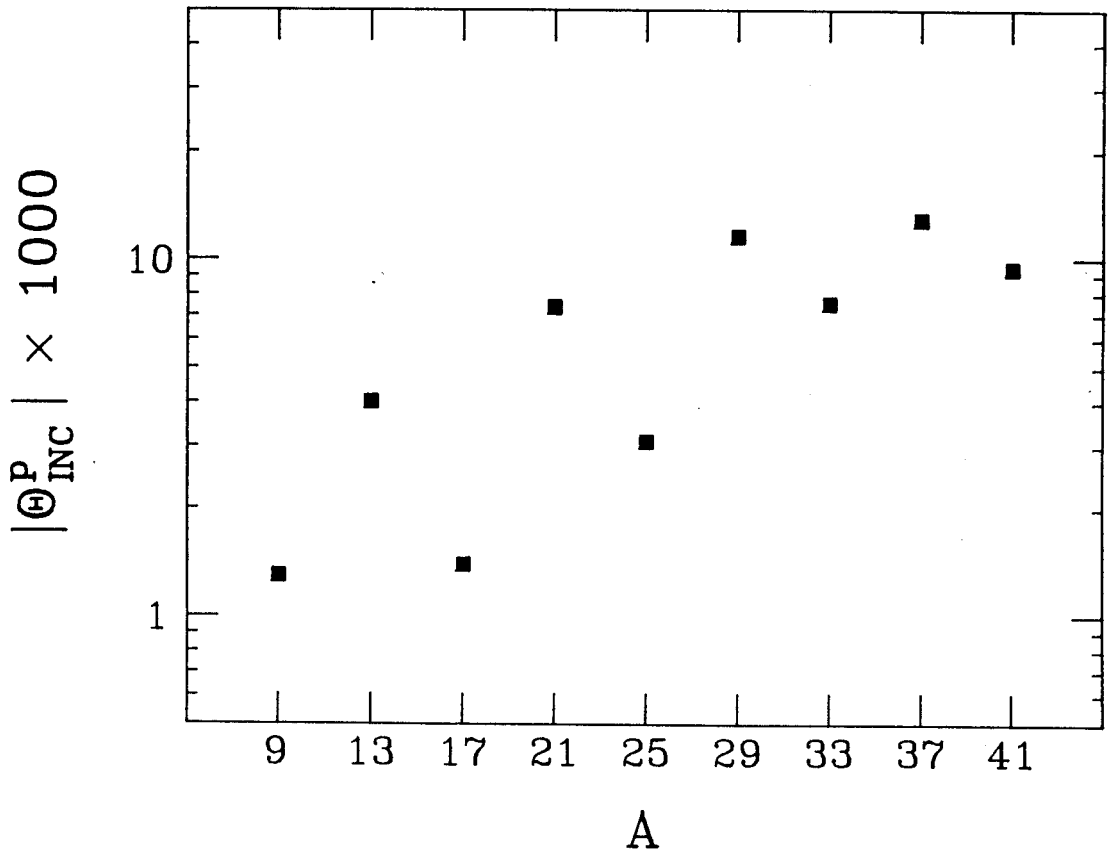

Figure 1.6: Plot of the isospin-forbidden spectroscopic amplitudes for decay of the lowest T=3/2 state in each nucleus by proton emission.

The second is due to mixing between nearby states (those contained in the shell-model basis) in both the parent and daughter nuclei. Here it is necessary to consider mixing between T=1/2 and T=3/2 parent states, and T=1 and 2 daughter states with T=0 ground state. (This last source of mixing is also the mechanism which produces the correction δ_{IM} to the Fermi matrix element). The contribution to Θ^{p}_{INC} due to the giant isovector monopole state has been evaluated [Lev 73] for several nuclei using an harmonic-oscillator basis, and was found to be "small but not negligible" [Aue 83] compared to experimental values. The harmonic-oscillator basis, however, tends to predict more isospin mixing in the ground state than does a more realistic Hartree-Fock calculation [Aue 83]. Therefore, this work concentrates on the contributions due to mixing with nearby states, and assumes that the isovector monopole contribution is negligible. A typical level scheme which illustrates the relative location of nearby states in both the parent and daughter nuclei is shown in Figure 1.7

In the past, there has been only a limited amount of theoretical analysis dealing with the contribution due to nearby states [Aue 71, Ari 71, and McD 78]. The most detailed work, was that of Arima and Yoshida [Ari 71] for the A=13 system. Their approach was to take into account the entire 0p shell and to determine the mixing with nearby states via perturbation theory. Their results generally agree with experiment, and were found to depend strongly on the location of the, then unknown, third $J^{\pi}=3/2^{-}$, T=1/2 state. The approach of McDonald and Adelberger [McD 78] and Auerbach and Lev [Aue 71] was to assume that the source of the isospin impurity was mixing with the anti-analog state (A $T_{<}$ state whose spatial and spin wave functions are similar to those of the $T_{>}$ analog

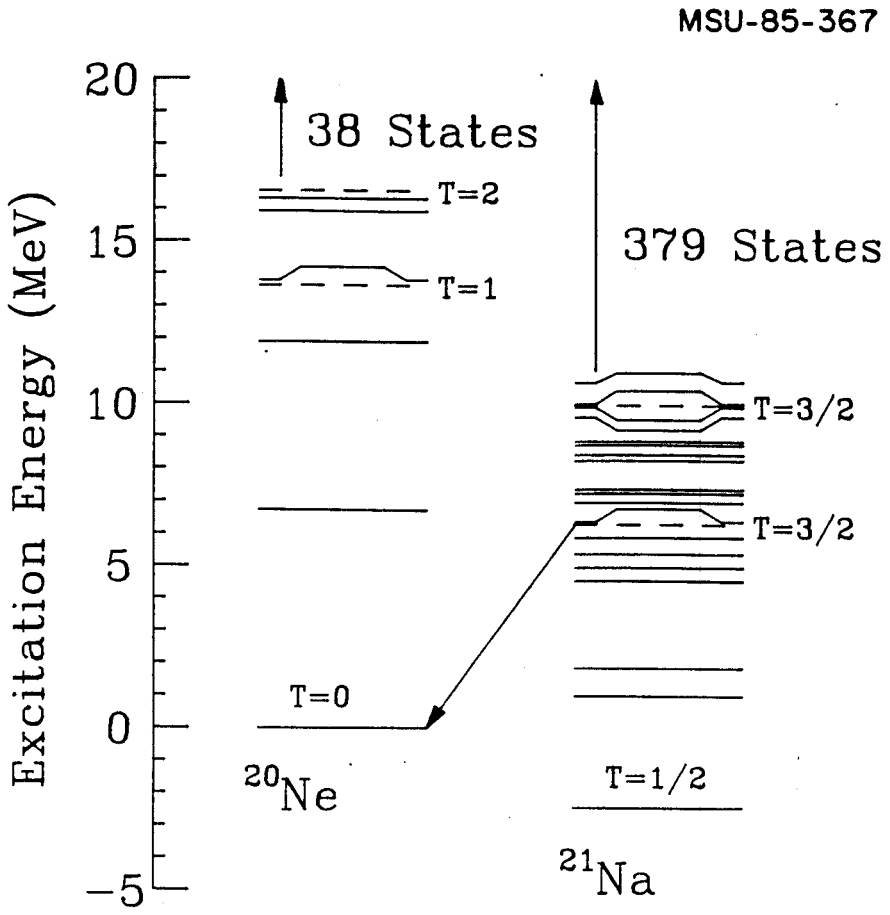

Figure 1.7: Level scheme of the relevant states in the decay of the $J^{\pi}=5/2^{+}$, T=3/2 state in ^{21}Na via isospin-forbidden proton emission. The isospin of the T=3/2 parent and the T=0 daughter states are represented by dashed lines and are labeled in the figure. The relative energies of the two ground states and the T=3/2 state were taken from experiment, while theoretical energies were used for the remaining states.

state. For a further discussion see page 309 of [Law 80]). Within the framework of this simple model, they were able to reproduce the qualitative behavior of the data, but were unable to explain the observed oscillation.

The isospin-forbidden spectroscopic amplitudes can be evaluated using perturbation theory (see Chapter Five, section 1), giving

$$\Theta^{p(n)}_{INC} = \sum_j a(j,T=1/2;T=3/2)\ \Theta^{p(n)}(j,T=1/2,T=0) + \sum_j \sum_{T'=1}^{2} a(j,T';T=0)\ \Theta^{p(n)}(T=3/2;j,T') \qquad (1.5.1)$$

where $a(j,T=1/2;T=3/2)$ is the isospin-mixing amplitude between the nearby T=1/2 states and the T=3/2 parent, $a(j,T';T=0)$ is the mixing amplitude between T=1 and 2 states and the T=0 ground state, and the $\Theta^{p(n)}$ are the isospin-allowed spectroscopic amplitudes of the mixed states. In first-order perturbation theory the amplitude of the state $|j,T'\rangle$ contained in the state $|i,T\rangle$ is simply

$$\frac{\langle j,T'|\ V_{INC}\ |i,T\rangle}{E(i,T) - E(j,T')} . \qquad (1.5.2)$$

Clearly, those states $|j,T'\rangle$ which satisfy the condition $E(i,T) - E(j,T')$ is small, can contribute significantly to the total value. As can be seen from Figure 1.7, this condition is satisfied for those T=1/2 states which are near the T=3/2 parent state. Unfortunately, both the allowed spectroscopic amplitudes and the exact location of these nearby T=1/2 states is uncertain theoretically and experimentally for all but

one case [Iko 76]. With this in mind, it is necessary to estimate the error in a calculation of $\Theta_{INC}^{p(n)}$. In this work, this was done by shifting the T=1/2 spectrum relative to the T=3/2 parent state by an amount ΔE in small steps, and evaluating $\Theta_{INC}^{p(n)}$ at each step with eq.(1.5.1). The "best" estimate of $\Theta_{INC}^{p(n)}$ is then the unweighted average of the absolute value of $\Theta_{INC}^{p(n)}$ obtained at each step, while upper and lower limits of the uncertainty are determined from the upper and lower rms deviations from this "best" value.

Results of the first detailed shell-model calculation for $\Theta_{INC}^{p(n)}$ in the region $21 \leq A \leq 37$, in which the full or nearly full 1s-0d shell-model space was taken into account, are presented here. The $\Theta_{INC}^{p(n)}$ are evaluated using perturbation theory (eq.(1.5.1)), and the influence of nearby states in both the parent and daughter nuclei is analyzed. The principal objective of these calculations is to give some insight into the cause of the observed oscillatory behavior.

Chapter Two

2.1 Introduction

In this chapter, a method for determining the isospin-nonconserving (INC) components of the nuclear Hamiltonian is developed. The procedure used is to assume an empirical form for the isovector and isotensor interactions, and, by performing a least squares fit to a set of experimental b- and c-coefficients (defined by eq.(1.2.3)), determine the parameters of these interactions.

The chapter is organized in the following manner. In section two, the isobaric mass multiplet equation (eq.(1.2.3)) is derived, and the procedure used to evaluate the b-and c-coefficients within the framework of the nuclear shell model is given. In the third section, the parameters of the isovector and isotensor interactions, determined from least-squares fits to experimental data, are presented for four separate configuration model spaces. Finally, the formalism needed to combine the isoscalar, isovector, and isotensor components of the Hamiltonian, in order that states of mixed isospin may be obtained, is given in the last section.

2.2 Isobaric Mass Multiplet Equation (IMME)

Wigner [Wig 57] was the first to demonstrate that the mass differences between members of the same isobaric multiplet can be parameterized by eq.(1.2.1). As was shown in Chapter One, the nuclear Hamiltonian can be decomposed into isoscalar, isovector, and isotensor components, i.e.

$$H_{tot} = \sum_{k=0}^{2} H^{(k)}. \qquad (2.2.1)$$

Since the dominant contribution to the total energy is due to the isoscalar part of the Hamiltonian, we start with states $\psi_A(\nu,J,T,T_Z)$ which are eigenstates of $H^{(0)}$, and evaluate the energy shift due to the isovector and isotensor components using first-order perturbation theory (the label ν represents all other relevant quantum numbers and A is the total number of nucleons). Applying the Wigner-Eckart theorem [Edm 60], the energy of the state $\psi_A(\nu,J,T,T_Z)$ is then

$$E(A,\nu,J,T,T_Z) = \langle\psi_A(\nu,J,T,T_Z)| H_{tot} |\psi_A(\nu,J,T,T_Z)\rangle$$

$$= \frac{1}{\sqrt{(2J+1)}} \sum_{k=0}^{2} (-1)^{T-T_Z} \begin{pmatrix} T & k & T \\ -T_Z & 0 & T_Z \end{pmatrix}$$

$$\times \langle\psi_A(\nu,J,T)|||\, H^{(k)} \,|||\psi_A(\nu,J,T)\rangle, \qquad (2.2.2)$$

where the three bars denote a reduction in both isospin and angular momentum space. Substituting explicit values for the 3-j coefficients into eq.(2.2.2), we obtain

$$E(A,\nu,J,T,T_Z) = E^{(0)}(A,\nu,J,T) + E^{(1)}(A,\nu,J,T)\, T_Z$$

$$+ [3T_Z^2 - T(T+1)]E^{(2)}(A,\nu,J,T), \qquad (2.2.3)$$

where

$$E^{(0)}(A,\nu,J,T) = \frac{1}{\sqrt{[(2J+1)(2T+1)]}} \langle\psi_A(\nu,J,T)|||\ H^{(0)}\ |||\psi_A(\nu,J,T)\rangle,$$

$$E^{(1)}(A,\nu,J,T) = \frac{1}{\sqrt{[(2J+1)T(2T+1)(T+1)]}}$$

$$\times \langle\psi_A(\nu,J,T)|||\ H^{(1)}\ |||\psi_A(\nu,J,T)\rangle,$$

$$E^{(2)}(A,\nu,J,T) = \frac{1}{\sqrt{[(2J+1)(2T-1)(2T+1)(T+1)(2T+3)]}}$$

$$\times \langle\psi_A(\nu,J,T)|||\ H^{(2)}\ |||\psi_A(\nu,J,T)\rangle. \qquad (2.2.4)$$

Eq.(2.2.3) has the same form as eq.(1.2.1), i.e.

$$E(A,\nu,J,T,T_Z) = a(A,\nu,J,T) + b(A,\nu,J,T)\ T_Z + c(A,\nu,J,T)\ T_Z^2$$

with

$$a(A,\nu,J,T) = E^{(0)}(A,\nu,J,T) - T(T+1)\ E^{(2)}(A,\nu,J,T), \qquad (2.2.5a)$$

$$b(A,\nu,J,T) = E^{(1)}(A,\nu,J,T), \qquad (2.2.5b)$$

$$c(A,\nu,J,T) = 3E^{(2)}(A,\nu,J,T). \qquad (2.2.5c)$$

Deviations from the parameterization of the isobaric mass multiplet equation are an indication that we must consider corrections due to higher-order perturbation theory, and/or the possibility of three-body interactions. For states with $T \geq 3/2$ these effects can be accounted for by adding the term dT_Z^3 to eq.(1.2.3). As was mentioned in Chapter One,

fourteen isobaric quintets have been analyzed to see if they fit the systematics of the IMME. In all but one case (A=9), the d-coefficients were found to be consistent with zero, with upper limits on their absolute values being approximately 5 keV [Ben 79]. This absence of experimental d-coefficients is a strong indication that a first-order perturbation theory calculation of the isotopic mass differences, which utilizes only two-body interactions, is adequate.

In this work, the reduced many-body matrix elements of the isospin-nonconserving components of H_{tot}, hereafter referred to as V_{INC}, are evaluated within the framework of the nuclear shell model. As was mentioned in Chapter One, the starting point of shell-model calculations is the many-body Slater determinants obtained within the spherical basis $|\psi(n,\ell,j)> = R_{n\ell j}(r)[Y^{\ell} \times s]^{j}$, in which (A-C) nucleons occupy n valence orbits outside a spherically closed core of C nucleons. Within this basis we need to account for the two-body interaction between particles occupying the valence orbits as well as with those inside the closed core. The reduced matrix element of $V_{INC}^{(k)}$ is then [Bru 77]

$$<\psi_A(\nu,J,T)||| V_{INC}^{(k)} |||\psi_A(\nu,J,T)> =$$

$$\sum_{orbits} OBTD_{A,\nu}(\rho,\rho';k) <core,\rho||| V_{INC}^{(k)} |||core,\rho'>$$

$$+ \sum_{orbits} TBTD_{A,\nu}(\rho_1\rho_2;\lambda_{12}:\rho_3\rho_4;\lambda_{34};k)$$

$$\times <\rho_1\rho_2;\lambda_{12}||| V_{INC}^{(k)} |||\rho_3\rho_4;\lambda_{34}>, \qquad (2.2.6)$$

where the one-body matrix element $\langle core,\rho \,|||\, V^{(k)} \,|||core,\rho\rangle$ represents the sum of two-body interactions between particles in the closed core and a particle in the ρth valence orbit, and $|\rho\rho';\lambda\rangle$ is the antisymmetric two-nucleon wave function with particles occupying the orbits ρ and ρ', coupled to the intermediate state λ. The labels ρ and λ denote all the available angular-momentum and isospin coupling quantum numbers. The general form of the one-body transition density (OBTD) and two-body transition density (TBTD) matrices are [Bru 77]

$$OBTD_{A,\nu\nu'}(\rho,\rho':\lambda) = \frac{1}{\sqrt{(2\lambda+1)}} \langle\psi_A(\nu,J,T)|||\,[a^{\dagger}_{\rho} \times \tilde{a}_{\rho'}]^{\lambda}\,|||\psi_A(\nu',J',T')\rangle,$$

$$TBTD_{A,\nu\nu'}(\rho_1\rho_2;\lambda_{12}:\rho_3\rho_4;\lambda_{34}:\lambda) = -\frac{1}{\sqrt{[(2\lambda+1)(1+\delta_{\rho_1\rho_2})(1+\delta_{\rho_3\rho_4})]}}$$

$$\times \langle\psi_A(\nu,J,T)|||\,[(a^{\dagger}_{\rho_1} \times a^{\dagger}_{\rho_2})^{\lambda_{12}} \times (\tilde{a}_{\rho_3} \times \tilde{a}_{\rho_4})^{\lambda_{34}}]^{\lambda}\,|||\psi_A(\nu',J',T')\rangle, \tag{2.2.7}$$

where $\sqrt{(2\lambda+1)}$ is shorthand for $\sqrt{[(2J+1)(2T+1)]}$, and $a^{\dagger}_{\rho}$ and $\tilde{a}_{\rho}$ are tensor operators which create and annihilate a nucleon in the ρth orbit, respectively. In eq.(2.2.6), the intermediate couplings λ_{12} and λ_{34} are restricted by the requirement that the final coupling λ must have angular momentum $\Delta J=0$ and isospin $\Delta T=k$.

A perturbative calculation of the isotopic mass differences within the framework of the shell model is then reduced to determining the isovector single-particle energies $\varepsilon^{(1)}(\rho) = \langle core,\rho|\, V^{(1)}_{INC} \,|core,\rho\rangle$, the two-body matrix elements of the isovector (k=1) and isotensor (k=2) components of $V^{(k)}_{INC}$, and the OBTD and TBTD matrices using wave functions obtained with a suitable isoscalar Hamiltonian.

2.3 Determination of the INC interaction

The starting point of a calculation of the b- and c-coefficients are the shell-model wave functions $\psi_A(\nu,J,T)$ (the label T_Z is unnecessary, as the matrix elements evaluated with these wave functions are reduced in isospin space) which are obtained with an appropriate isoscalar Hamiltonian. Due to the wide range of nuclei ($14 \leq A \leq 54$) under investigation in this work, four separate configuration spaces and isoscalar Hamiltonians are used. These are:

(1) $0p_{3/2}$ and $0p_{1/2}$ orbits (0p shell) and the interaction of Cohen and Kurath (referred to as CKPOT) [Coh 65],

(2) $0d_{5/2}$, $1s_{1/2}$, and $0d_{3/2}$ orbits (1s-0d shell) and the mass-dependent sd-shell Hamiltonian of Wildenthal (W) [Wil 84],

(3) $0d_{3/2}$ and $0f_{7/2}$ orbits and the isoscalar Hamiltonian of Hsieh and Wildenthal (HW) [Hsi 85], and

(4) $0f_{7/2}$, $1p_{3/2}$, $0f_{5/2}$, and $1p_{1/2}$ orbits (0f-1p shell) and the van Hees interaction (FPV) [van 81].

Listed in Table 2.1 are the configuration spaces, isoscalar Hamiltonians, and the mass number A of the isobaric multiplets considered in this work.

The many-body wave functions $\psi_A(\nu,J,T)$ used to evaluate the one-body and two-body transition density matrices were obtained with the Oxford-Buenos Aires-MSU shell-model code [Rae 85]. In order that the calculation of the TBTD matrices remain tractable, some truncations on the configuration space were found necessary, and are also listed in Table 2.1. The effects of the model space truncations were checked by

Table 2.1

List of configuration spaces, isoscalar Hamiltonians, and model-space truncations used for each isobaric multiplet.

Configuration Space	Isoscalar Hamiltonain	Mass Number A	Model Space Truncations
0p Shell	CKPOT	10-15	None
1s-0d Shell	W	22	No more than four particles outside the $0d_{5/2}$ orbit
		34	No more than two holes in the $0d_{5/2}$ orbit
		35-39	None
$0d_{3/2}$-$0f_{7/2}$ orbits	HW	36-41	None
		43 & 53	No more than two holes in the $0d_{3/2}$ orbit
0f-1p Shell	FPV[a])	42	None
		43,45,46, 53, & 55	No more than one particle outside the $0f_{7/2}$ orbit
		57 & 59	No more than one hole in the $0f_{7/2}$ orbit

[a])This isoscalar interaction was designed to be used with the model space truncations indicated.

adding the empirically determined INC interaction onto the isoscalar Hamiltonian, and obtaining the eigenenergies in proton-neutron formalism (see section 2.4). The isotopic mass shifts evaluated using perturbation theory and the truncated model spaces were found to be in good agreement with those of the full-space proton-neutron calculation.

As was mentioned in the first Chapter, the explicit form of the isovector and isotensor components is unknown, and must therefore be determined empirically. With this in mind, the isospin-nonconserving potential is assumed to have the form

$$V_{INC}^{(k)} = [C^{(k)}V_C(r) + P^{(k)}V_\pi(r) + R^{(k)}V_\rho(r) + A^{(k)}V_{Iso}]\, I^{(k)}, \quad (2.3.1)$$

where $V_C(r)$ is the Coulomb potential e^2/r, $V_\pi(r)$ and $V_\rho(r)$ are Yukawa potentials of the form

$$V_\mu(r) = \frac{e^{-\mu r}}{\mu r},$$

with $\mu_\pi = 0.7\text{fm}^{-1}$ and $\mu_\rho = 3.9\text{fm}^{-1}$, and V_{Iso} represents the T=1 two-body matrix elements of the isoscalar Hamiltonian. The strength of each part of the interaction in eq.(2.3.1) is embodied in the coefficients $C^{(k)}$, $P^{(k)}$, $R^{(k)}$, and $A^{(k)}$, which are assumed to depend only on the isospin tensor rank k (note, however, that the condition $C^{(1)}=C^{(2)}$ must be satisfied). $I^{(k)}$ is an isospin operator whose form permits the components $V_{INC}^{(k)}$ to correspond to the T=1 part of the proton-proton ($v^{(pp)}$), neutron-neutron ($v^{(nn)}$), and proton-neutron ($v^{(pn)}$) interactions by

$$V_{INC}^{(1)} = v^{(pp)} - v^{(nn)} + C^{(1)} \frac{e^2}{r}$$

$$V_{INC}^{(2)} = v^{(pp)} + v^{(nn)} - 2v^{(pn)} + C^{(2)} \frac{e^2}{r}.$$

In this work, the two-body matrix elements of the Coulomb and Yukawa-like potentials are evaluated using harmonic-oscillator radial wave functions [Law 80]. These wave functions are used because they are a good approximation to more realistic wave functions, such as those obtained with a Woods-Saxon potential, the separation into center-of-mass and relative coordinates is straightforward, and the variation with mass number A is easily accounted for by the oscillator parameter $\hbar\omega$. Here the matrix elements were evaluated for value A=39, and then multiplied by the scaling factor

$$SF(A) = \left(\frac{\hbar\omega(A)}{\hbar\omega(39)}\right)^{1/2} \qquad (2.3.2)$$

to account for dependence on A. For most nuclei under consideration in this work ($20 \leq A \leq 50$) the oscillator parameter can be approximated by

$$\hbar\omega(A) = 45A^{-1/3} - 25A^{-2/3} \text{MeV}. \qquad (2.3.3)$$

For other nuclei ($A < 20$ and $A > 50$), however, this formula is inadequate, and values of $\hbar\omega$ determined from experimental root mean square (rms) charge radii must be used. The procedure followed to determine $\hbar\omega$ from rms charge radii is outlined by Brown, Chung, and Wildenthal [Bro 80], and a review of the most recent experimental data is given by Brown, Bronk, and Hodgson [Bro 84] and Sherrill [She 85].

Table 2.2

Comparison between experimental and parameterized values of $\hbar\omega$.

A	Exp.	Eq.(2.3.3))	A	Exp.	Eq.(2.3.3)
10	15.408*	15.501	39	10.982	11.173*
11	15.687*	15.179	40	10.760	11.021*
12	15.667*	14.886	41	10.746*	10.948*
13	16.239	14.616	42	10.687	10.877
14	15.194*	14.367	43	10.629[a]	10.808[b]
15	14.740*	14.136	45	10.572*	10.675
22	12.528	12.876*	46	10.516*	10.612
34	11.820	11.508*	53	10.608*	10.208
35	11.310	11.421*	55	10.652*	10.104
36	11.090	11.335*	57	10.559*	10.005
37	11.304	11.253*	59	10.272*	9.910
38	10.982	11.173*			

* Indicates the values of $\hbar\omega$ used in the present work.

[a] This value was used for A=43 for the fit in the 0f-1p shell.

[b] This value was used for A=43 for the fits in the 0d3/2 and 0f7/2 orbits.

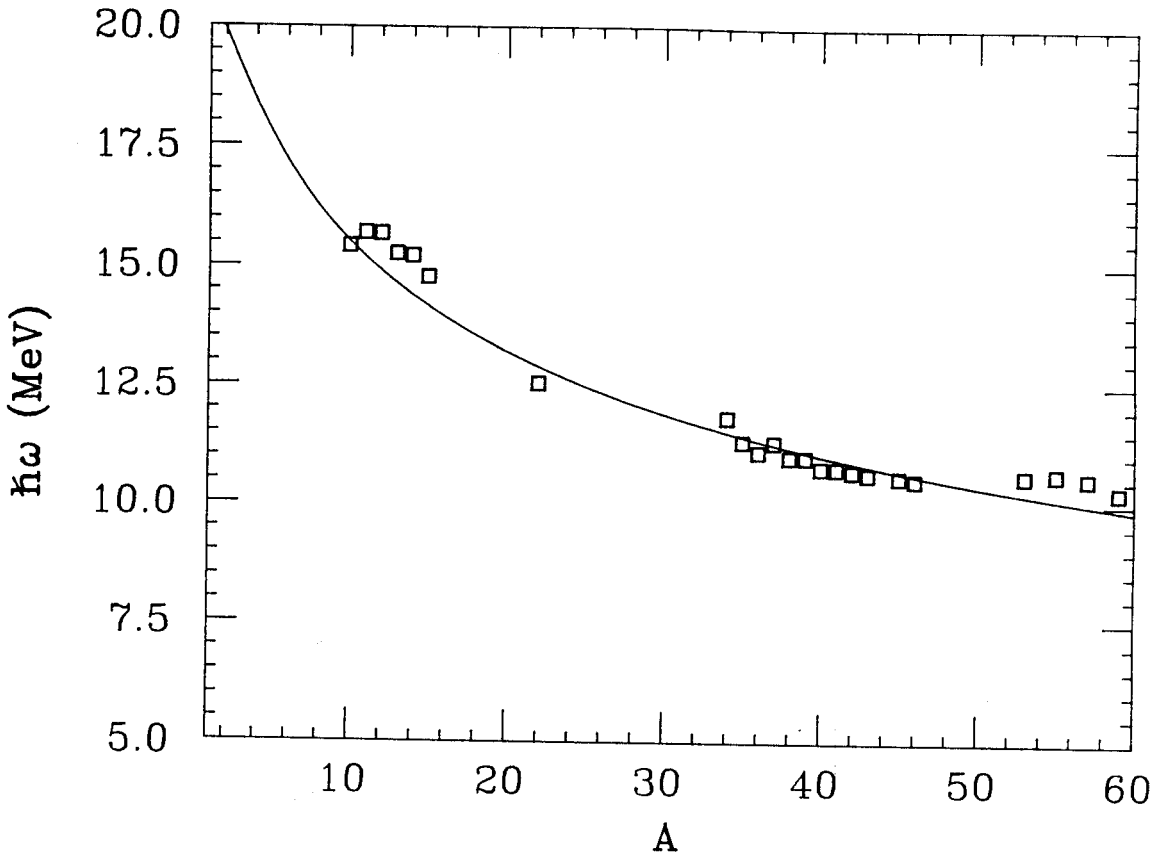

Figure 2.1: Comparison between experimental and parameterized values of $\hbar\omega$ (eq.(2.3.3)). The quantities are also given in Table 2.1.

Values of $\hbar\omega$ determined from experimental rms charge radii and eq.(2.3.3) for the isobaric mass multiplets considered here are listed in Table 2.2, and are shown graphically in Figure 2.1. The values of $\hbar\omega$ used in the present work are also indicated in Table 2.2.

Using eqs.(2.2.4) and (2.2.6) the b- and c-coefficients can be written as a sum of terms depending on the isovector single-particle energies $\varepsilon^{(1)}(\rho)$ and the strength parameters $C^{(k)}$, $P^{(k)}$, $R^{(k)}$, and $A^{(k)}$. Hence, the b- and c-coefficients of the analog states $\psi_A(\nu,J,T)$ $(-T \leq T_Z \leq T)$ can be written as

$$b(A,\nu) = \sum_{\rho} SP^{(1)}(A,\nu,\rho)\ \varepsilon^{(1)}(\rho) + C^{(1)}\gamma^{(1)}(A,\nu,V_C)$$

$$+ P^{(1)}\gamma^{(1)}(A,\nu,V_\pi) + R^{(1)}\gamma^{(1)}(A,\nu,V_\rho) + A^{(1)}\gamma(a,\nu,V_{Iso}), \quad (2.3.3a)$$

$$c(A,\nu) = C^{(2)}\gamma^{(2)}(A,\nu,V_C) + P^{(2)}\gamma^{(2)}(A,\nu,V_\pi) +$$

$$R^{(2)}\gamma^{(2)}(A,\nu,V_\rho) + A^{(2)}\gamma^{(2)}(A,\nu,V_{Iso}), \quad (2.2.3b)$$

where the quantities $SP^{(1)}(\nu,A,\rho)$ and $\gamma^{(k)}(\nu,A,V_\mu)$ are given by

$$SP^{(1)}(A,\nu,\rho) = \frac{SF(A)}{\sqrt{[(2J_i+1)T_i(2T_i+1)(T_i+1)]}}\ OBTD_{A,\nu}(\rho,\rho;1) \quad (2.3.4a)$$

$$\gamma^{(1)}(A,\nu,V_\mu) = \frac{SF(A)}{\sqrt{[(2J_i+1)T_i(2T_i+1)(T_i+1)]}}$$

$$\times \sum_{\text{orbits}} TBTD_{A,\nu}(j_1j_2;J,T=1:j_3j_4:J,T=1;\Delta J=0,k=1)$$

$$\times \langle j_1 j_2; J, T=1 \| \| V_\mu I^{(1)} \| \| j_3 j_4; J, T=1 \rangle_{A=39}, \quad (2.3.4b)$$

$$\gamma^{(2)}(A,\nu,V_\mu) = \frac{SF(A)}{\sqrt{[(2J_i+1)(2T_i-1)(2T_i+1)(T_i+1)(2T_i+3)]}}$$

$$\times \sum_{\text{orbits}} TBTD_{A,\nu}(j_1 j_2; J, T=1 : j_3 j_4; J, T=1; \Delta J=0, k=2)$$

$$\times \langle j_1 j_2; J, T=1 \| \| V_\mu I^{(2)} \| \| j_3 j_4; J, T=1 \rangle_{A=39}. \quad (2.3.4c)$$

The reduced two-body matrix elements in eq.(2.3.4) are given by

$$\langle j_1 j_2; J, T=1 \| \| V_\mu I^{(1)} \| \| j_3 j_4; J, T=1 \rangle = [\tfrac{3}{2}(2J+1)]^{1/2}$$

$$\times \langle j_1 j_2, J | V_\mu | j_3 j_4; J \rangle,$$

$$\langle j_1 j_2; J, T=1 \| \| V_\mu I^{(2)} \| \| j_3 j_4; J, T=1 \rangle = [\tfrac{5}{6}(2J+1)]^{1/2}$$

$$\times \langle j_1 j_2, J | V_\mu | j_3 j_4; J \rangle.$$

The single-particle energies $\varepsilon^{(1)}(\rho)$ and the strength parameters $C^{(k)}$, $P^{(k)}$, $R^{(k)}$, and $A^{(k)}$ can then be determined by performing a least-squares fit to a set of experimental b- and c-coefficients.

2.3a Fit to b-coefficients

In this section, results of the least-squares fit to experimental b-coefficients are presented. Four separate isovector interactions were

determined, and the results are given in Tables 2.3 (0p shell), 2.4 (1s-0d shell), 2.5 (0d3/2 and 0f7/2 orbits), and 2.6 (0f-1p shell). Given in each table are the fitted parameters, the uncertainty of each parameter, and the rms deviation between fitted and experimental values for each fit. The data base for each of the fits was determined from the ground-state binding energies tabulated by Wapstra and Boos [Wap 82] and the excitation energies compiled by Endt and Van Der Leun [End 78] and Ajzenberg-Selove [Ajz 82]. The free parameters were taken to be the isovector single-particle energies, $\varepsilon^{(1)}(\rho)$, for each valence orbit, the the Coulomb strength coefficient $C^{(1)}$ and any one of coefficients $P^{(1)}$, $R^{(1)}$, and $A^{(1)}$. The restriction on the number of parameters was imposed because the experimental data were not sensitive to the determination of more than one parameter of the charge-asymmetric interaction ($v^{(A)} = v^{(pp)} - v^{(nn)}$). In addition, fits to 0f-1p-shell b-coefficients were performed while requiring that $\varepsilon^{(1)}(0f_{7/2}) = \varepsilon^{(1)}(0f_{5/2}) = \varepsilon^{(1)}(0f)$ and $\varepsilon^{(1)}(1p_{3/2}) = \varepsilon^{(1)}(1p_{1/2}) = \varepsilon^{(1)}(1p)$. This last condition was imposed because of the insensitivity of the experimental data to the single-particle energies $\varepsilon^{(1)}(0f_{5/2})$ and $\varepsilon^{(1)}(1p_{1/2})$. This assumption, however, is not unreasonable, as the single-particle energies of the orbits $n\ell j$, $j=\ell-1/2$ and $\ell+1/2$, are identical when evaluated with harmonic-oscillator wave functions.

As can be seen from Tables 2.3, 2.4, 2.5, and 2.6, an optimal fit is obtained for all configuration spaces except the 0p shell by varying the isovector single-particle energies and restricting $C^{(1)}$ to unity and $P^{(1)}$, $R^{(1)}$ and $A^{(1)}$ to zero. Subsequent variations of these parameters do not lead to a significant reduction in either the rms deviation or the parameter uncertainties. For the 0p shell, however, the inclusion of

Table 2.3

Single-particle energies and potential strength parameters obtained from fits to 0p-shell b-coefficients.

$\varepsilon^{(1)}(p_{3/2})$	$\varepsilon^{(1)}(p_{1/2})$	$C^{(1)}$	$P^{(1)}$ (MeV)	$R^{(1)}$ (MeV)	$A^{(1)}$ ($\times 10^{-2}$)	RMS (keV)
0.909(44)	0.887(45)	1.00	-	-	-	73.2
1.001(139)	0.964(111)	0.94(7)	-	-	-	70.3
0.909(131)	0.887(117)	1.00	0.0(5)	-	-	73.2
0.829(71)	0.786(84)	1.00	-	58(42)	-	64.8
0.941(30)	0.804(38)	1.00	-	-	-3.5(1)	44.6
1.052(88)	0.914(71)	0.49(14)	2.9(8)	-	-	41.0
0.052(88)	0.914(71)	0.83(6)	-	122(36)	-	41.0
1.057(82)	0.891(68)	0.93(4)	-	-	-3.6(1)	38.1

Single-particle energies are given in MeV, while potential strengths are defined in eq.(2.3.1) of the text. Uncertainties for each parameter are given in parenthesis. Note that the single-particle energies are appropriate for A=39.

Table 2.4

Single-particle energies and potential strength parameters obtained from fits to 1s-0d-shell b-coefficients.

$\varepsilon^{(1)}(d_{5/2})$	$\varepsilon^{(1)}(s_{1/2})$	$\varepsilon^{(1)}(d_{3/2})$	$C^{(1)}$	$P^{(1)}$ (MeV)	$R^{(1)}$ (MeV)	$A^{(1)}$ ($\times 10^{-2}$)	RMS (keV)
3.325(15)	3.305(16)	3.346(7)	1.00	-	-	-	26.5
3.348(74)	3.445(18)	3.484(12)	0.96(2)	-	-	-	25.0
3.348(81)	3.418(18)	3.454(15)	1.00	-0.2(2)	-	-	25.8
3.323(43)	3.294(17)	3.337(17)	1.00	-	4(18)	-	26.5
3.312(18)	3.291(16)	3.330(11)	1.00	-	-	-0.8(7)	25.8
3.345(80)	3.430(18)	3.473(15)	0.94(4)	0.2(4)	-	-	24.8
3.342(78)	3.426(18)	3.469(15)	0.96(2)	-	11(18)	-	24.8
3.351(78)	3.440(22)	3.476(15)	0.96(2)	-	-	-0.6(7)	24.5

Single-particle energies are given in MeV, while potential strengths are defined in eq.(2.3.1) of the text. Uncertainties for each parameter are given in parenthesis. Note that the single-particle energies are appropriate for A=39.

Table 2.5

Single-particle energies and potential strength parameters obtained from fits to b-coefficients in the $0d_{3/2}$ and $0f_{7/2}$ orbits.

$\varepsilon^{(1)}(d_{3/2})$	$\varepsilon^{(1)}(f_{7/2})$	$C^{(1)}$	$P^{(1)}$ (MeV)	$R^{(1)}$ (MeV)	$A^{(1)}$ ($\times 10^{-2}$)	RMS (keV)
6.262(10)	6.019(13)	1.00	-	-	-	28.8
6.262(20)	6.018(35)	1.00(2)	-	-	-	28.8
6.256(20)	6.008(23)	1.00	0.1(2)	-	-	28.7
6.253(17)	6.006(23)	1.00	-	13(18)	-	29.1
6.254(11)	6.015(13)	1.00	-	-	-1.6(10)	30.5
6.250(20)	6.013(35)	0.93(7)	0.5(6)	-	-	31.3
6.259(21)	6.022(35)	0.98(3)	-	23(25)	-	31.2
6.247(22)	6.003(35)	1.01(2)	-	-	-1.7(11)	29.4

Single-particle energies are given in MeV, while potential strengths are defined in eq.(2.3.1) of the text. Uncertainties for each parameter are given in parenthesis. Note that the single-particle energies are appropriate for A=39.

Table 2.6

Single-particle energies and potential strength parameters obtained from fits to 0f-1p-shell b-coefficients.

$\varepsilon^{(1)}(f)$	$\varepsilon^{(1)}(p)$	$C^{(1)}$	$P^{(1)}$ (MeV)	$R^{(1)}$ (MeV)	$A^{(1)}$ ($\times 10^{-2}$)	RMS (keV)
7.460(10)	7.200(84)	1.00	-	-	-	30.5
7.454(13)	7.176(92)	1.01(1)	-	-	-	29.7
7.454(14)	7.175(95)	1.00	0.1(1)	-	-	29.7
7.462(17)	7.210(99)	1.00	-	-4(2)	-	30.7
7.467(18)	7.209(89)	1.00	-	-	0.6(13)	31.0
7.461(18)	7.199(105)	1.04(6)	-0.4(7)	-	-	30.5
7.464(17)	7.202(98)	1.02(2)	-	-25(29)	-	30.6
7.460(21)	7.184(99)	1.01(1)	-	-	0.5(13)	30.2

Single-particle energies are given in MeV, while potential strengths are defined in eq.(2.3.1) of the text. Uncertainties for each parameter are given in parenthesis. Note that the single-particle energies are appropriate for A=39.

Table 2.7

Parameters for the "best" isovector interaction for each configuration shell-model space.

0p Shell

$\varepsilon^{(1)}(p_{3/2})$	$\varepsilon^{(1)}(p_{1/2})$	$C^{(1)}$	$P^{(1)}$	$R^{(1)}$	$A^{(1)}$
1.057(82)	0.891(67)	0.93(4)	0.0	0.0	-3.6(1)

1s-0d Shell

$\varepsilon^{(1)}(d_{5/2})$	$\varepsilon^{(1)}(s_{1/2})$	$\varepsilon^{(1)}(d_{3/2})$	$C^{(1)}$	$P^{(1)}$	$R^{(1)}$	$A^{(1)}$
3.325(15)	3.305(16)	3.346(7)	1.00	0.0	0.0	0.0

$0d_{3/2}$ and $0f_{7/2}$ orbits

$\varepsilon^{(1)}(d_{3/2})$	$\varepsilon^{(1)}(f_{7/2})$	$C^{(1)}$	$P^{(1)}$	$R^{(1)}$	$A^{(1)}$
6.262(10)	6.019(13)	1.00	0.0	0.0	0.0

0f-1p Shell

$\varepsilon^{(1)}(f)$	$\varepsilon^{(1)}(p)$	$C^{(1)}$	$P^{(1)}$	$R^{(1)}$	$A^{(1)}$
7.460(10)	7.200(84)	1.00	0.0	0.0	0.0

The parameters are given in the same units as they appear in Tables 2.3 (0p shell), 2.4 (1s-0d shell), 2.5 ($d_{3/2}$ and $0f_{7/2}$ orbits), and 2.6 (0f-1p shell).

Table 2.8

Comparison between fitted b-coefficients and experimental values for 0p-shell nuclei.

A	J^π	T	b (exp) (MeV)	b (fit) (MeV)
10	0^+	1	2.329(2)	2.306
11	$1/2^-$	1/2	2.640(2)	2.682
	$3/2^-$	1/2	2.765(2)	2.724
12	1^+	1	2.767(1)	2.795
	2^+	1	2.770(1)	2.787
13	$1/2^-$	1/2	3.003(2)	2.951
	$3/2^-$	1/2	2.829(2)	2.894
14	0^+	1	3.276(4)	3.228
15	$1/2^-$	1/2	3.536(1)	3.550
	$3/2^-$	1/2	3.388(10)	3.387

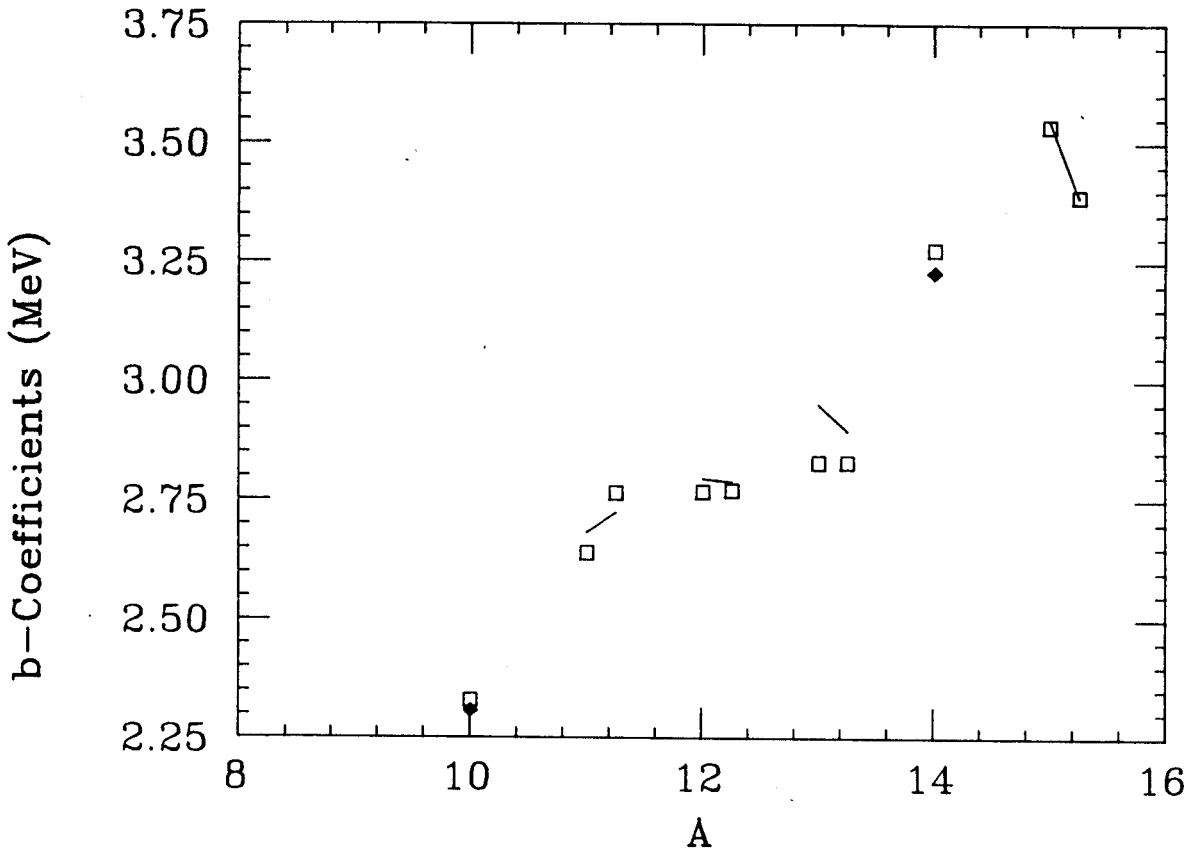

Figure 2.2: Plot of 0p-shell b-coefficients. Experimental data are represented by open boxes, while the fitted values are given by the line and the solid diamonds. The coefficients are plotted in the same order as they appear in Table 2.8.

Table 2.9

Comparison between fitted b-coefficients and experimental values for 1s-0d-shell nuclei.

A	J^{π}	T	b (exp) (MeV)	b (fit) (MeV)
22	0^+_+	1	4.597(2)	4.593
	2^+_+	1	4.583(2)	4.586
	4^+_+	1	4.573(10)	4.587
	2^+	1	4.571(10)	4.584
34	0^+_+	1	6.559(1)	6.546
	2^+_+	1	6.541(1)	6.525
	2^+_+	1	6.551(2)	6.533
	0^+	1	6.537(2)	6.521
35	$3/2^+_+$	1/2	6.747(2)	6.736
	$1/2^+_+$	1/2	6.712(2)	6.677
	$5/2^+_+$	1/2	6.734(2)	6.716
	$3/2^+_+$	1/2	6.654(2)	6.673
	$5/2^+_+$	1/2	6.727(3)	6.659
	$1/2^+_+$	1/2	6.664(2)	6.661
	$3/2^+$	3/2	6.666(10)	6.673
36	2^+_+	1	6.830(4)	6.832
	3^+_+	1	6.836(7)	6.833
	1^+	1	6.806(7)	6.821
	0^+	2	6.827(13)	6.837
37	$3/2^+_+$	1/2	6.931(1)	6.924
	$1/2^+_+$	1/2	6.890(10)	6.929
	$5/2^+_+$	1/2	6.884(10)	6.966
	$3/2^+_+$	3/2	6.983(10)	6.997
	$1/2^+$	3/2	6.947(12)	6.969
38	0^+_+	1	7.109(5)	7.116
	2^+	1	7.129(6)	7.159
39	$3/2^+_+$	1/2	7.313(4)	7.317
	$1/2^+$	1/2	7.257(4)	7.292

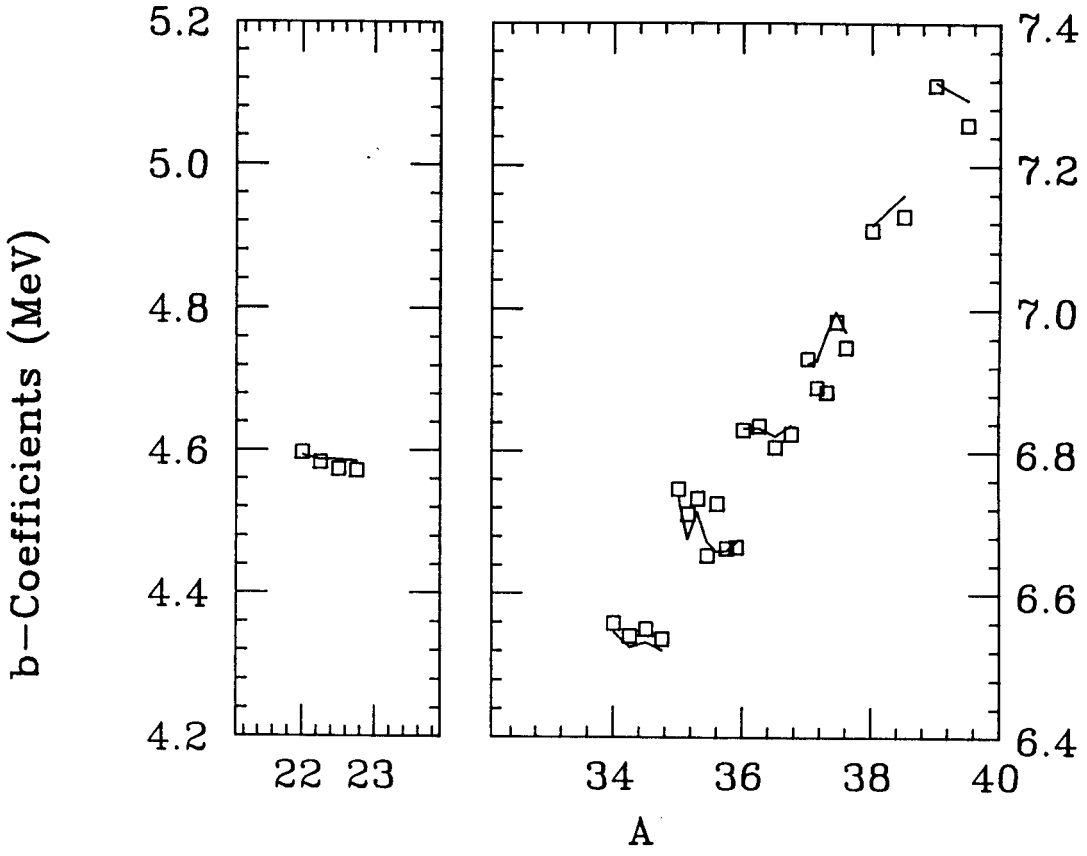

Figure 2.3: Plot of 1s-0d-shell b-coefficients. Experimental data are represented by open boxes, while the fitted values are given by the line. The coefficients are plotted in the same order as they appear in Table 2.9.

Table 2.10

Comparison between fitted b-coefficients and experimental values for nuclei in the $0d_{3/2}$ and $0f_{7/2}$ orbits.

A	J^{π}	T	b (exp) (MeV)	b (fit) (MeV)
36	2^+_+	1	6.830(4)	6.838
	3^+_+	1	6.836(7)	6.837
	1^+	1	6.806(7)	6.825
37	$3/2^+$	1/2	6.931(1)	6.945
38	0^+_+	1	7.109(5)	7.103
	2^+_+	1	7.129(6)	7.141
	0^+_+	1	6.951(6)	6.962
	2^+	1	6.989(6)	6.933
39	$3/2^+_-$	1/2	7.313(4)	7.284
	$3/2^-_-$	1/2	7.318(4)	7.286
	$7/2^-$	1/2	7.295(4)	7.300
40	2^-_-	1	7.272(5)	7.311
	4^-_-	1	7.286(6)	7.313
	5^-	1	7.289(6)	7.310
41	$7/2^-$	1/2	7.278(4)	7.321
43	$7/2^-$	1/2	7.644(4)	7.631
53	$7/2^-$	1/2	9.086(18)	9.060

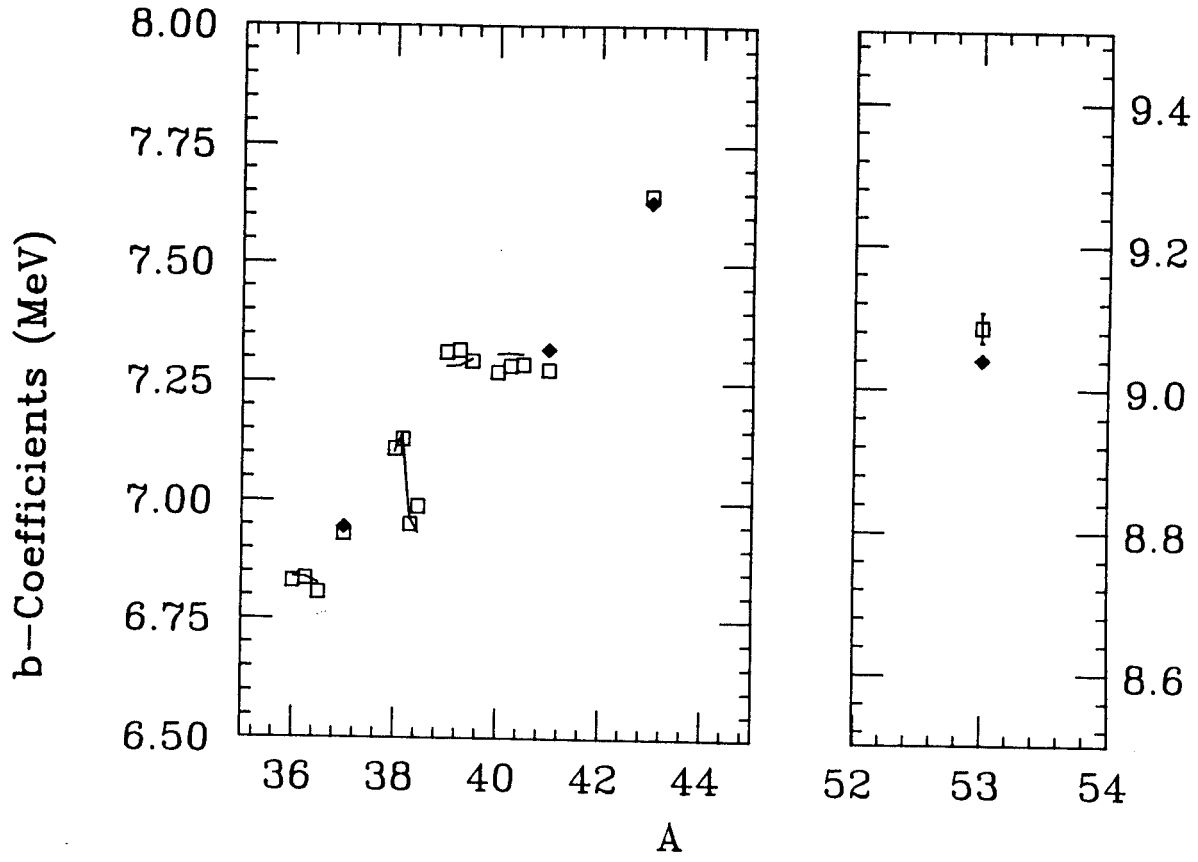

Figure 2.4: Plot of $0d_{3/2}$-$0f_{7/2}$-orbit b-coefficients. Experimental data are represented by open boxes, while the fitted values are given by the line and the solid diamonds. The coefficients are plotted in the same order as they appear in Table 2.10.

Table 2.11

Comparison between fitted b-coefficients and experimental values of 1p-shell nuclei.

A	J^{π}	T	b (exp) (MeV)	b (fit) (MeV)
42	0^+	1	7.495(4)	7.515
	2^+	1	7.510(7)	7.484
	4^+	1	7.457(7)	7.474
	6^+	1	7.421(7)	7.473
43	$7/2^-$	1/2	7.644(1)	7.667
45	$7/2^-$	1/2	7.902(27)	7.900
	$3/2^-$	1/2	7.929(27)	7.875
46	0^+	1	8.113(13)	8.057
53	$7/2^-$	1/2	9.086(18)	9.082
55	$7/2^-$	1/2	9.473(10)	9.462
57	$3/2^-$	1/2	9.510(50)	9.530
59	$3/2^-$	1/2	9.882(40)	9.877

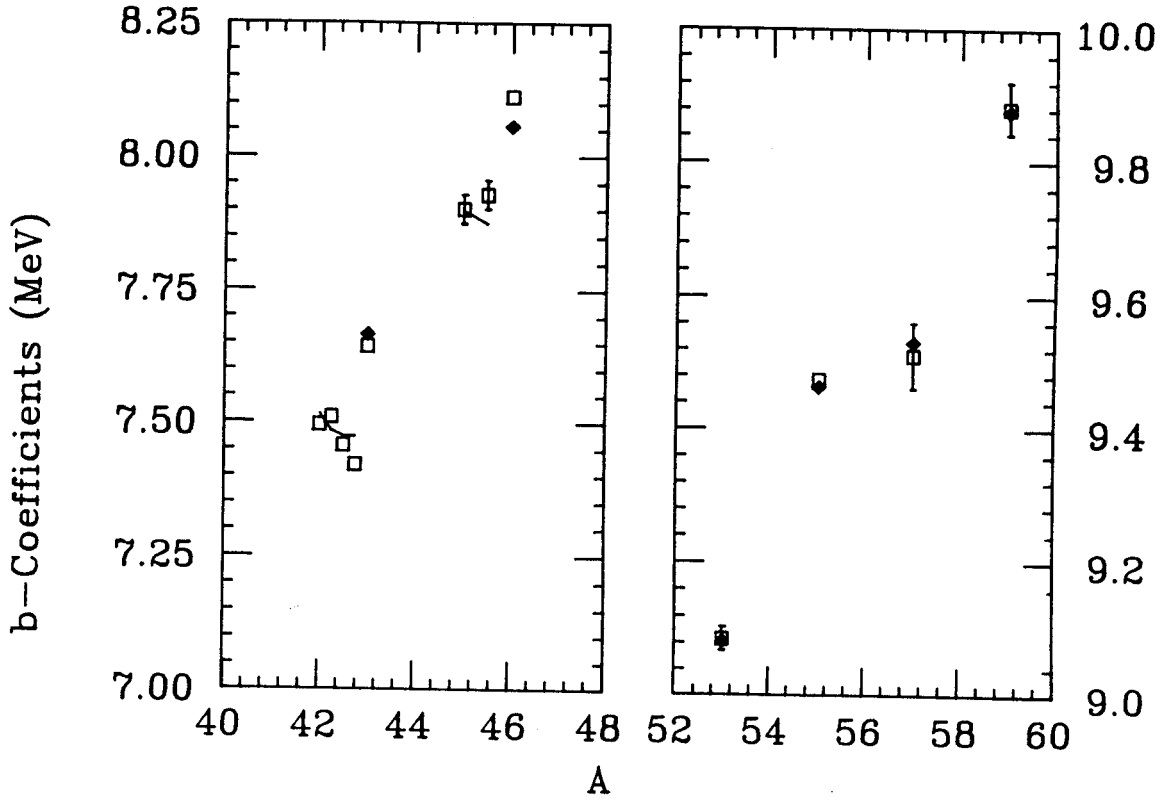

Figure 2.5: Plot of 0f-1p-shell b-coefficients. Experimental data are represented by open boxes, while the fitted values are given by the line and the solid diamonds. The coefficients are plotted in the same order as they appear in Table 2.11.

a two-body charge-asymmetric interaction proportional to the isoscalar two-body matrix elements is necessary to improve the rms deviation of the fit. The "best" set of parameters for each isovector interaction studied is given in Table 2.7. Experimental b-coefficients and those obtained with these isovector interactions are presented in Tables 2.8 (0p shell), 2.9 (1s-0d shell), 2.10 (0d3/2 and 0f7/2 orbits), and 2.11 (0f-1p shell), and are shown graphically in Figures 2.2, 2.3, 2.4, and 2.5.

As can be seen from the figures, the results of the fits are generally good. There are, however, a few salient features which must be pointed out. The fitted isovector single-particle energies extrapolated to A=17 (1s-0d shell) are $\varepsilon^{(1)}_{fit}(0d_{5/2})$ = 3.697 MeV, $\varepsilon^{(1)}_{fit}(1s_{1/2})$ = 3.674 MeV, and $\varepsilon^{(1)}_{fit}(0d_{3/2})$ = 3.721 MeV. These are not in good agreement with the experimental values of 3.543 MeV, 3.168 MeV, and 3.561 MeV, respectively, determined from ^{17}F and ^{17}O [Wap 82 and Ajz 82]. The tendency for the experimental values to be smaller than those needed for the upper sd shell is most likely due to the fact that these levels are loosely bound relative to ^{17}O (unbound in the case of the $0d_{3/2}$ orbit in ^{17}F), and, therefore, have a larger rms radius and a smaller Coulomb energy. This effect is particularly large for the $0s_{1/2}$ orbit because of the absence of a centrifugal barrier.

Another feature of the 1s-0d shell fits is that better results were obtained using values of $\hbar\omega$ given by eq.(2.3.3) than with the experimental values shown in Table 2.2. The parameters of the isovector interaction were also determined using the experimental values shown in Table 2.2. The rms deviation of these fits, however, were generally 20 keV greater than those obtained using $\hbar\omega$ given by eq.(2.3.3). The cause

of this discrepancy is not understood, but since the parameterization of $\hbar\omega$ gives generally better results, it is assumed that this procedure leads to a better determination of $V_{INC}^{(1)}$ in the 1s-0d shell. A comparison between fits using experimental and parameterized values of $\hbar\omega$ in the $0d_{3/2}$ and $0f_{7/2}$ orbits was not performed, but good results were obtained using the parameterized values. It should be remarked, however, that the fits in the 1s-0d shell and the $0d_{3/2}$ and $0f_{7/2}$ orbits are in stark contrast with those in the 0p and 0f-1p shells, where experimental values were essential in order to reduce the rms deviations.

The somewhat larger rms deviation of the fit in the 0p shell is most likely due to limitations of the configuration space and the loosely bound nature of these light nuclei. There is strong experimental evidence (low lying J=1/2 and 5/2 positive parity states in odd-A nuclei) which indicates that the $1s_{1/2}$ and $0d_{5/2}$ orbits contribute significantly to the structure of nuclei in this mass region ($12 \leq A \leq 16$). At present, however, there is no reliable isoscalar interaction which accounts for configurations due to both the 0p and 1s-0d shells (the interaction of Zucker, Buck, and McGory (ZBM) [Zuc 69a and Zuc 69b] allows excitations into the $1s_{1/2}$ and $0d_{5/2}$ orbits, but excludes particle-hole excitations of the $0p_{3/2}$ orbit). An additional feature of these light nuclei is that they are rather loosely bound to particle breakup, indicating that particle clustering effects are important. This shows that perhaps some correction to the matrix elements evaluated with harmonic-oscillator wave functions is needed.

In all but the 0p shell the fits do not give a strong indication that a charge-asymmetric interaction is necessary. The importance of the charge-asymmetric interaction in the 0p shell, however, can be partly

interpreted as being an effect due to differences between proton and neutron radial wave functions (radial-wave-function (RWF) correction). Coulomb repulsion tends to push proton radial wave functions out relative to neutrons, and therefore, matrix elements of $v^{(pp)}$ will differ from those of $v^{(nn)}$ even if $v^{(pp)} = v^{(nn)}$. This effect can be particularly important for light nuclei because of their loosely bound nature. Lawson [Law 79] has estimated the RWF corrections for the 0p shell by assuming that the Cohen-Kurath two-body matrix elements are effected in the same manner as a δ-function potential. With this assumption he finds that the two-body matrix element $\langle(0p3/2)^2;J=0|\ V\ |(0p3/2)^2;J=0\rangle$ for the neutron-neutron system is 5.6% larger than that for the proton-proton system. The value of 3.6% obtained with the fitting procedure is not inconsistent with the results of Lawson. Unfortunately, however, it is impossible to determine how much of this 3.6% correction is due to the RWF correction or the presence of a charge-asymmetric two-body interaction. With this, and the results of Lawson in mind, the charge asymmetric potential obtained for the 0p shell is taken to be due to the RWF correction.

Recently, effects of the radial-wave-function correction have also been estimated for 1s-0d-shell nuclei by Sagawa [Sag 85], using wave functions obtained from a self consistent Hartree-Fock calculation which utilizes a Skyrme-type interaction (a description of this type of Hartree-Fock calculation is given in Chapter Three, section 3). RWF correction effects on the 1s-0d-shell two-body matrix elements are smaller than in the 0p shell, being typically 1% or less. To determine the effect on the previous fits to 1s-0d-shell b-coefficients, the components of $V_{INC}^{(1)}$ were redetermined while including the estimates of

Table 2.12

Single-particle energies and potential strength parameters obtained from fits to 1s-0d-shell b-coefficients while including the RWF correction to the b-coefficients.

$\varepsilon^{(1)}(d_{5/2})$	$\varepsilon^{(1)}(s_{1/2})$	$\varepsilon^{(1)}(d_{3/2})$	$C^{(1)}$	$P^{(1)}$ (MeV)	$R^{(1)}$ (MeV)	$A^{(1)}$ ($\times 10^{-2}$)	RMS (keV)
3.315(17)	3.100(19)	3.168(8)	1.00	-	-	-	29.5
3.359(73)	3.387(17)	3.450(11)	0.92(2)	-	-	-	23.9
3.356(90)	3.304(20)	3.462(16)	1.00	-0.5(2)	-	-	27.4
3.300(49)	3.046(19)	3.122(16)	1.00	-	20(21)	-	29.0
3.287(20)	3.070(18)	3.132(12)	1.00	-	-	-1.8(7)	26.6
3.354(74)	3.339(17)	3.411(13)	0.85(4)	0.7(4)	-	-	22.1
3.340(70)	3.324(16)	3.404(14)	0.91(2)	-	36(16)	-	21.7
3.320(70)	3.325(16)	3.483(14)	0.93(2)	-	-	-1.5(6)	21.4

Single-particle energies are given in MeV, while potential strengths are defined in eq.(2.3.1) of the text. Uncertainties for each parameter are given in parenthesis. Note that the single-particle energies are appropriate for A=39.

Sagawa. The results of these fits are given in Table 2.12, where it is seen that an optimal fit was obtained by renormalizing the Coulomb strength to 0.93, and including a charge asymmetric interaction equal to $-1.5 \times 10^{-2} V_{Iso}$. This is consistent with the results of Negele [Neg 71], Sato [Sat 76], and Shlomo [Shl 78], where it was found that a small (approximately -1%) phenomenological nuclear charge-asymmetric interaction could account for at least part of the Nolen-Schiffer anomaly. It should be pointed out, however, that at present, there is no theoretical model for a charge-asymmetric interaction which can account for the Nolen-Schiffer anomaly. A recent experiment by Winfield et al. [Win 85] also indicates that the nucleon-nucleon interaction between neutrons is slightly more attractive than it is for protons. Their results, however, do not rule out the possibility that $v^{(pp)}$ is equal to $v^{(nn)}$. In addition, these studies are not contradicted by free nucleon-nucleon scattering data. The nucleon scattering lengths are: $a^{(pn)}$ = -23.715±0.015 fm [Hen 79], $a^{(nn)}$ = -18.6±0.5 fm [Gab 81], and $a^{(pp)}$ = -17.1±1.0 fm (corrected for electromagnetic effects; the error reflects the uncertainty in this correction) [Hen 73]. The change in the potential ΔV is related to change in the scattering length, Δa, for Yukawa potentials by [Hen 69]

$$\frac{\Delta a}{a} \approx 14 \frac{\Delta V}{V}.$$

Using this relation, the proton-proton and neutron-neutron scattering lengths indicate that the $v^{(nn)}$ is 0.6±0.4% times more attractive than $v^{(pp)}$.

The choice as to which isovector interaction to use in the 1s-0d shell is somewhat arbitrary, and must be checked. The calculations in the present work were performed using the interaction given by the parameters in Table 2.11. This is because the RWF corrections of Sagawa are rather recent and that the 1s-0d-shell calculations reported here are quite time consuming. Therefore, rather than re-performing all the calculations reported here, a comparison is made between results obtained using both interactions for a simple case. This comparison then gives some indication of the uncertainty that is caused by the two alternative isovector interactions.

A final feature of the fits is that in some cases a renormalization of the Coulomb strength is needed in order to reduce the rms deviation between fitted and experimental values. Renormalizing the Coulomb strength, however, is not unreasonable, as a number of corrections are expected. These are primarily due to neglecting short range correlations, higher order Coulomb effects ($(v/c)^2$ corrections to the Coulomb interaction and vacuum polarization), and the fact that harmonic-oscillator wave functions were used. It should be kept in mind, however, the strengths of the isovector and isotensor parts of the Coulomb interaction must be the same.

2.3b Fit to c-coefficients

In this section, results of the least-squares fit to experimental c-coefficients for 0p- and 1s-0d-shell nuclei are presented. Fits to nuclei in the $0d_{3/2}$-$0f_{7/2}$ orbits and the 0f-1p shell were not performed because there is very little experimental data in this region. There is,

however, evidence [Hen 69] that the isotensor interaction can be accurately approximated by

$$V_{INC}^{(2)} = V_C + (-4 \times 10^{-2})\, V_{Iso}. \qquad (2.3b.1)$$

Note if $v^{(pp)} = v^{(nn)}$, this parameterization is equivalent to increasing the T=1 proton-neutron matrix elements by 2%. With this in mind, a fit to 0p and 1s-0d shell c-coefficients is made to test whether eq.(2.3b.1) can be applied to $0d_{3/2}$-$0f_{7/2}$-orbit and the 0f-1p-shell nuclei.

The data base for the fits was again determined from the ground state masses tabulated by Wapstra and Boos [Wap 82] and the excitation energies compiled by Endt and Van Der Leun [End 78] and Ajzenberg-Selove [Ajz 82]. The free parameters were the Coulomb strength coefficient $C^{(2)}$ and any one of coefficients $P^{(2)}$, $R^{(2)}$, and $A^{(2)}$. This restriction was imposed because, as in the case of the b-coefficients, the experimental data were not sensitive to the determination of more than one parameter of the nuclear charge-dependent interaction ($v^{(CD)} = v^{(pp)} + v^{(nn)} - 2\, v^{(pn)}$). Results of the fits are given in Tables 2.13 (0p shell) and 2.14 (1s-0d shell), where it is seen that a charge-dependent interaction is necessary in order to reduce the rms deviation between fitted and experimental values. Clearly, the results of the 1s-0d-shell fits support the parameterization of $V_{INC}^{(2)}$ given by eq.(2.3b.1), while those of the 0p shell do not. It should be noted, however, that the results in the 0p shell are not expected to be as good as those in the 1s-0d shell because of model-space limitations and the loosely bound nature of these nuclei. These effects, however, are not as strong as they are in the case for the b-coefficients because c-coefficients are

Table 2.13

Fitted parameters obtained from fits to 0p-shell c-coefficients.

$C^{(2)}$	$P^{(2)}$ (MeV)	$R^{(2)}$ (MeV)	$A^{(2)}$ ($\times 10^{-2}$)	RMS (keV)
1.00	-	-	-	27.5
1.06(4)	-	-	-	24.5
1.00	0.4(1)	-	-	20.1
1.00	-	36(8)	-	14.1
1.00	-	-	-1.5(2)	10.8
0.75(5)	1.4(2)	-	-	8.3
0.92(3)	-	60(9)	-	8.3
0.98(2)	-	-	-1.6(3)	10.3

Strengths are defined in eq.(4.3.1) of the text. Uncertainties for each parameter are given in parenthesis.

Table 2.14

Fitted parameters obtained from fits to 1s-0d-shell c-coefficients.

$C^{(2)}$	$P^{(2)}$ (MeV)	$R^{(2)}$ (MeV)	$A^{(2)}$ ($\times 10^{-2}$)	RMS (keV)
1.00	-	-	-	35.0
1.17(3)	-	-	-	20.1
1.00	1.05(8)	-	-	12.8
1.00	-	78(4)	-	8.2
1.00	-	-	-4.2(2)	7.0
0.82(4)	2.0(2)	-	-	8.2
0.99(2)	-	81(9)	-	8.1
1.00(2)	-	-	-4.1(3)	7.0

Strengths are defined in eq.(4.3.1) of the text. Uncertainties for each parameter are given in parenthesis.

Table 2.15

Parameters of the best isotensor interaction for each configuration shell-model space.

Configuration space	$C^{(2)}$	$P^{(2)}$ (MeV)	$R^{(2)}$ (MeV)	$A^{(2)}$ ($\times 10^{-2}$)
0p Shell	0.93(3)	0.0	60(9)	0.0
1s-0d Shell	1.00	0.0	78(4)	0.0
$0d_{3/2}$-$0f_{7/2}$ orbits	1.00	0.0	0.0	-4.0
0f-1p Shell	1.00	0.0	0.0	-4.0

The strength coefficients are defined in eq.(4.3.1) of the text.

Table 2.16

Comparison between fitted c-coefficients and experimental values for 0p-shell nuclei.

A	J^{π}	T	c (exp) (keV)	c (fit) (keV)
10	0^+	1	363(2)	369
12	1^+	1	244(2)	232
	2^+	1	203(2)	209
13	$3/2^-$	3/2	258(10)	266
14	0^+	1	337(4)	325
	2^+	1	264(7)	265

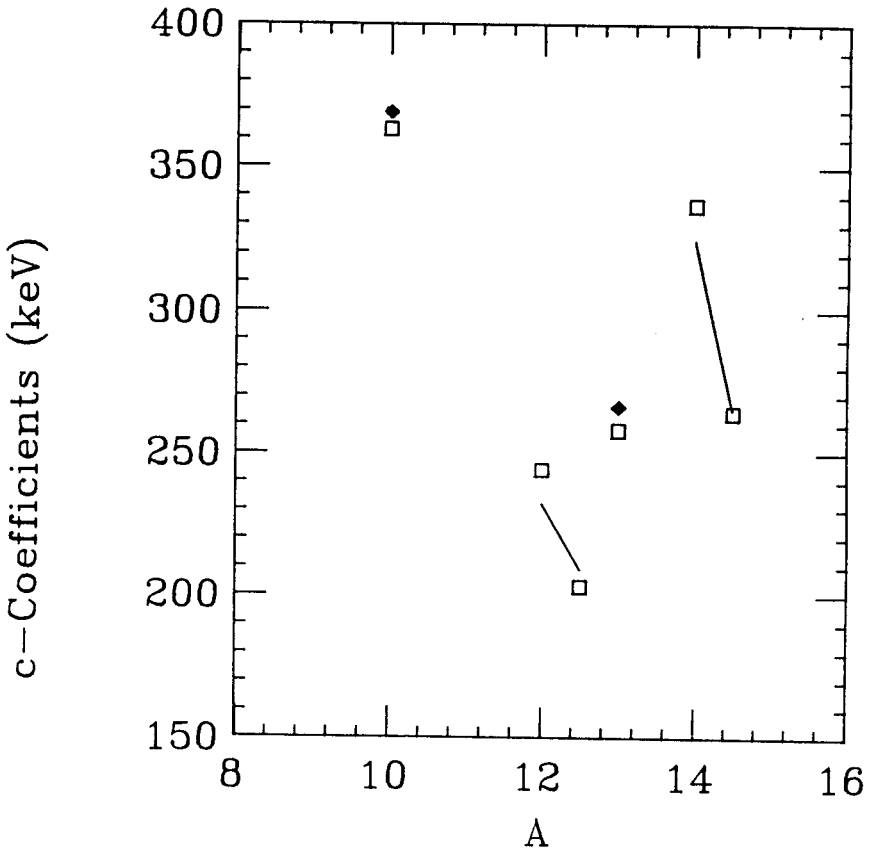

Figure 2.6: Plot of 0p-shell c-coefficients. Experimental data are represented by open boxes, while the fitted values are given by the line and the solid diamonds. The coefficients are plotted in the same order as they appear in Table 2.16.

Table 2.17

Comparison between fitted c-coefficients and experimental values for 1s-0d-shell nuclei.

A	J^{π}	T	c (exp) (keV)	c (fit) (keV)
22	0^+_+	1	316(2)	315
	2^+_+	1	282(2)	272
	4^+_+	1	235(10)	226
	2^+	1	231(10)	228
34	0^+_+	1	284(2)	282
	2^+_+	1	235(2)	228
	2^+_+	1	196(2)	197
	0^+	1	235(2)	252
35	$3/2^+$	3/2	214(10)	204
36	2^+_+	1	146(4)	145
	3^+_+	1	214(7)	229
	1^+_+	1	188(7)	199
	0^+	2	201(13)	204
37	$3/2^+_+$	3/2	196(10)	204
	$1/2^+$	3/2	210(14)	218
38	0^+_+	1	285(5)	282
	2^+	1	199(6)	198

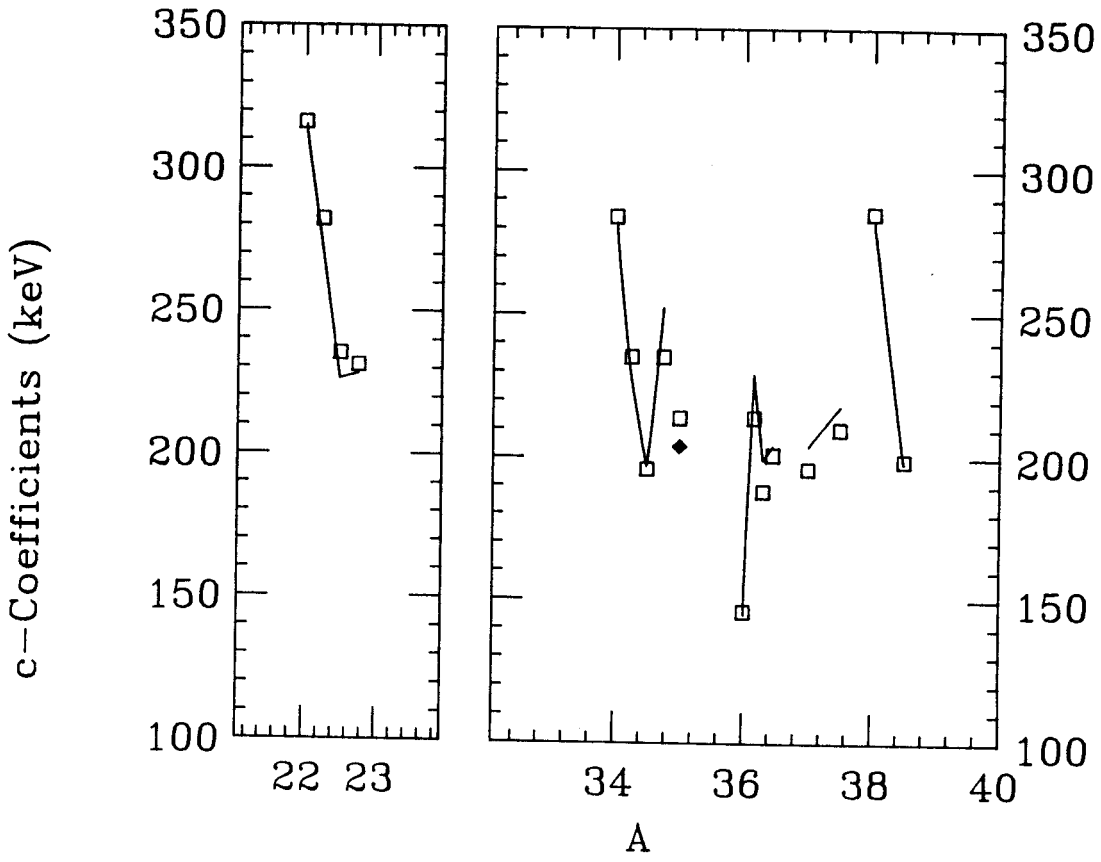

Figure 2.7: Plot of 1s-0d-shell c-coefficients. Experimental data are represented by open boxes, while the fitted values are given by the line. The coefficients are plotted in the same order as they appear in Table 2.17.

less effected by the differences in the radial wave functions. Heavier nuclei ($22 \leq A \leq 60$), on the other hand, are not as sensitive to model space limitations and are not as loosely bound. Therefore, the results obtained in the 1s-0d shell are expected to be typical for the $0d_{3/2}$ and $1f_{7/2}$ orbits and the 0f-1p shell.

The "best" parameter set for each isotensor interaction is listed in Table 2.15, while a comparison between experimental values and those obtained with these interactions for 0p and 1s-0d shell nuclei is given in Tables 2.16 and 2.17 and Figures 2.6 and 2.7, respectively. Note that since $C^{(1)}$ must equal $C^{(2)}$ the values $C^{(1)} = C^{(2)} = 0.93$ are chosen.

2.4 The Total Hamiltonian

Once the isovector and isotensor components of H have been determined the total Hamiltonian is obtained by inverting eq.(1.1.8). The T=1 part of the proton-proton, neutron-neutron, and proton-neutron matrix elements is given by

$$h^{(pp)}_{ijkl} = v^{(0)}_{ijkl}(T=1) + \frac{1}{2} v^{(1)}_{ijkl} + \frac{1}{6} v^{(2)}_{ijkl}, \qquad (2.4.1a)$$

$$h^{(nn)}_{ijkl} = v^{(0)}_{ijkl}(T=1) - \frac{1}{2} v^{(1)}_{ijkl} + \frac{1}{6} v^{(2)}_{ijkl}, \qquad (2.4.1b)$$

$$h^{(pn)}_{ijkl}(T=1) = v^{(0)}_{ijkl}(T=1) - \frac{1}{3} v^{(2)}_{ijkl}, \qquad (2.4.1c)$$

where the subscript ijkl represents the antisymmetric two-body matrix element $\langle j(i),j(j);J| V |j(k),j(l);J\rangle$, and $v^{(0)}_{ijkl}(T=1)$ represents the T=1 two-body matrix elements of the isoscalar Hamiltonian. The total proton-neutron two-body matrix elements are given by

$$\langle j_p(i), j_n(j); J | \; h^{(pn)} \; | j_p(k), j_n(l); J \rangle =$$

$$\{(1-(-1)^{J+1}\delta_{j_1 j_2})^2 + (1+(-1)^J\delta_{j_1 j_2})^2\}^{-1/2}$$

$$\times \{(1-(-1)^{J+1}\delta_{j_3 j_4})^2 + (1+(-1)^J\delta_{j_1 j_2})^2\}^{-1/2}$$

$$\times [(1-(-1)^{J+1}\delta_{j_1 j_2})(1-(-1)^{J+1}\delta_{j_3 j_4})\; h^{(pn)}_{ijkl}(T=1)$$

$$+ \; (1+(-1)^J\delta_{j_1 j_2})(1+(-1)^J\delta_{j_3 j_4})\; v^{(0)}_{ijkl}(T=0)] \qquad (2.4.2)$$

where $v^{(0)}(T=0)$ represents the T=0 two-body matrix elements of the isoscalar Hamiltonian. Note the that terms $(1-(-1)^{J+1}\delta_{jj'})$ and $(1+(-1)^J\delta_{jj'})$ are due to the Pauli exclusion principle. The proton and neutron single-particle energies are

$$\varepsilon^{(p)} = \varepsilon^{(0)} + \frac{1}{2}\varepsilon^{(1)}, \qquad (2.4.3a)$$

$$\varepsilon^{(n)} = \varepsilon^{(0)} - \frac{1}{2}\varepsilon^{(1)}. \qquad (2.4.3b)$$

From the total Hamiltonian, determined from the procedure outlined by eqs.(2.4.1), (2.4.2), (2.4.3), one obtains the states $\psi_A(\nu, J, T_Z)$ which have mixed isospin and eigenenergies which can be very accurately parameterized by eq.(1.2.1). With these isospin-mixed wave functions it is then possible to make predictions as to the extent of isospin-symmetry violation in nuclei.

Chapter Three

3.1 Introduction

In this chapter, corrections to the Fermi matrix element for superallowed β-transitions due to isospin impurities are investigated. The important feature of these decays is that once all nucleus dependent corrections have been applied to the experimental ft values, these quantities should be constant and given by

$$ft = \frac{K}{2G_V^2}, \qquad (3.1.1)$$

where $K = 2\pi^3 \ln 2 \hbar^7 c^6/(mc^2)^5$, and G_V is the effective vector coupling constant for nucleon β-decay. Although many superallowed transitions have been observed experimentally, at present, ft values for only eight transitions have been measured with sufficient accuracy to permit a test of eq.(3.1.1). For this reason, this work concentrates on corrections for the ground state β-decay of ^{14}O, ^{34}Cl, ^{42}Sc, ^{46}V, ^{50}Mn, and ^{54}Co and the decay of the metastable state in ^{26}Al and ^{38}K.

As was mentioned in the first chapter, there are two classes of corrections which must be evaluated within the frame work of the nuclear shell model. The first arises because the isospin-nonconserving (INC) force mixes states of different isospin which are contained within the shell-model configuration space. The second is due to mixing with states which lie outside the range of the configuration space. The effects of this last type of isospin mixing is to change proton radial wave functions relative to neutrons. These corrections have been evaluated

previously by Towner, Hardy, and Harvey [Tow 73, Har 75, and Tow 77], and have failed to yield constant ft values for the eight transitions mentioned above. There have been many improvements, however, in nuclear models since these first calculations, and therefore it is prudent to re-evaluate these corrections, making use of these recent advances in our understanding of nuclear structure. Perhaps the most important improvement in regards to this problem are radial wave functions obtained from a self-consistent Hartree-Fock calculation utilizing a Skyrme-type interaction. In addition, revised isoscalar Hamiltonians and an INC interaction which reproduces experimental isotopic mass shifts (Chapter Two) are used in this work.

In the second section of this chapter, the matrix element of the Fermi operator is derived within the formalism of the nuclear shell model, taking into account the two corrections mentioned above. In the third section, values of the correction due to the difference in the radial wave functions are presented, while those due to configuration-space mixing are presented in the fourth section. A comparison between values obtained in the present work with those evaluated previously [Tow 73, Har 75, and Tow 77] is given in the fifth section. Finally, in the sixth section, the implications of the corrections evaluated here on eq.(3.1.1) are given.

3.2 Corrections to the Fermi Matrix Element, δ_C

The starting point of a shell-model calculation of the Fermi matrix element are the states $\Psi_A(\Gamma,J,T_Z)$, which are eigenstates of the total Hamiltonian, that is $[H^{(0)} + V_{INC}^{(1)} + V_{INC}^{(2)}]\ \Psi_A(i) = E(i)\Psi_A(i)$. Within the

frame work of the nuclear shell model, the Fermi matrix element for the positron decay of the state $\Psi_A(\Gamma,J,T_Z)$ to $\Psi_A(\Gamma',J,T_Z-1)$ is

$$M_F = \langle\Psi_A(\Gamma',J,T_Z-1)|\ \tau_-\ |\Psi_A(\Gamma,J,T_Z)\rangle =$$

$$(2J+1)^{-1/2} \sum_j \mathrm{OBTD}(j_n,j_p;\Delta J=0)\ \sqrt{(2j+1)}\ \Omega_j\ \langle n|\ \tau_-\ |p\rangle, \quad (3.2.1)$$

where

$$\Omega_j = \int dr\ r^2\ R_n(r)\ R_p(r),$$

$$\langle n|\ \tau_-\ |p\rangle = 1.$$

The analogous formulae for the electron decay are obtained by operating with τ_+ and interchanging the n/p labels. The general form of the one-body transition density matrix (OBTD) in eq.(3.2.2) is given in proton-neutron formalism by [Bru 77]

$$\mathrm{OBTD}(j'\mu',j\mu;\Delta J) =$$

$$\frac{1}{\sqrt{(2\Delta J+1)}}\ \langle\Psi(\Gamma',J',T_Z')||\ [a^\dagger_{j'\mu'} \times \tilde{a}_{j\mu}]^{\Delta J}\ ||\Psi(\Gamma,J,T_Z)\rangle, \quad (3.2.2)$$

where $a^\dagger_{j\mu}$ is the tensor operator that creates a nucleon with $\tau_Z = 2\mu$ in the orbit j, and $\tilde{a}_{j\mu}$ is the tensor operator that destroys a nucleon in the orbit j. Here we freely interchange the values $\mu=1/2(-1/2)$ with the labels p(n). The double bar in the reduced matrix element in eq.(3.2.2) denotes a reduction in angular momentum space.

If the effects of the INC forces are neglected, the states $\Psi_A(\Gamma,J,T_Z)$ have definite isospin T, and the sum in eq.(3.2.1) is given just as:

$$|M_{FO}|^2 = [T(T+1) - T_{Zi}T_{zf}]\,\delta_{if}, \qquad (3.2.3)$$

where the Kronecker delta insures that only transitions between analog states are allowed. Deviations from this value occur at two levels. First, the one-body transition density matrix is slightly changed because of isospin mixing among shell-model configuration states, and second, the radial overlap integral Ω_j differs from unity because the proton single-particle wave functions are pushed out relative to the neutron wave functions. This last correction is due to the one-body Coulomb potential causing mixing with states which are not contained in the shell-model configuration space (see Chapter One).

The correction to the one-body transition density matrix can be accounted for by the quantity $\beta(j_n,j_p;\Delta J=0)$, defined as

$$\beta(j_n,j_p;0) = OBTD^T(j_n,j_p,;0) - OBTD(j_n,j_p;0) \qquad (3.2.4)$$

where the superscript T denotes the one-body transition density matrix obtained when both the initial and final states possess good isospin.

The proton and neutron single-particle wave functions used to evaluate Ω_j are dependent on the selection of the single-particle potential parameters, such as the well depth. In order to specify the separation energies needed for the calculations of the radial wave functions we insert a complete set of states $\Psi(\pi)$ of the A-1 nucleon

system between the creation and annihilation operators of $OBTD^T(j_n,J_p;0)$. The one-body transition density matrix $OBTD^T(j'\mu',j\mu;\Delta J)$ is then

$$OBTD^T(j'\mu',j\mu;\Delta J) = \sum_{\pi} (-1)^{J_{\Gamma'}+J_\pi+j+\Delta J} \sqrt{[(2J_\Gamma+1)(2J_{\Gamma'}+1)]}$$

$$\times \begin{Bmatrix} J_{\Gamma'} & J_\Gamma & \Delta J \\ j' & j & J_\pi \end{Bmatrix} \sqrt{[\, S(j'\mu';\Gamma',\pi)\; S(j\mu;\Gamma,\pi)\,]}. \qquad (3.2.5)$$

The spectroscopic factor $S(j\mu;\Gamma,\pi)$ is given in terms of the matrix element of $a^\dagger_{j\mu}$, reduced in angular momentum space, by

$$S(j\mu;\Gamma,\pi) = \left| \frac{\langle \Psi(\Gamma,T_Z) || \; a^\dagger_{j\mu} \; || \Psi(\pi)\rangle}{\sqrt{(2J_\Gamma+1)}} \right|^2.$$

The proton-neutron spectroscopic factor, $S(j\mu;\Gamma,\pi)$, is related to the spectroscopic factor in isospin formalism by

$$S(j\mu;\Gamma,\pi) = C^2(\mu)\; S(j;\Gamma,\pi) \qquad (3.2.6)$$

where

$$C(\mu) = (T_\pi \; T_{\pi Z} \; \tfrac{1}{2} \; \mu \mid T_\Gamma \; T_{\Gamma Z}).$$

$S(j;\Gamma,\pi)$ is given in terms of the matrix element of $a^\dagger_j$, reduced in angular momentum and isospin space, by

$$S(j;\Gamma,\pi) = \left| \frac{\langle \Psi(\Gamma) \,|||\, a_j^{\dagger} \,|||\, \Psi(\pi)\rangle}{\sqrt{[(2J_\Gamma+1)(2T_\Gamma+1)]}} \right|^2 .$$

The proton and neutron radial wave functions are then evaluated with the appropriate separation energy of the intermediate parent state $\Psi(\pi)$, and the radial integral of these wave functions, $\Omega_{j,\pi}$, is weighted by the factor $\sqrt{[S(j;\Gamma',\pi)S(j;\Gamma,\pi)]}$.

Utilizing equations (3.2.4), (3.2.5) and (3.2.6), with $\Delta J=0$, the Fermi matrix element can now be rewritten as

$$M_F = (2J+1)^{-1/2} \Big[\sum_j OBTD^T(j_n,j_p;0)\ \sqrt{(2j+1)}$$

$$- \sum_j \beta(j_n,j_p;0)\ \sqrt{(2j+1)}$$

$$- \sum_{j,\pi} C(\tfrac{1}{2})\ C(-\tfrac{1}{2})\ \sqrt{(2J_\Gamma+1)}\ \sqrt{[S(j;\Gamma',\pi)S(j;\Gamma,\pi)]}\ (1-\Omega_{j,\pi}) \Big]. \qquad (3.2.7)$$

For superallowed decays, eq.(3.2.7) gives

$$|M_F|^2 = |M_{F0}|^2\ (1 - \delta_C) = |M_{F0}|^2\ (1 - (\delta_{RO} + \delta_{IM})) \qquad (3.2.8)$$

where δ_{RO} and δ_{IM} are given by

$$\delta_{RO} = \frac{2}{M_{F0}} \sum_{j,\pi} C(1/2)C(-1/2)\ \sqrt{(2J_\Gamma+1)}$$

$$\times \sqrt{[S(j;\Gamma,\pi)S(j;\Gamma,\pi)]}\ (1 - \Omega_{j,\pi}), \qquad (3.2.9a)$$

$$\delta_{IM} = \frac{2}{M_{FO}} \sum_{j} \beta(j_n, j_p; 0) \sqrt{(2j+1)}. \qquad (3.2.9b)$$

3.3 Radial-Overlap Contribution, δ_{RO}

Previously [Tow 73, Har 75, and Tow 77], values for δ_{RO} have been calculated using proton and neutron radial wave functions obtained with a central Woods-Saxon plus Coulomb potential. This procedure overestimates the difference between the proton and neutron radial wave functions by neglecting an induced isovector interaction that arises from the difference between the proton and neutron densities. To take into account the effects of this induced interaction a self-consistent Hartree-Fock calculation utilizing a Skryme-type interaction has been performed.

Skyrme proposed [Sky 56 and Sky 59] that interactions between nucleons within the nuclear environment can be approximated by an effective force which is composed of two parts. The first is a two-body potential of the form

$$v(\vec{r}_1, \vec{r}_2) = t_0(1 + x_0 P_\sigma)\delta(\vec{r}_1 - \vec{r}_2)$$

$$+ \frac{1}{2} t_1[\delta(\vec{r}_1 - \vec{r}_2)k^2 + k'^2\delta(\vec{r}_1 - \vec{r}_2)]$$

$$+ t_2\vec{k}'\cdot\delta(\vec{r}_1 - \vec{r}_2)\vec{k} + i\, w_0(\vec{\sigma}_1 + \vec{\sigma}_2)\cdot\vec{k}'\times\delta(\vec{r}_1 - \vec{r}_2)\vec{k},$$

where t_0, t_1, t_2, x_0, and w_0 are adjustable parameters, $\vec{k}$ denotes the operator $(\vec{\nabla}_1 - \vec{\nabla}_2)/2i$ acting on the right, $\vec{k}'$ is the operator $-(\vec{\nabla}_1 - \vec{\nabla}_2)/2i$ acting on the left, and $P_\sigma = \frac{1}{2}(1 + \vec{\sigma}_1\cdot\vec{\sigma}_2)$ is the spin exchange

operator. The second component of the interaction is the three-body potential

$$v(\vec{r}_1,\vec{r}_2,\vec{r}_3) = t_3\delta(\vec{r}_1 - \vec{r}_2)\delta(\vec{r}_2 - \vec{r}_3),$$

where t_3 is a free parameter. The qualitative effect of t_0 and t_1 is to determine the strength of that part of the interaction which acts on relative even states (s- and d-states), while t_2 determines that part acting on relative odd states (p-states). Since the operator x_0P_σ is equivalent to $-x_0P_\tau$ (P_τ is the isospin exchange operator) when acting on antisymmetrized states, the parameter x_0 determines the strength of the component which is sensitive to proton-neutron asymmetries. The one-body spin-orbit potential is governed by the parameter w_0. The potential $v(\vec{r}_1,\vec{r}_2,\vec{r}_3)$ should not be thought of as a real three-body interaction, but rather a convenient way of simulating the density dependence of the effective interaction. In fact, in Hartree-Fock calculations this three-body potential is equivalent to a two-body zero-range interaction with a linear density dependence [Vau 72].

The parameters of the Skyrme interaction are determined by requiring that they reproduce bulk properties of closed-shell (magic) nuclei [Vau 72, Dov 72, Bei 75, Van 81b, and Van 81c], such as ground state binding energies, proton distributions, excitation energies of the giant isoscalar monopole and quadrupole resonances, and Gamow-Teller strengths. The parameters used in this work are those of the SGII interaction of Van Giai and Sagawa [Van 81b and Van 81c]. For this interaction, it was found that in order to describe the giant isoscalar

monopole state, the linear density dependence suggested by the three-body potential had to be replaced by a dependence on $\rho^{1/6}$.

Hartree-Fock calculations using the Skyrme interaction lead to a set of spherical nonlocal differential equations with eigenfunctions $\psi^{NL}_{\alpha}(r) = u^{NL}_{\alpha}(r)/r$ and eigenvalues ε_{α} [Vau 72, Dov 72, and Bei 75]. The nonlocal eigenfunctions and eigenvalues can be obtained from the following equivalent set of differential equations, which involve a local energy-dependent potential [Dov 72]

$$-\frac{\hbar^2}{2m}\frac{d^2}{dr^2}u^{L}_{\alpha,\mu}(r) + \frac{\hbar^2}{2m}\frac{\ell(\ell+1)}{r^2}u^{L}_{\alpha,\mu}(r)$$

$$+ V^{L}_{\mu}(r)\,u^{L}_{\alpha,\mu}(r) = \varepsilon_{\alpha\mu}\,u^{L}_{\alpha,\mu}(r), \qquad (3.3.1)$$

with

$$V^{L}_{\mu}(r) = \left[1 - \frac{m^{*}(r)}{m}\right]\varepsilon_{\alpha,\mu} + U_{\mu}(r) + U^{SO}_{\mu}(r)\,\vec{\sigma}\cdot\vec{\ell} + \delta_{\frac{1}{2},\mu}\,V_{Coul}(r),$$

$$m^{*}_{\mu}(r)/m = \left\{1 + C_0[\rho_p(r) + \rho_n(r)] + 2\mu C_1[\rho_p(r) + \rho_n(r)]\right\}^{-1},$$

$$\psi^{NL}_{\alpha,\mu}(r) = N\left[\frac{m^{*}(r)}{m}\right]^{1/2}\psi^{L}_{\alpha,\mu}(r).$$

N is a normalizing constant determined by the condition

$$\int |\psi^{NL}_{\alpha,\mu}(r)|^2 r^2 dr = 1.$$

The subscript μ denotes the z-projection of the isospin of the nucleon, and α denotes all other single-particle quantum numbers.

The central and spin-orbit potentials, $U_\mu(r)$ and $U_\mu^{SO}(r)$, are dependent on the nucleon densities, their derivatives, and the Skyrme parameters [Bei 75]. The coefficients C_0 and C_1 expressed in terms of the Skyrme parameters t_1 and t_2 are

$$C_0 = \frac{2m}{\hbar^2}\left[\frac{5t_2 + 3t_1}{16}\right],$$

$$C_1 = \frac{2m}{\hbar^2}\left[\frac{t_2 - t_1}{16}\right].$$

The Coulomb potential, V_{Coul}, is

$$V_{Coul}(r) = e^2\left[\int \frac{\rho_p(r')}{|\vec{r}' - \vec{r}|} d^3r - \frac{3}{2}\left(\frac{3}{\pi}\right)^{1/3} \rho_p^{1/3}(r)\right]$$

where the first of these contributions is the direct term, and the second the exchange term in the Fermi-gas approximation [Bei 75] . The nucleon densities, $\rho_\mu(r)$, are given by

$$\rho_\mu(r) = \sum_j n_{j,\mu} \left| \psi^{NL}_{\alpha,\mu}(r)\right|^2$$

where $n_{j,\mu}$ is the occupation number of the j^{th} orbit as determined from the shell model wave functions obtained with the isoscalar Hamiltonian.

The radial overlap correction was evaluated in the following manner. First, the average central potential $U_\mu(r)$ was obtained by

performing the self-consistent calculation with eq.(3.3.1). Then the single-particle wave functions were obtained by solving eq.(3.3.1) using this average potential shape, and scaling its overall strength to reproduce the separation energy. The separation energies were determined from experimental ground state masses [Wap 82] and excitation energies [Ajz 80, Ajz 81, Ajz 83, End 77, and Led 78] of the intermediate parent state $\Psi(\pi)$. Where experimental excitation energies were not available, excitation energies obtained with the isoscalar Hamiltonian were used. The spectroscopic amplitudes $S(j,\Gamma\pi)$ were also evaluated using the shell-model wave functions.

The quantities δ_{RO} obtained from a Hartree-Fock (HF) calculation for ^{14}O, ^{26m}Al, ^{34}Cl, ^{38m}K, ^{42}Sc, ^{46}V, ^{50}Mn, and ^{54}Co are presented in Table 3.1. The shell-model configuration spaces used for these calculations are also listed in Table 3.1, while the corresponding isoscalar Hamiltonians are listed in Table 2.1. The only model-space truncations imposed were for ^{42}Sc (no more than four holes in the $0d_{3/2}$ orbit) and the 0f-1p-shell nuclei (no more than one particle outside the $0f_{7/2}$ orbit). For the purpose of comparison, the calculation was also performed with the usual method of using a Woods-Saxon (WS) plus Coulomb single-particle potential [Bro 82]. As can be seen from the table, with the exception of ^{38m}K, values of δ_{RO} obtained from the HF wave functions are systematically reduced relative to the WS calculation. This reduction is due to the effects of both the Coulomb and nuclear potentials used in each calculation. The Coulomb potential of the WS procedure was that of a uniformly charged sphere containing Z-1 protons, whose radius was chosen to reproduce the experimental rms charge radii, with no exchange term. The WS isovector potential is

Table 3.1

Values for the radial overlap correction, δ_{RO}, obtained with the Woods-Saxon (WS) and Hartree-Fock (HF) calculations.

Decaying Nucleus	Shell-Model Configuration Space	δ_{RO}(%) (WS)	(HF)
^{14}O	0p shell	0.299	0.134
^{26m}Al	1s-0d shell	0.283	0.255
^{34}Cl	1s-0d shell	0.552	0.432
^{38m}K	$0d_{3/2}$ & $0f_{7/2}$ orbits	0.390	0.453
^{42}Sc	$0d_{3/2}$ & $0f_{7/2}$ orbits	0.413	0.209
^{46}V	0f-1p shell	0.470	0.230
^{50}Mn	0f-1p shell	0.586	0.296
^{54}Co	0f-1p shell	0.747	0.359

generally assumed to be proportional to N-Z, whereas the isovector interaction in the HF procedure arises from the difference in the neutron and proton densities, leading to an isovector potential even for N=Z nuclei.

To understand the difference between the proton and neutron wave functions generated with the WS and HF procedures, we consider protons perturbatively relative to neutrons in ^{34}Cl. The perturbing Hamiltonian in the WS procedure, δH_{WS}, is simply $V_{Coul}^{(WS)}(r)$, while in the HF procedure we have

$$\delta H_{HF} = \frac{m}{m^*(r)} \left[U_p(r) - U_n(r) \right] + V_{Coul}^{(HF)}(r),$$

where the small isovector spin-orbit term has been neglected. Plotted in Figure 3.1 are the quantities

$$\delta H_{Coul} = V_{Coul}^{(HF)}(r) - V_{Coul}^{(WS)}(r),$$

$$\delta H_{isov} = \frac{m}{m^*(r)} \left[U_p(r) - U_n(r) \right],$$

$$\delta H = \delta H_{Coul} + \delta H_{isov}. \qquad (3.3.2)$$

δH is then the extra potential exerted on protons in the HF procedure relative to WS. In Hartree-Fock calculations, protons are effectively in a potential well which is both deeper at the origin and has a higher barrier at the nuclear surface than protons in a Woods-Saxon calculation. The effect on δ_{RO} due to these perturbing potentials can be

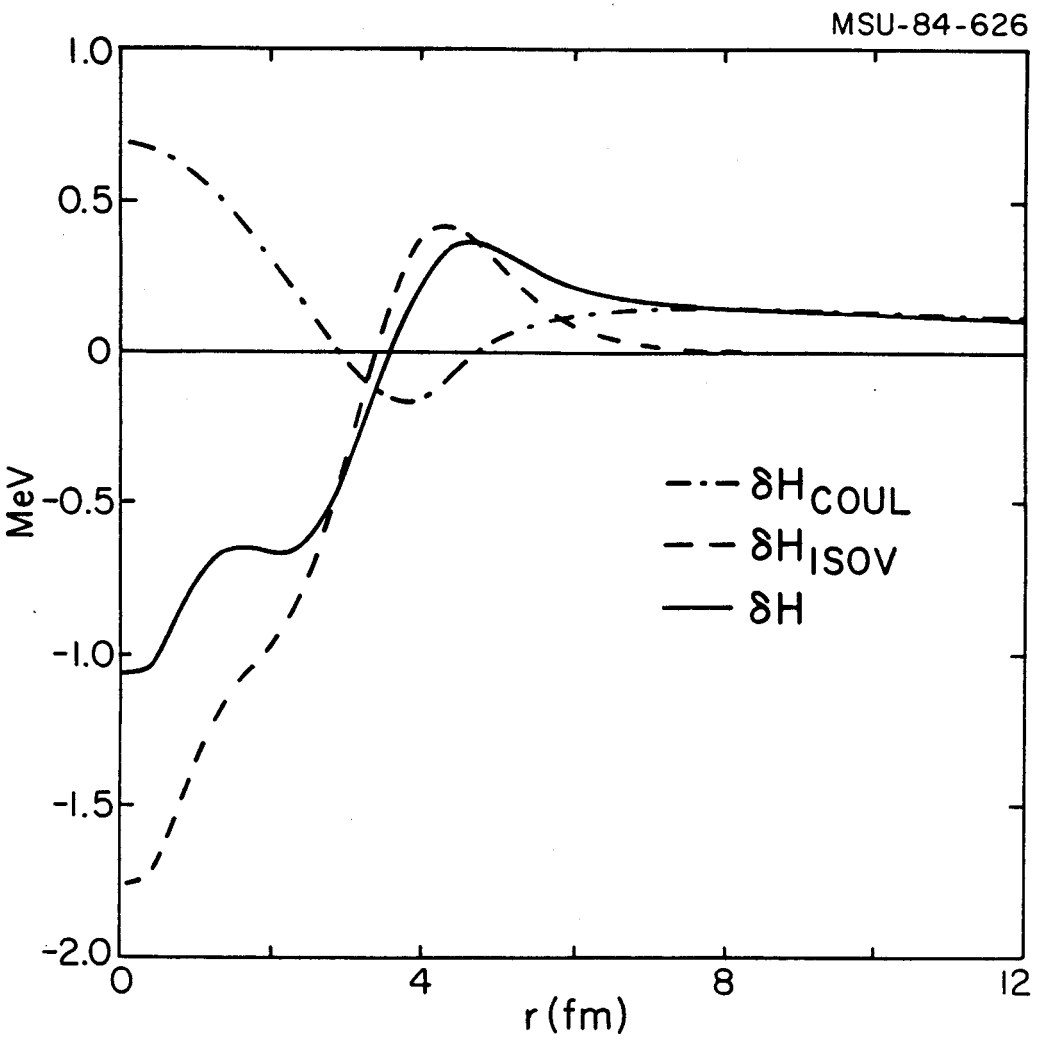

Figure 3.1: Plot of the perturbing Hamiltonians δH_{Coul}, δH_{isov}, and δH, defined in eq.(3.3.2), as a function of r.

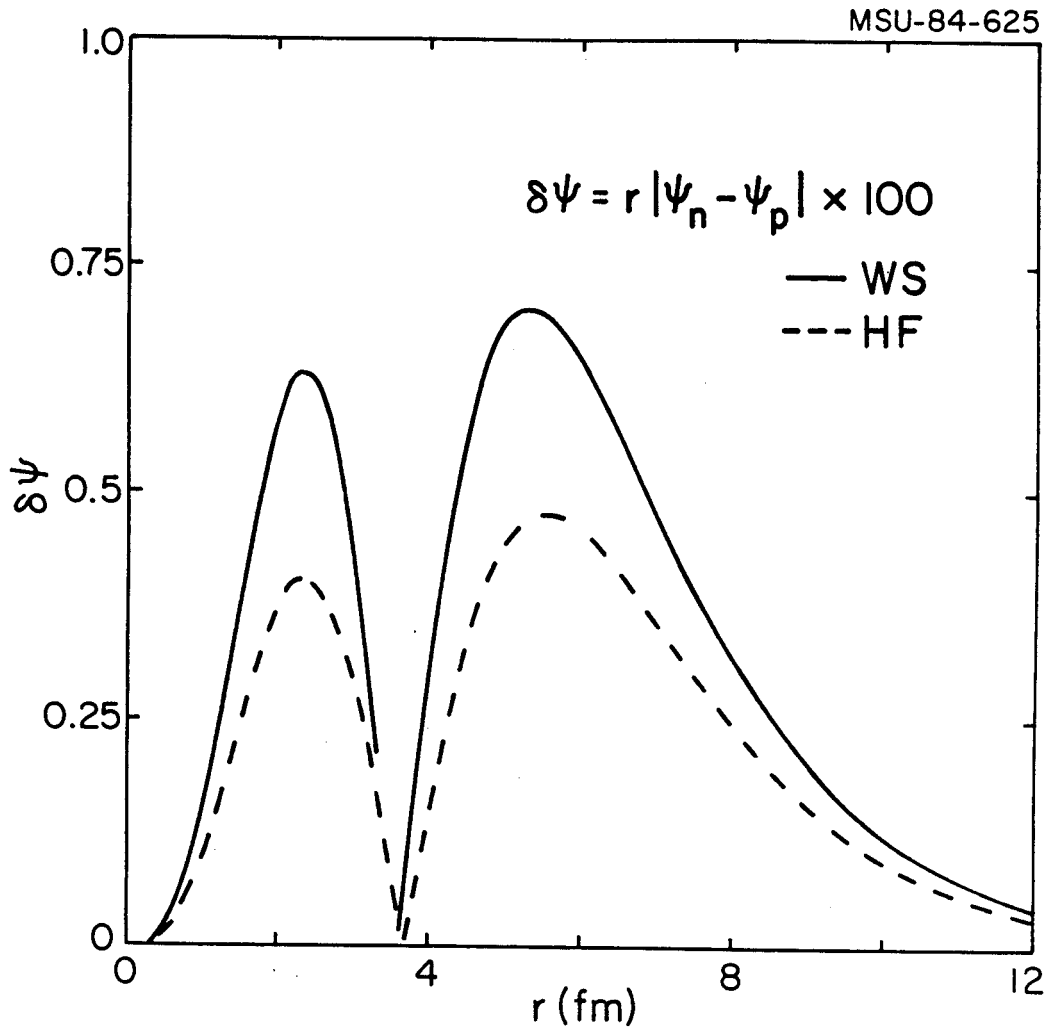

Figure 3.2: Plot of the difference $\delta\psi = r|\psi_n - \psi_p| \times 100$ for Hartree-Fock (HF) and Woods-Saxon (WS) wave functions.

seen in Figure 3.2 where the difference, $\delta\psi = r|\psi_n - \psi_p|$, is plotted for $0d_{3/2}$ radial wave functions obtained from both the WS and HF calculations. This additional potential tends to draw in the proton radial wave functions relative to the neutrons and thus reduce the value of δ_{RO}.

3.4 Isospin-Mixing Contribution, δ_{IM}

The contribution to δ_C due to isospin mixing within the shell-model configuration space can be calculated with two equivalent methods. The first is to obtain isospin-mixed wave functions from the shell model by adding the isospin-nonconserving (INC) interaction directly onto the isoscalar Hamiltonian. The Fermi matrix element correction δ_{IM} can then be evaluated by simply calculating the OBTD matrix of eq.(3.2.2). The second method is to consider the effects of the INC potential perturbatively. The Fermi matrix element is then calculated with wave functions corrected to first order, and δ_{IM} becomes a sum of terms which are dependent on the matrix element of the INC potential between the ground state and all other states (see below).

Since the perturbation is small, the two methods are equivalent. However, each of the methods have particular advantages and disadvantages. The primary advantage of the perturbative approach is that it is easier to determine the contribution to δ_{IM} due to either specific nuclear states, or particular parts of the interaction, such as that due to the single-particle energies, the two-body matrix elements, or the isovector and isotensor components of the interaction. The disadvantage of the perturbative method is that it involves a sum over many matrix elements connecting to a large number of excited states. In

addition, this procedure requires the calculation of the two-body transition densities (see Chapter Two, section two), which is often time consuming. The diagonalization procedure has the advantage that corrections due to higher-order perturbations and the sum over the matrix elements performed in the perturbative method is done automatically during the diagonalization of the Hamiltonian.

In the present work, both procedures are used. Since the diagonalization procedure is generally easier to perform, this method is chosen for the evaluation of δ_{IM}. On the other hand, since the perturbation expansion lends itself to determining how much of δ_{IM} is due to mixing with individual states, this procedure is used to help understand the differences between the results presented here and those of previous works.

3.4a Perturbation Expansion for δ_{IM}

In this section, δ_{IM} is derived using first-order perturbation theory. Following the method of Blin-Stoyle [Bli 69] and Towner and Hardy [Tow 73], the wave function $\Psi(\Gamma,T_Z)$ is given by

$$\Psi(\Gamma,T_Z) = N(\Gamma,T,T_Z)\ \Psi_0(\Gamma,T,T_Z) + \sum_{\nu} \sum_{t=|T_Z|}^{T+2} a(\nu,t,T_Z)\Psi_0(\nu,t,T_Z), \qquad (3.4a.1)$$

where the sum over ν represents the sum over all quantum numbers other than isospin, and the states $\Psi_0(k)$ satisfy the eigenvalue equation

$H^{(0)}|\Psi_0(k)\rangle = E_0(k)|\Psi_0(k)\rangle$. The coefficients $a(\nu,t,T_Z)$ are given in first-order nondegenerate perturbation theory by

$$a(\nu,t,T_Z) = \frac{\langle\psi(\nu,t,T_Z)|\ V_{INC}\ |\psi(\Gamma,T,T_Z\rangle}{E(\nu,t) - E(\Gamma,T)}\ , \qquad (3.4a.2)$$

and the normalizing constant $N(\Gamma,T,T_Z)$ satisfies the constraint

$$\{N(\Gamma,T,T_Z)\}^2 + \sum_{\nu} \sum_{t=|T_Z|}^{T+2} \{a(\nu,t,T_Z)\}^2 = 1. \qquad (3.4a.3)$$

To calculate the effects of isospin mixing on superallowed Fermi β-decay, we square the matrix element of the τ_- operator between the state $\Psi_A(\Gamma,J,T_Z)$ and its analog $\Psi_A(\Gamma,J,T_Z-1)$ to obtain

$$|M_F|^2 = |\langle\ \Psi(\Gamma,T_Z-1)\ |\ \tau_-\ |\ \Psi(\Gamma,T_Z)\ \rangle|^2 =$$

$$[T(T+1)-T_Z(T_Z-1)]\ \{\ N(\Gamma,T,T_Z)N(\Gamma,T,T_Z-1)$$

$$+\sum_{\nu} \sum_{t=|T_Z|}^{T+2} \left(\frac{t(t+1)-T_Z(T_Z-1)}{T(T+1)-T_Z(T_Z-1)}\right)^{1/2} a(\nu,t,T_Z)a(\nu,t,T_Z-1)\}^2. \qquad (3.4a.4)$$

Expanding eq.(3.4a.4) and keeping terms only up to second order in $a(\nu,t,T_Z)$ we find

$$|M_F|^2 = [T(T+1)-T_Z(T_Z-1)]\ \{N^2(\Gamma,T,T_Z)\ N^2(\Gamma,T,T_Z-1)$$

$$+\ 2N(\Gamma,T,T_Z)N(\Gamma,T,T_Z-1)$$

$$\times \sum_{\nu} \sum_{t=|T_z|}^{T+2} \left(\frac{t(t+1)-T_z(T_z-1)}{T(T+1)-T_z(T_z-1)}\right)^{1/2} a(\nu,t,T_z)a(\nu,t,T_z-1)\}. \quad (3.4a.5)$$

By inserting eq.(3.4a.3) into eq.(3.4a.5) we obtain

$$\delta_{IM}(T_z) = \sum_{\nu} [\sum_{t=|T_z|}^{T+2} \{a(\nu,t,T_z)\}^2 + \sum_{t=|T_z-1|}^{T+2} \{a(\nu,T_z-1)\}^2$$

$$- 2 \sum_{t=|T_z|}^{T+2} \left(\frac{t(t+1)-T_z(T_z-1)}{T(T+1)-T_z(T_z-1)}\right)^{1/2} a(\nu,t,T_z)\, a(\nu,t,T_z-1)]. \quad (3.4a.6a)$$

Similarly, it can be shown that, for the forbidden (off diagonal) β-decay of the state $\Psi(\Gamma,T_z)$ to $\Psi(\Gamma',T_z-1)$, $|M_F|^2$ is given by

$$|M_F|^2 = [T(T+1)-T_z(T_z-1)]\, \{a(\Gamma,T,T_z-1) + a(\Gamma',T,T_z)\}^2. \quad (3.4a.6b)$$

3.4b Results for δ_{IM}

The isospin-mixing correction δ_{IM} for the superallowed β-decay of ^{14}O, ^{26m}Al, ^{34}Cl, ^{38m}K, ^{42}Sc, ^{46}V, ^{50}Mn, and ^{54}Co have been evaluated and are presented in Table 3.2. The configuration spaces and isoscalar Hamiltonians used were the same as for the radial-overlap correction, and the isovector and isotensor interactions were determined with the parameters given in Tables 2.7 and 2.15, respectively.

As was mentioned in the second chapter, there is some uncertainty in the selection of the isovector and isotensor interactions. At this point then, it is necessary to discuss the differences between the isovector and isotensor interactions determined with the parameters

Table 3.2

Values for the isospin-mixing correction δ_{IM}.

Decaying Nucleus	δ_{IM}(%)
^{14}O	0.010
^{26m}Al	0.012
^{34}Cl	0.056
^{38m}K	0.111
^{42}Sc	0.109
^{46}V	0.013
^{50}Mn	0.004
^{54}Co	0.005

Table 3.3

Comparison between isospin-mixing matrix elements for the lowest $J^{\pi}=1/2^{+}$ T=3/2 state in ^{21}Na evaluated with $R^{(2)}$ = 81 MeV and $A^{(2)} = -4.2 \times 10^{-2}$.

k	$R^{(2)}$ = 81 MeV	$A^{(2)} = -4.2 \times 10^{-2}$
1	15.0	12.0
2	-12.6	-12.1
3	16.1	19.3
4	-6.7	-10.5
5	7.1	6.7
6	32.1	36.7
7	6.7	8.1
8	13.4	19.5
rms deviation 3.4 keV		

Table 3.4

Comparison between isospin-mixing matrix elements for the lowest $J^{\pi}=1/2^{+}$ T=3/2 state in ^{21}Na evaluated with parameters given Table 2.7 and the last row of Table 2.12.

k	Table 2.7	Table 2.12
1	15.0	9.5
2	-12.6	-23.6
3	16.1	19.7
4	-6.7	-3.6
5	7.1	9.5
6	32.1	51.4
7	6.7	10.2
8	13.4	16.9
	rms deviation 8.5 keV	

given in Tables 2.7 and 2.15, respectively, and their alternatives. Comparisons are made between the isospin-mixing matrix elements obtained for the lowest $J^{\pi}=1/2^{+}$ T=3/2 state in ^{21}Na, and the isospin-mixing correction for A=34 superallowed decays. The purpose of these comparisons is to determine what effect these alternative interactions might have on the present calculation of δ_{IM}.

Isospin-mixing matrix elements between the lowest $J^{\pi}=1/2^{+}$ T=3/2 state and the lowest eight $J^{\pi}=1/2^{+}$ T=1/2 states in ^{21}Na have been evaluated using the isotensor interactions in which $R^{(2)}$ = 81 MeV and $A^{(2)} = -4.2 \times 10^{-2}$, and are shown in Table 3.3. The rms deviation of the isospin-mixing matrix elements evaluated with these interactions is 3.4 keV. In addition, values of δ_{IM} for the superallowed β-decay of ^{34}Cl and ^{34}Ar have been evaluated with these interactions. These are 0.056×10^{-2} and 0.006×10^{-2} for ^{34}Cl and ^{34}Ar, respectively, with $R^{(2)}$ = 81 MeV, and are close to the values 0.054×10^{-2} and 0.014×10^{-2}, obtained with $A^{(2)} = -4.2 \times 10^{-2}$. Note that the correction for the ^{34}Ar decay does not appear in Table 3.2 because of the large experimental error in the ft value for this transition.

The situation with the isovector interactions, however, is not so clear-cut. The isospin-mixing matrix elements that appear in Table 3.3 have been re-evaluated using the parameters given in the last row of Table 2.12, and are shown in Table 3.4. The companion isotensor interaction was obtained by fixing $C^{(2)}$ to 0.93 and fitting on $A^{(2)}$, giving $A^{(2)} = (-5.5\pm0.2) \times 10^{-2}$ with an rms deviation of 9.7 keV. As can be seen from the table, the isospin-mixing matrix elements evaluated with these interactions differ somewhat, with an rms deviation of 8.5

keV. The values δ_{IM} obtained with this INC interaction are 0.080×10^{-2} and 0.014×10^{-2} for ^{34}Cl and ^{34}Ar, respectively.

When the deviation in δ_{IM} found in the above analysis is added onto the the values of 0.432×10^{-2} and 0.369×10^{-2} obtained for the δ_{RO}, the total correction δ_C changes by only 5%/or less. Therefore, it is expected that the uncertainty in the isovector interactions will not significantly effect the calculation of the total correction δ_C.

3.6 Total Correction δ_C

Shown in Table 3.5 and Figure 3.3 is a comparison of the values for δ (IM, RO, and C) obtained in the present work with those obtained previously [Tow 73 and Tow 77]. The difference that exists between values of the radial-overlap corrections evaluated from the Woods-Saxon potential shown in Table 3.1 and those of Towner, Hardy, and Harvey [Tow 77] (also evaluated with a Woods-Saxon potential and eq.(2.10a)) is primarily due to different Woods-Saxon potential parameters. Using the Woods-Saxon potential parameters of Towner, Hardy, and Harvey we find δ_{RO} for ^{54}Co to be 0.593%, which is in good agreement with the value shown in Table 3.5. Again, it is important to note that by including the effects of the induced isovector interaction the radial overlap contribution to δ_C is reduced relative to previous estimates.

In order to understand the difference between the values of δ_{IM} in the present work and those of Towner and Hardy [Tow 73], we examine the correction for A=34 superallowed transitions in detail. Shown in Table 3.6 are the values of δ_{RO} and δ_{IM} obtained previously [Tow 73 and Tow 77] and in the present work for ^{34}Cl and ^{34}Ar. The discrepancy observed for δ_{IM} can be attributed to different zeroth-order wave functions

Table 3.5

Comparison of the corrections to the Fermi matrix element obtained in the present work and those of Towner, Hardy, and Harvey [Tow 73 and Tow 77] (Values of δ are given in %).

Decaying nucleus	Present Work			Previous Values		
	δ_{IM}	δ_{RO}	δ_C	δ_{IM} [a]	δ_{RO} [b]	δ_C
^{14}O	0.010	0.134	0.144	0.05	0.23	0.33
^{26m}Al	0.012	0.255	0.267	0.07	0.27	0.34
^{34}Cl	0.056	0.432	0.488	0.23	0.62	0.85
^{38m}K	0.111	0.453	0.564	0.16	0.54	0.70
^{42}Sc	0.109	0.209	0.318	0.13	0.35	0.48
^{46}V	0.013	0.230	0.243	0.04	0.36	0.40
^{50}Mn	0.004	0.296	0.300	0.03	0.40	0.43
^{54}Co	0.005	0.359	0.364	0.04	0.56	0.60

[a]) values presented in Table 6 of [Tow 73]

[b]) values presented in Table 3 of [Tow 77]

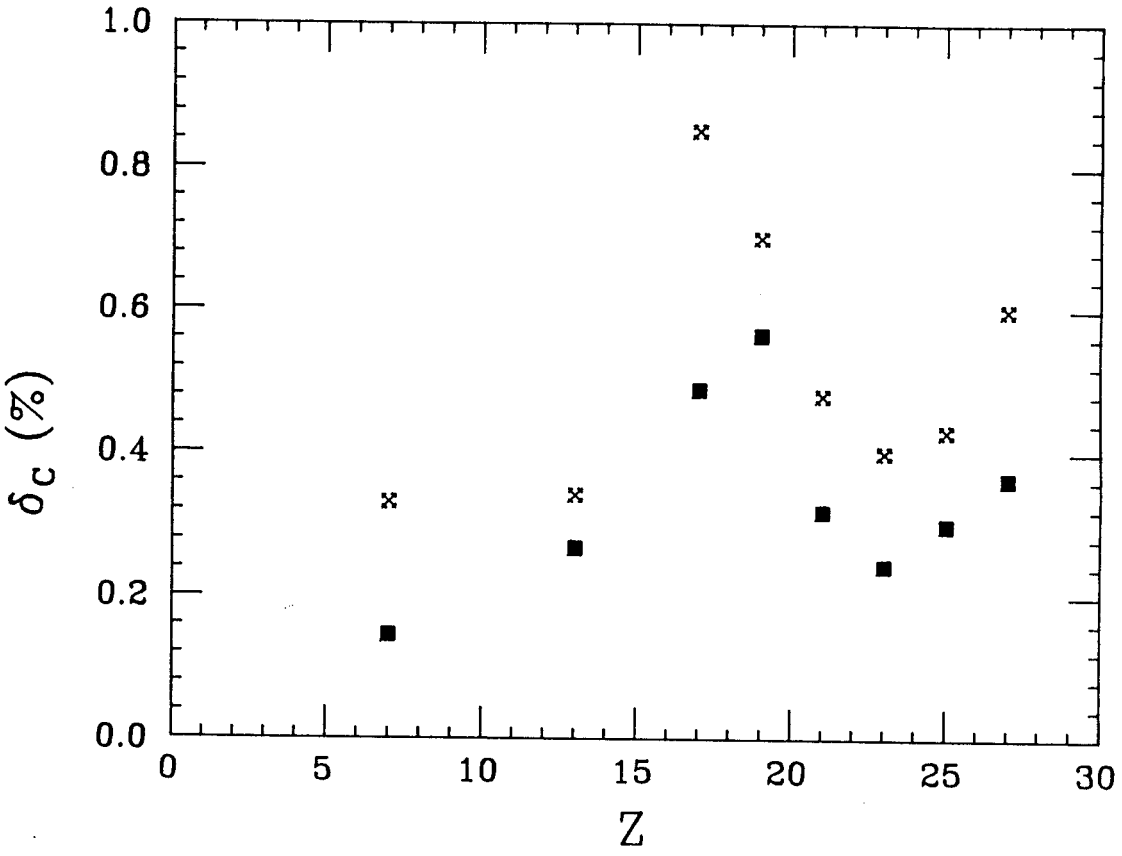

Figure 3.3: Comparison between values of δ_C evaluated in the present work (squares) and those of Towner, Hardy, and Harvey (crosses).

Table 3.6

Comparison of the corrections to the Fermi matrix element obtained in the present work and those of Towner, Hardy and Harvey [Tow 73 and Tow 77] for A=34 superallowed β-emitters (Values of δ are given in %).

Decaying nucleus	Present Work			Previous Values		
	δ_{IM}	δ_{RO}	δ_C	δ_{IM}	δ_{RO}	δ_C
^{34}Ar	0.006	0.369	0.375	0.13	0.91	1.04
^{34}Cl	0.056	0.432	0.488	0.23	0.62	0.85

and/or the INC interaction used. The zeroth-order wave functions used by Towner and Hardy were obtained with a modified surface delta interaction (MSDI) in a truncated 1s-0d shell-model space. The truncation restriction was that no more than two holes in the $0d_{5/2}$ orbit were allowed. Towner and Hardy's INC interaction (V_{INC}(Tow)) was obtained by:

(1) adding Coulomb matrix elements evaluated with harmonic oscillator wave functions to the proton-proton two-body matrix elements,

(2) increasing the T=1 part of the MSDI proton-neutron matrix elements by 2%, and

(3) using the A=17 energy levels to determine the isovector single-particle energies (i.e. $\varepsilon^{(1)}(0d_{5/2})$ = 3.544 MeV, $\varepsilon^{(1)}(1s_{1/2})$ = 3.168 MeV and $\varepsilon^{(1)}(0d_{3/2})$ = 3.56 MeV).

In addition, no A dependence in the single-particle energies was assumed, and the value of $\hbar\omega$ for A=34 was 11.2 MeV, while the value of 11.5 MeV is used in the present work.

The effects of the model-space truncation were investigated by evaluating δ_{IM} with the total Hamiltonian of the present work in the truncated model space used by Towner and Hardy. The values of δ_{IM} obtained for ^{34}Ar and ^{34}Cl in the truncated model space are 0.004% and 0.048% respectively, and do not differ significantly from the full-space values of 0.006% and 0.056%.

In order to determine whether the starting wave functions or the INC interaction are responsible for the discrepancy in δ_{IM}, both the IMME coefficients and δ_{IM} for A=34 were evaluated with all the possible

Table 3.7

Comparison of IMME coefficients and δ_{IM} evaluated with the combinations of the isoscalar interaction, isovector single-particle energies, and the two-body INC interaction.

Isoscalar	INC		b	c	δ_{IM} (%)	
	Single-Particle	Two-Body	(MeV)	(keV)	^{34}Ar	^{34}Cl
MSDI	A	A	6.594	277	0.136	0.276[a]
MSDI	A	B	6.636	293	0.135	0.276
MSDI	B	A	6.479	284	0.019	0.078
MSDI	B	B	5.521	300	0.016	0.076
W	A	A	6.641	292	0.055	0.186
W	A	B	6.684	285	0.052	0.178
W	B	A	6.497	297	0.009	0.061
W	B	B	6.548	281	0.006	0.056
Experimental IMME Coefficients			6.559	284		

The labels MSDI and A refer to the isoscalar and INC interactions used by Towner and Hardy, while the labels W and B represent the mass-dependent sd-shell hamiltonian [Wil 84] and fitted INC interaction of the present work.

[a]) Values obtained by Towner and Hardy [Tow 84] for these quantities are b=6.596 MeV, c=278 keV, $\delta_{IM}(^{34}Ar)$=0.132%, and $\delta_{IM}(^{34}Cl)$=0.234%.

Table 3.8

Comparison between MSDI, W-interaction, and experimental excitation energies (in MeV) for A = 34.

J	T	EXP	USD	MSDI
0	1	0.000	0.000	0.00
3	0	0.146	0.133	-0.13
1	0	0.461	0.317	-0.45
1	0	0.666	0.661	-0.19
2	0	1.230	1.142	0.39
2	0	1.887	1.712	1.43
2	1	2.127	2.200	1.99
3	0	2.181	2.032	1.19
4	0	2.376	2.394	2.07
2	1	3.303	3.138	2.68
5	0	3.646	3.762	3.59
0	1	3.914	3.905	3.32
4	0	3.964	3.897	3.20
1	1	4.074	4.302	3.87
2	1	4.114	4.896	5.09
3	1	4.876	4.773	4.18

No more than two excitation energies with a given J and T value are tabulated.

combinations of the isoscalar interaction, isovector single-particle energies, and the two-body INC interaction of the present work and that of Towner and Hardy. The results of these calculations are presented in Table 3.7, along with the experimental IMME coefficients. The values of δ_{IM} evaluated with the mass-dependent sd-shell Hamiltonian of Wildenthal (W-interaction) are consistently smaller in magnitude than those evaluated with MSDI, suggesting a dependence on the isoscalar Hamiltonian in δ_{IM}. A comparison of the lowest T=0 and T=1 excitation energies obtained with both the MSDI and W-interactions with experimental values is presented in Table 3.8. A generally better agreement with experiment is obtained with the W-interaction excitation energies.

A further difference arises in the selection of the isovector single-particle energies. From a comparison between the values of δ_{IM} obtained with the single-particle energies of V_{INC}(Tow) and the fitted single-particle energies of this work, it is apparent that δ_{IM} is sensitive to the single-particle energies. The isospin-mixing amplitudes of eq.(4.2.6a) in fact are sensitive to the relative difference in the isovector single-particle energies, $\varepsilon^{(1)}(\rho) - \varepsilon^{(1)}(0d_{5/2})$. For A=34 the relative difference in the isovector single-particle energies for the $1s_{1/2}$ and $0d_{3/2}$ orbits are -21 keV and 21 keV, respectively, for the INC interaction of the present work, and -370 keV and 20 keV for V_{INC}(Tow). It is this difference between the isovector single-particle energies which is primarily responsible for the discrepancy that exists between the values of δ_{IM} of the present work and those of Towner and Hardy. Single-particle energies obtained via the fitting procedure, however,

are perhaps more appropriate than those determined from closed-core-plus-proton and -neutron nuclei, because of the loosely bound nature of these "single-particle" states.

To further understand the values of δ_{IM} presented here and those of Towner and Hardy, the perturbation expansion of eq.(3.4a.6a) was obtained for the A=34 analogs by evaluating the direct overlap between the isospin mixed ground state wave functions and 16 $J^{\pi}=0^{+}$ states of the unperturbed system, with $0 \leq T \leq 2$. Results of the perturbation expansion are presented in Tables 3.9 and 3.10 for the interactions of Towner and Hardy and the present work, respectively. From this expansion it is apparent that the fitted INC interaction predicts less mixing to excited states than does V_{INC}(Tow), while both interactions predict that isospin mixing in ^{34}S is more pronounced than in either ^{34}Ar or ^{34}Cl. In the expansions presented in both tables, the contributions due to these 16 states differ from the total values shown in Table 3.6, indicating mixing to still higher states. These differences, however, are larger for the expansion presented in Table 3.9, and in fact, the the total values are considerably smaller than those shown in Table 3.9. As can be seen from eq.(4.2.6), negative contributions to the expansion can occur only via mixing with T=2 and T=3 states, and therefore V_{INC}(Tow) predicts more mixing to these higher isospin states than does the fitted INC interaction. Finally, since the contribution to δ_{IM} due to T=1 states is the square of the difference between the mixing amplitudes, the small value obtained for ^{34}Ar with the fitted interaction is explained by the fact that the mixing amplitudes for the lowest T=1 states are approximately equal in both ^{34}Ar and ^{34}Cl.

Table 3.9

Isospin-mixing amplitudes and contribution to δ_{IM} due to the 15 lowest 0^+ states (T=0 and 1) and the first T=2 state evaluated with the INC interaction of Towner and Hardy [Tow 73].

Excitation Energy (MeV)	T	Isospin-Mixing Amplitudes ($\times 10^{-4}$)			δ_{IM} (%)	
		^{34}Ar	^{34}Cl	^{34}S	^{34}Ar	^{34}Cl
3.314	1	47	291	696	0.0595	0.1640
4.924	0	0	-96	0	0.0092	0.0092
5.400	1	-310	-83	119	0.0515	0.0408
5.437	0	0	2	0	0.0000	0.0000
5.749	0	0	68	0	0.0046	0.0046
6.305	1	-125	182	-222	0.0942	0.1632
7.020	1	69	138	90	0.0048	0.0023
7.812	1	45	-31	-87	0.0058	0.0031
7.950	0	0	8	0	0.0001	0.0001
8.462	1	21	-4	103	0.0006	0.0114
8.943	1	-55	13	-53	0.0046	0.0044
8.983	0	0	-1	0	0.0000	0.0000
9.335	0	0	1	0	0.0000	0.0000
9.766	0	0	-11	0	0.0001	0.0001
9.929	1	14	-3	30	0.0003	0.0011
12.538	2	69	80	-67	-0.0080	0.0295
	TOTAL				0.2273	0.4338

Excitation energies are the unperturbed values given by the MSDI Hamiltonian.

Table 3.10

Isospin-mixing amplitudes and contribution to δ_{IM} due to the 16 lowest 0^+ states (T=0 and 1) evaluated with the INC interaction of the present work.

Excitation Energy (MeV)	T	Isospin Mixing Amplitudes ($\times 10^{-4}$)			δ_{IM} (%)	
		^{34}Ar	^{34}Cl	^{34}S	^{34}Ar	^{34}Cl
3.905	1	36	36	227	0.0000	0.0365
5.172	1	48	-39	-22	0.0076	0.0003
6.111	0	0	39	0	0.0015	0.0015
7.116	1	-10	-44	3	0.0012	0.0022
7.605	0	0	3	0	0.0000	0.0000
7.919	1	-5	4	5	0.0001	0.0000
8.296	0	0	-8	0	0.0001	0.0001
8.877	1	15	13	-68	0.0000	0.0066
9.881	1	-10	21	-7	0.0010	0.0008
10.400	0	0	2	0	0.0000	0.0000
11.373	1	-25	14	-44	0.0015	0.0034
11.422	1	-3	-7	-4	0.0000	0.0000
11.949	0	0	0	0	0.0000	0.0000
12.168	2	26	22	12	-0.0008	0.0015
12.495	0	0	1	0	0.0000	0.0000
12.531	1	16	-22	-16	0.0014	0.0000
TOTAL					0.0136	0.0526

Excitation energies are the unperturbed values given by the W-interaction.

Although comparisons of this type have not been made for each superallowed β-emitter shown in Table 3.5, it is expected that the differences in the values obtained in the present work and by Towner and Hardy are due to the same causes as in the case of A=34. This is because in all cases Towner and Hardy used a different isoscalar Hamiltonian and an INC interaction obtained using the procedure outlined above, rather than an empirical interaction which is constrained to reproduce the diagonal matrix elements of V_{INC}.

3.6 Determination of G_V/G_μ

With the total correction δ_C evaluated, it is then possible to invert eq.(1.3.1) and obtain empirical values of the effective vector coupling constant G_V. A more useful relation, however, is the ratio G_V/G_μ, where G_μ is the effective vector coupling constant for muon decay, the experimental value of which is $G_\mu/(\hbar c)^3 = (1.166347 \pm 0.00013) \times 10^{-5}$ GeV^{-2} [PDG 84 and Gio 84]. The relationship between these two coupling constants is

$$\frac{G_V^2}{G_\mu^2} = \cos^2\theta_C \, (1 + \Delta_\beta - \Delta_\mu). \qquad (3.6.1)$$

θ_C is the Cabibbo angle, whose value determined from hyperon decays is $\theta_C = 0.232 \pm 0.003$ [Roo 74]. The quantities Δ_β and Δ_μ are "inner" radiative corrections to the nucleon and muon decays. The difference $\Delta_\beta - \Delta_\mu$ is given by [Sir 78]

$$\Delta_\beta - \Delta_\mu = \frac{\alpha}{2\pi}\left[\, 3\ell n\left(\frac{M_Z}{M_p}\right) + 6\bar{Q}\ell n\left(\frac{M_Z}{M_A}\right) + 2C + \ldots \,\right], \qquad (3.6.2)$$

with $3\ell n(M_Z/M_p)$ actually being the difference $3[\ell n(M_W/M_p) - \ell n(M_Z/M_W)]$, where M_W is the W-boson mass, M_Z = 92.9±1.6 GeV [Arn 83 and Bag 83] is the Z-boson mass, and M_p = 938.2592±0.0052 MeV [Tay 69 and Mat 65] is the proton mass. The first of two these terms is due to the vector current in the the local V-A theory, while the second is due to Z-boson exchange between the muon and electron in the muon decay. The remaining terms, $6\bar{Q}\ell n(M_Z/M_A)$ and 2C, arise from corrections to β-decay due to the axial-vector current mediated by an axial-vector boson of mass M_A = 1.275±0.0030 GeV (the A_1 meson mass [PDG 84]). $\bar{Q}$ is the average charge of the participating quarks (for u and d quarks $\bar{Q}$ is 1/6). The quantity C is the least understood part of eq.(6.2), and present estimates are C = 1 [Sir 74] and C = -0.5 [Abe 68]. Using the conservative estimate C = 0±1, we find $\Delta_\beta - \Delta_\mu = (2.10\pm0.24) \times 10^{-2}$. With sufficient accuracy in the experimental ft values and the nuclear corrections δ_C, it might be possible to use superallowed Fermi transitions as a test for current theoretical estimates of C.

Given in Table 3.11 are the experimental $ft(1+\delta_R)$ values [Kos 85] for ^{14}O, ^{26m}Al, ^{34}Cl, ^{38m}K, ^{42}Sc, ^{46}V, ^{50}Mn, and ^{54}Co, the ratio G_V/G_μ for these transitions determined with the total isospin-mixing correction δ_C of Towner, Hardy, and Harvey and that of the present work, and the unweighted average of these values (the uncertainty quoted is the standard deviation from the norm). In addition, a comparison between the results of the present study and those previous works is shown in Figure 3.4. The quantities $\Delta_\beta - \Delta_\mu$ and C determined for each

Table 3.11

Values of G_V/G_μ

Decaying Nucleus	$ft(1+\delta_R)$[a] (sec)	Present Work	Towner, Hardy, and Harvey
^{14}O	3085.7(22)	0.9842(4)	0.9851(4)
^{26m}Al	3083.3(14)	0.9852(3)	0.9855(3)
^{34}Cl	3103.3(28)	0.9831(5)	0.9849(5)
^{38m}K	3098.1(26)	0.9843(4)	0.9849(4)
^{42}Sc	3104.2(63)	0.9821(10)	0.9829(10)
^{46}V	3100.9(19)	0.9822(3)	0.9830(3)
^{50}Mn	3099.2(38)	0.9828(6)	0.9834(6)
^{54}Co	3105.9(23)	0.9821(4)	0.9832(4)
Average values:		0.9833(12)	0.9841(11)

[a]) [Kos 85]

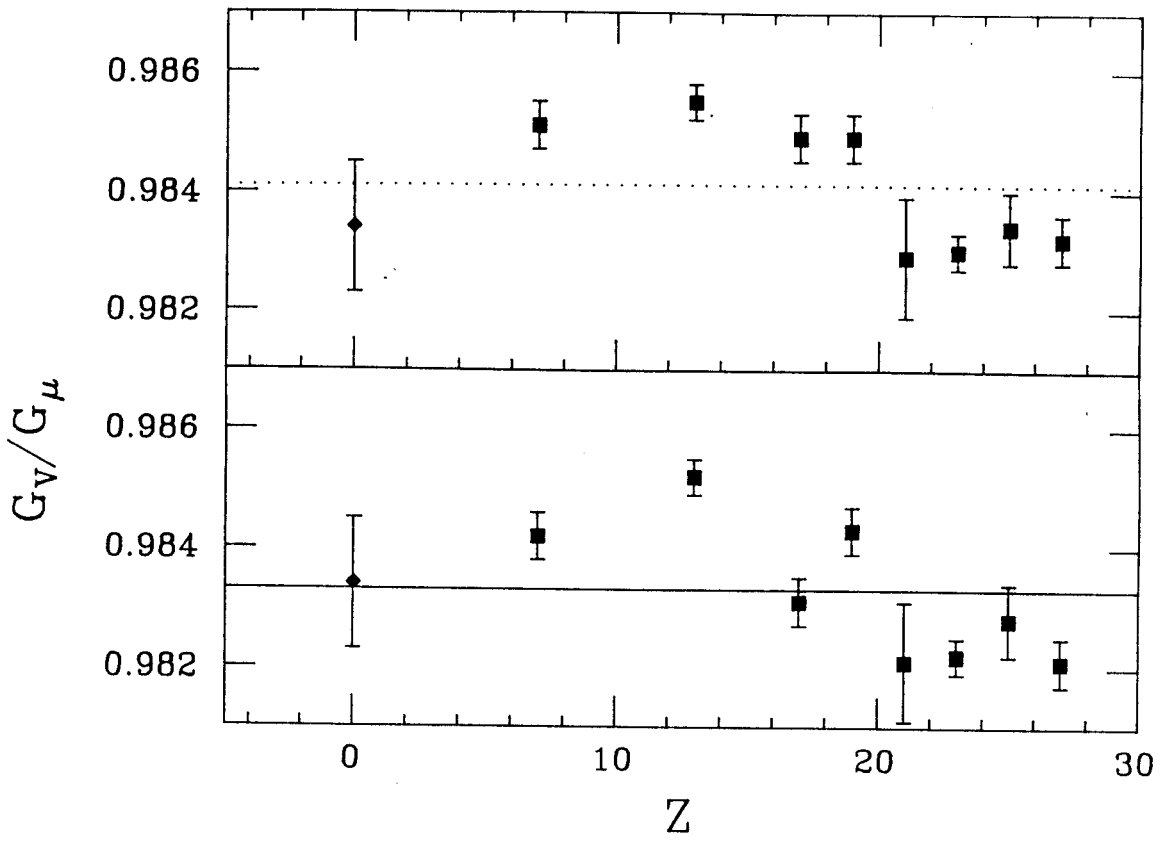

Figure 3.4: Comparison between values of the ratio G_V/G_μ determined from experimental ft values and the corrections to the Fermi matrix element of (a) Towner, Hardy, and Harvey and (b) the present work. The value plotted at Z=0 is determined from eqs.(3.6.1) and (3.6.2) with C=0.0±1.0.

Table 3.12

Values of $\Delta_\beta - \Delta_\mu$ and C

Decaying Nucleus	Present Work		Previous Values	
	$\Delta_\beta - \Delta_\mu$ ($\times 10^{-2}$)	C	$\Delta_\beta - \Delta_\mu$ ($\times 10^{-2}$)	C
^{14}O	2.27(7)	0.73(30)	2.45(7)	1.51(30)
^{26m}Al	2.48(4)	1.64(17)	2.54(4)	1.89(17)
^{34}Cl	2.04(9)	-0.26(39)	2.42(9)	1.38(39)
^{38m}K	2.29(8)	0.82(34)	2.42(8)	1.38(34)
^{42}Sc	1.90(20)	-0.86(86)	2.00(21)	-0.43(87)
^{46}V	1.86(6)	-1.03(26)	2.02(6)	-0.34(26)
^{50}Mn	1.98(13)	-0.52(56)	2.11(12)	0.04(56)
^{54}Co	1.81(7)	-1.25(30)	2.06(7)	-0.17(30)
Average values:	2.08(24)	-0.09(104)	2.25(22)	0.66(97)

superallowed transition, along with their average values, are presented in Table 3.12. As can be seen from Figure 3.4a, the corrections δ_C of Towner, Hardy, and Harvey yield values of G_V/G_μ which are consistent for low Z ($Z < 21$) or high Z ($Z \geq 21$), but not both. The results of the calculations reported here are in this sense an improvement; the ratio G_V/G_μ for Z=17 is consistent with that for Z = 21 and 25. However, there are still large variations in this quantity, as those values for higher Z are still consistently smaller than those for lower Z. Unfortunately, even though the procedures used here represent an improvement over those of previous works, they do not as yet yield corrections δ_C which can lead to a test of the radiative correction $\Delta_\beta - \Delta_\mu$.

At present, the discrepancy between values of G_V/G_μ for high and low Z is not yet resolved. As was mentioned in the first chapter, possible causes of this discrepancy are experimental error in the ft values, an error in the evaluation of the "particle-physics" corrections δ_R, and of course the nuclear correction δ_C. There are, however, some clues in the present work which point to improvements that can be made in future calculations of δ_C. One important question is whether the model-space truncations in the 0f-1p shell are causing the calculated values of δ_{RO} to be too small. In the present work, only one nucleon is allowed outside the $0f_{7/2}$ orbit, causing the radial-overlap correction to be dominated by the integral $\Omega_{j,\pi}$ of particles in this orbit. Nucleons in this orbit, however, feel the effects of a strong centrifugal barrier. The effect of this barrier is to counteract Coulomb repulsion, thereby reducing the deviation from unity of the integral $\Omega_{j,\pi}$ relative to, say, the $0p_{3/2}$ orbit. Therefore, one might expect values of δ_{RO} to increase with an expanded shell-model configuration

space. Unfortunately, the large number of basis states that exist in even a moderately expanded configuration space (eg. four particles in the $0p_{3/2}$ orbit) renders the calculation of the spectroscopic factors $S(j,\Gamma,\pi)$ computationally impractical. With this in mind, it is necessary to turn to another source for the values $S(j,\Gamma,\pi)$, such as experimental data. A problem that arises with using experimental quantities, however, is that often these values are normalized arbitrarily, leading to some uncertainty in the application of eq.(3.2.7). Since values of δ_{RO} may be too small, it is therefore important to re-investigate these corrections for 0f-1p-shell nuclei, before turning to the possibility of experimental error in the ft values or other "particle-physics" corrections to explain the high- and low-Z discrepancy.

Chapter Four

4.1 Introduction

In this chapter, a comparison between predicted and experimentally observed isospin-forbidden Fermi transitions is presented. A schematic of the decay process under study here, the β-decay to a state which is not the analog of the parent as defined by eq.(1.1.4), is shown in the level diagram of Figure 1.5. The chapter is separated into two parts. In the first, a discussion on isospin-forbidden Fermi transitions between $J^{\pi}=0^{+}$ states is presented. For this class of decays the ft value gives a direct measurement of the forbidden Fermi matrix element. In the last section, the forbidden β^{+} decay of ^{24}Al is discussed. In this case, the Gamow-Teller matrix element is nonzero, and the transition rate does not directly give the small Fermi matrix element. Therefore, a comparison between theoretical and experimental values for the Fermi to Gamow-Teller mixing ratio is given.

4.2 Isospin-Forbidden $0^{+} \rightarrow 0^{+}$ Fermi Transitions

In this section, results for isospin-forbidden $0^{+} \rightarrow 0^{+}$ Fermi transitions are presented and compared with experimental results when these are available. Since these transitions are purely vector, i.e., the Gamow-Teller matrix element is zero, the measured ft value directly gives the forbidden Fermi matrix element, as

$$ft = \frac{K}{G_V^2 |M_F|^2}.$$

The quantities in this equation are $K = 2\pi^3 \ln 2 \hbar^7 c^6/(mc^2)^5$, the effective vector coupling constant G_V, and the Fermi matrix element M_F.

At present two isospin-forbidden $0^+ \rightarrow 0^+$ Fermi transitions have been examined experimentally. These are the β^+ decay of the T=1 ground state of ^{42}Sc to the 1.837 MeV, T=1 level in ^{42}Ca [Ing 77, Del 78, San 80, and Dae 85] and the β^- decay of the T=2 ground state of ^{28}Mg to the 0.972 MeV, T=1 level in ^{28}Al [Alb 79]. Values of $|M_F|^2$ obtained from the experimental ft values are shown in Table 4.1.

A shell-model calculation of the isospin-forbidden Fermi matrix element is done using eq.(3.2.7), except that the sum

$$\sum_{\text{orbits}} OBTD^T(j_n, j_p; \Delta J=0)\sqrt{[2j+1]}$$

is equal to zero. In addition, the radial-overlap contribution to the matrix element is generally quite small (typically $M_F(RO) \approx 10^{-4}$), and can be neglected. In this work, $|M_F|^2$ for the decay of ^{28}Mg and ^{42}Sc was evaluated using the 1s-0d shell and the $0d_{3/2}$ and $0f_{7/2}$ orbits, respectively. The corresponding isoscalar interactions are listed in Table 2.1, while the isovector and isotensor interactions were determined with the parameters given in Tables 2.7 and 2.15, respectively. In addition, the ^{42}Sc calculation was performed by allowing no more than four holes in the $0d_{3/2}$ orbit. The theoretical estimates for $|M_F|^2$ are compared with experimental results in Table 4.1. Although these values deviate somewhat from the experiment, they are of the right order of magnitude, and the ^{42}Sc value presented here is a significant improvement over the previous result of 31×10^{-4} obtained

Table 4.1

Comparison between theoretical and experimental values of the isospin-forbidden Fermi matrix elements for ^{28}Mg and ^{42}Sc.

Decaying Nucleus	$\|M_F\|^2 \times 10^{-4}$ Experiment	Theory
^{28}Mg	6.7 ± 0.8	14.4
^{42}Sc	9.4 ± 1.6[a]	5.7
^{34}Ar	-	4.6×10^{-4}
^{34}Cl	-	7.2

[a]The branching ratio of Daehnick and Rosa [Dae 85] was used to determine $|M_F|^2$.

by Towner [Tow 73a], in which the INC interaction was the same as that used for the calculation of the isospin-mixing correction, δ_{IM}, for the superallowed transition.

Although both the isospin-forbidden Fermi matrix element and the correction δ_{IM} are a measure of isospin-symmetry violation, they are in a sense measuring different quantities. For isospin-forbidden $0^+ \rightarrow 0^+$ T=1 decays, the Fermi matrix element is given by

$$|M_F|^2 = 2\,[a(\Gamma,T=1,T_Z-1) + a(\Gamma',T=1,T_Z)]^2,$$

where $a(\Gamma',T=1,T_Z)$ and $a(\Gamma,T=1,T_Z-1)$ are the mixing amplitudes between the ground state and the excited T=1 state in the parent and daughter nuclei, respectively. On the other hand, the contribution to δ_{IM} due to these two states is

$$\delta_{IM} = [a(\Gamma',T=1,T_Z) - a(\Gamma,T=1,T_Z-1)]^2.$$

Therefore, a measurement of the forbidden matrix element does not in general give an indication as to the value of δ_{IM} for the superallowed transition. For example, in the case for ^{42}Sc, the correction δ_{IM} for the superallowed transition is 0.109×10^{-2}, while the quantity $[a(\Gamma,T=1,T_Z-1) + a(\Gamma',T=1,T_Z)]^2$ determined for the forbidden decay above is 0.017×10^{-2}.

In addition to the transitions reported above, Fermi matrix elements for the β^+ decay of ^{34}Ar and ^{34}Cl to the first excited $J^\pi=0^+$, T=1 state in ^{34}Cl and ^{34}S, respectively, are also given in Table 4.1. Here we see that the matrix element for ^{34}Ar is essentially zero. The

reason for this small value can be seen in Table 3.12, where the mixing amplitude to the first excited state in both the parent and daughter nuclei is 36×10^{-4}. On the other hand, the forbidden matrix element for ^{34}Cl is rather large, and is primarily due to mixing in ^{34}S (see Table 3.12). This transition, however, is difficult to observe experimentally because of high-energy background γ-rays which are due to the β-decay of the $J^{\pi}=3^{+}$ metastable state in ^{34}Cl.

4.3 Isospin-Forbidden Fermi Transitions in ^{24}Al

In this section, a comparison between predicted and experimentally observed isospin-symmetry violation in the β-decay of ^{24}Al is presented. Here we are interested in the β-decay of the $J^{\pi}=4^{+}$, T=1 ground state of ^{24}Al to an excited $J^{\pi}=4^{+}$, T=0 state in ^{24}Mg. A schematic level diagram for this transition is shown in Figure 4.1. This transition has an allowed Gamow-Teller component, and an isospin-forbidden Fermi component which is due to mixing with the $J^{\pi}=4^{+}$, T=1 analog state in ^{24}Mg. The ft value for this transition is given by

$$ft = \frac{K}{G_V^2 |M_F|^2 + G_A^2 |M_{GT}|^2}, \qquad (4.3.1)$$

where G_A is the effective axial-vector coupling constant, and M_{GT} is the Gamow-Teller matrix element. Since the transition is predominantly Gamow-Teller, the transition rate will not in general provide an unambiguous measurement of the small Fermi matrix element. Therefore, it is necessary to measure a quantity which is sensitive to the Fermi to Gamow-Teller mixing ratio

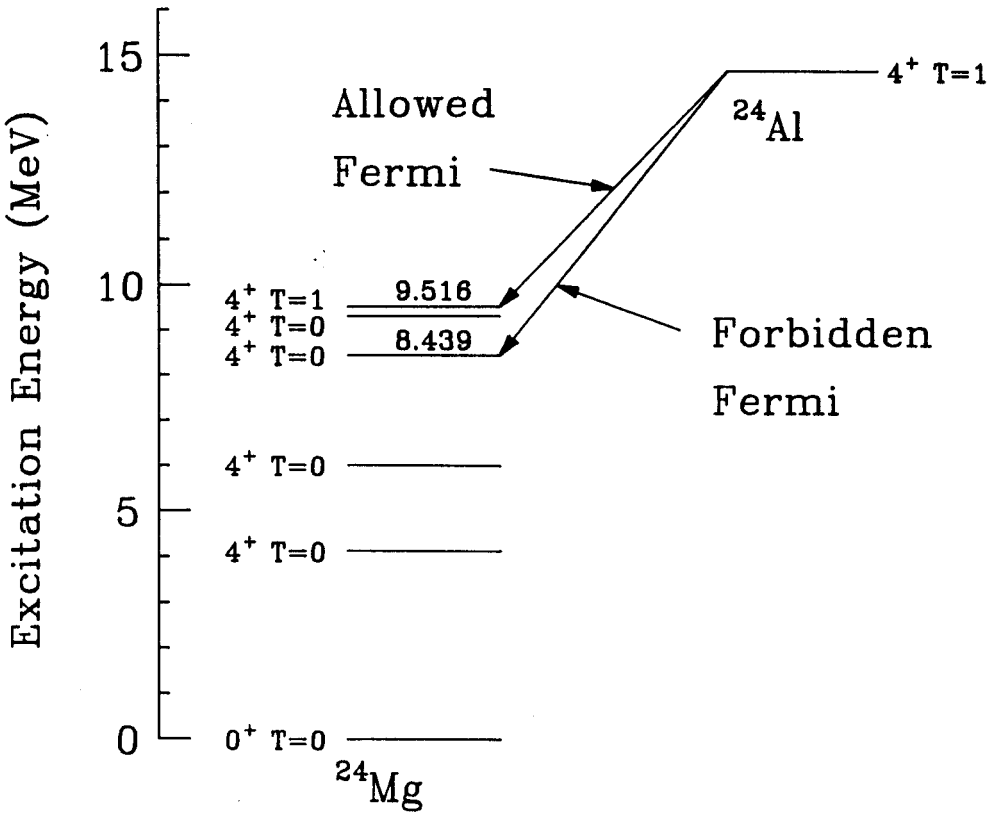

Figure 4.1: Level diagram indicating the allowed and forbidden Fermi transitions in ^{24}Al.

$$y = \frac{G_V M_F}{G_A M_{GT}}.$$

Such an experiment has been performed by Hoyle et al. [Hoy 83], who measured the asymmetry coefficient $\tilde{A}$ of the β-γ circular polarization correlation. The value found in this experiment was $\tilde{A} = -0.145 \pm 0.030$. This measured value, however, cannot be directly compared with theoretical estimates of y for the 8.439 MeV state in ^{24}Mg, because this level is fed by the γ-decay of the 9.516 MeV level. In the measurement mentioned above, it was found that, for each time the 8.438 MeV level is directly produced by the β-decay of ^{24}Al, it was fed $f = 0.303 \pm 0.019$ times by the β-decay to the 9.516 MeV state. The observed asymmetry coefficient $\tilde{A}$ is given in terms of the coefficients $\tilde{A}_8$ and $\tilde{A}_9$ by

$$\tilde{A} = \frac{1}{1 + f} [\, \tilde{A}_8 + f\, \tilde{A}_9],$$

where the subscripts 8 and 9 denote the 8.439 and 9.516 MeV states, respectively. The coefficients $\tilde{A}_8$ and $\tilde{A}_9$ are given by [Hoy 83]

$$\tilde{A}_8 = \frac{1}{1 + y_8^2} \left[-\frac{1}{12} + \frac{\sqrt{5}}{3} y_8 \right], \qquad (4.3.2a)$$

$$\tilde{A}_9 = \frac{0.95}{1 + y_9^2} \left[-\frac{1}{12} + \frac{\sqrt{5}}{3} y_9 \right]. \qquad (4.3.2b)$$

To calculate the asymmetry coefficients we start with the states $\Psi_0(8)$ and $\Psi_0(9)$ which are eigenstates of the isoscalar Hamiltonian. In the presence of the INC interaction these two states mix, giving

$$\Psi(8) = \alpha\Psi_0(8) - \beta\Psi_0(9),$$

$$\Psi(9) = \beta\Psi_0(8) + \alpha\Psi_0(9),$$

where

$$\alpha^2 + \beta^2 = 1.$$

The relationship between the mixing amplitude β and the matrix element $V_{8,9} = \langle\Psi_0(8)| V_{INC} |\Psi_0(9)\rangle$ is

$$V_{8,9} = \sqrt{[1-\beta^2]}\beta\Delta E, \qquad (4.3.3)$$

where $\Delta E = (9.516 - 8.439)$ MeV. The Fermi and Gamow-Teller matrix elements for these mixed states become

$$M'_F(8) = \beta\sqrt{2}, \qquad M'_{GT}(8) = \alpha M_{GT}(8) - \beta M_{GT}(9), \qquad (4.3.4a)$$

$$M'_F(9) = \sqrt{[2(1 - \delta_C)]}, \qquad M'_{GT}(9) = \beta M_{GT}(8) + \alpha M_{GT}(9), \qquad (4.3.4b)$$

where δ_C is the total isospin-mixing correction for the allowed Fermi transition. Theoretical values for the Gamow-Teller matrix elements are [Bro 83 and Bro 85]

$$g_A M_{GT}(8) = -0.8790,$$

$$g_A M_{GT}(9) = 0.0850,$$

where $g_A = G_A/G_V$.

The isospin-mixing matrix element was evaluated with proton-neutron shell-model wave functions, and the total Hamiltonian was obtained by adding the sd-shell INC interaction determined with the parameters given in Tables 2.7 and 2.15 onto the mass-dependent sd-shell Hamiltonian of Wildenthal. Due to the large number of $J^\pi=4^+$ states in a proton-neutron calculation, a truncation based on the monopole energy of the diagonal matrix elements was applied. Using this truncation, the number of 4^+ states in ^{24}Mg was reduced from the full space value of 15089 to 3113. The mixing matrix element $V_{8,9}$ was then determined by evaluating the direct overlap $\langle\Psi_0(9)|\Psi(8)\rangle$ and inverting eq.(4.3.3), giving $V_{8,9}$ = -66.0 keV.

The correction δ_C to the allowed Fermi transition was evaluated using the procedure outlined in Chapter Three. The values are δ_{RO} = 0.14% and $\delta_{IM} = 1 - \beta^2 = 0.38\%$, giving $\delta_C = 0.52\%$.

Before evaluating the asymmetry coefficients $\tilde{A}_8$ and $\tilde{A}_9$, it is instructive to compare theoretical and experimental values of the Fermi and Gamow-Teller matrix elements. Values of $|M'_F|^2 + g_A|M'_{GT}|^2$ determined from experimental ft values are 0.722±0.034 [War 81] and 1.977±0.020 [Ade 85] for the β-decay to the 8.439 and 9.516 MeV states, respectively. Theoretical values for these transitions are 0.786 and 1.991. The theoretical value for the allowed Fermi transition to the 9.516 MeV state is in good agreement with the experimental value. The theoretical value for the 8.439 MeV level, however, is significantly larger than the experimental result. Since $M_{GT}(8)$ and $M_{GT}(9)$ add coherently in eq.(4.3.4a) (β = -0.0614) and $M_{GT}(8)$ dominates the total value of $|M'_F|^2 + g_A|M'_{GT}|^2$, it is not unreasonable to suspect that $M_{GT}(8)$

is too large. Therefore, we renormalize $M_{GT}(8)$ to reproduce the experimental ft value, giving $g_A M_{GT}(8) = -0.867 \pm 0.020$. The Fermi to Gamow-Teller mixing ratios are then

$$y_8 = -0.107 \pm 0.002,$$

$$y_9 = 44.0 \pm 1.2,$$

and the asymmetry coefficients $\tilde{A}_8$ and $\tilde{A}_9$ are:

$$\tilde{A}_8 = -0.162 \pm 0.001,$$

$$\tilde{A}_9 = 0.015 \pm 0.001.$$

The total asymmetry coefficient is then $\tilde{A} = -0.121 \pm 0.001$, which is in fair agreement with the experimental value of -0.145 ± 0.030. Taking $M_{GT}(9) = 0.0$ and assuming $\delta_{RO} = 0.0$, Hoyle et al. [Hoy 83] determined the isospin-mixing matrix element between the 8.439 and 9.516 MeV levels to be 106 ± 40 keV. The theoretical value for this quantity given above is in agreement with this measurement.

In addition, to the transition mentioned above, the isospin-forbidden Fermi component has also been measured in the β^- decay of ^{24}Na to the 4.123 MeV $J^\pi = 4^+$, T=0 state in ^{24}Mg [Ram 75]. This transition gives an isospin-mixing matrix element between the 4.123 MeV, T=0 state and 9.516 MeV, T=1 level of 5.4 ± 2.2 keV. Using the INC interaction of the present work, this matrix element is found to be 10.4 keV. The explanation for the large isospin-mixing matrix element for the 8.439

MeV state relative to that of the 4.123 MeV level is that the former state is thought to be the anti-analog of the 4^+, T=1 state in ^{24}Mg.

It should also be pointed out that the calculations presented here were performed within a truncated shell-model space. It would therefore be interesting at some point to examine the effects of the model-space truncations on the results reported above.

Chapter Five

5.1 Introduction

In this chapter, the decay of T=3/2 states in A=4n+1 ($21 \leq A \leq 37$) nuclei to the $J^{\pi}=0^{+}$, T=0 ground state in A=4n nuclei by proton and neutron emission is discussed. As was mentioned in the first chapter, this decay process is forbidden in first order because it violates isospin symmetry, and can only take place by mixing T=1/2 states into the T=3/2 parent state, or by mixing T=1 and 2 states with the T=0 daughter ground state. One of the most striking features of these decays is that the experimentally determined spectroscopic amplitudes, θ^{p}_{INC}, exhibit an oscillation with period $\Delta A=8$ (see Figure 1.6). The cause of this oscillation is not yet understood. In this work, contributions to $\theta^{p(n)}_{INC}$ due to mixing with individual states in both the parent and daughter nuclei are studied with the hope that some indication as to cause of this oscillation might be given.

The organization of this chapter is as follows. In the second section, the perturbation theory expansion for $\theta^{p(n)}_{INC}$ is derived, and a discussion about one of the principal uncertainties in the calculation of $\theta^{p(n)}_{INC}$ is presented. In the third section, the method used to determine the isospin-mixing matrix elements is described. Results of a calculation of $\theta^{p(n)}_{INC}$ for A = 21, 25, 29, 33, and 37 nuclei are presented in the fourth section. In the fifth section, θ^{p}_{INC} for the lowest $J^{\pi}=1/2^{+}$, T=3/2 state in ^{33}Cl is evaluated using experimental values for the excitation energies of the nearby T=1/2 states and the allowed spectroscopic amplitudes of these states and of the lowest T=1/2 state (this is the only case under investigation in the present work in which

these quantities have been measured experimentally). In section six, a recently developed procedure for determining the decay width Γ from the spectroscopic amplitudes is discussed, along with the application of this method to the decay of the $J^{\pi}=1/2^{+}$, T=3/2 state in ^{33}Cl. Finally, suggestions for future work are given in the seventh section.

5.2 Isospin-Forbidden Spectroscopic Amplitude $\Theta^{p(n)}_{INC}$

A calculation of the spectroscopic amplitude $\Theta^{p(n)}_{INC}$ starts with the isospin-mixed states, $\Psi(\Gamma,J,T_Z)$, which are eigenstates of the total Hamiltonian, i.e. $[H^{(0)} + V^{(1)}_{INC} + V^{(2)}_{INC}]\ |\Psi(k)> = E(k)\ |\Psi(k)>$, and have definite angular momentum J and z-projection of the isospin T_Z (all other relevant quantum numbers are represented by Γ). The spectroscopic amplitude which connects the parent and daughter states $\Psi(\Gamma,J,T_Z+\mu)$ and $\Psi(\Gamma',J',T_Z)$ is given by [Bru 77]

$$\Theta^{\mu}_{INC}(\Gamma,J;\Gamma',J';j_{\mu})$$

$$= \frac{1}{\sqrt{[2J+1]}} <\Psi(\Gamma,J,T_Z+\mu)||\ a^{\dagger}_{j\mu}\ ||\Psi(\Gamma',J',T_Z)> \quad (5.2.1)$$

where $a^{\dagger}_{j\mu}$ creates a nucleon with z-component of the isospin μ in an orbit with angular momentum j.

Since the transitions of interest are isospin-forbidden, it is useful to expand the isospin-mixed states Ψ in terms of wave functions with good isospin, $\Psi_0(\Gamma,J,T,T_Z)$, which satisfy the eigenvalue equation $H^{(0)}\ |\Psi_0(i)> = E_0(i)\ |\Psi_0(i)>$, giving

$$\Psi(i) = N(i)\Psi_0(i) + \sum_{k\neq i} a(i;k)\Psi_0(k). \qquad (5.2.2)$$

Inserting eq.(5.2.2) into eq.(5.2.1) and specializing to the decay of T=3/2 states to the $J^{\pi}=0^{+}$ T=0 daughter ground state we have

$$\Theta^{\mu}_{INC}(\Gamma,J;\Gamma',J'=0;j_{\mu}) =$$

$$\sum_{\gamma\neq\Gamma} N(\Gamma',J',T=0,T_Z)\; a(\Gamma,T=3/2;\gamma,T=1/2)\; \Theta^{\mu}(\gamma,J,T=1/2;\Gamma',J'=0,T'=0;j_{\mu})$$

$$+ \sum_{\gamma'\neq\Gamma'} \sum_{T'=1}^{2} N(\Gamma,J,T=3/2,T_{Z+\mu})\; a(\Gamma',T=0;\gamma',T')$$

$$\times\; \Theta^{\mu}(\Gamma,J,T=3/2;\gamma',J'=0,T';j_{\mu}), \qquad (5.2.3)$$

where the allowed spectroscopic amplitudes Θ^{μ} in the right-hand side of eq.(5.2.3) are given by eq.(5.2.1), with Ψ replaced by Ψ_0. The first sum in eq.(5.2.3) is the contribution to $\Theta^{p(n)}_{INC}$ due to mixing between T=3/2 and T=1/2 parent states, while the second is that due to mixing between the T=0 ground state and T=1 and 2 daughter states.

In first-order nondegenerate perturbation theory the mixing amplitudes $a(\Gamma_1,T_1;\Gamma_2,T_2)$ are given by

$$a(\Gamma_1,T_1;\Gamma_2,T_2) = \frac{\langle\Psi_0(\Gamma_1,J,T_1,T_Z) \mid V_{INC} \mid \Psi_0(\Gamma_2,J,T_2,T_Z)\rangle}{E(\Gamma_1,J,T_Z) - E(\Gamma_2,J,T_Z)}, \qquad (5.2.4)$$

where $V_{INC} = V^{(1)}_{INC} + V^{(2)}_{INC}$. From equations (5.2.3) and (5.2.4) it is clear that $\Theta^{p(n)}_{INC}$ is sensitive to those T=1/2 parent states whose excitation

energies are comparable with the T=3/2 state. There are at least three sources of uncertainty in these nearby states which can influence the calculation of $\theta_{INC}^{p(n)}$. These are:

(1) the exact location of these states relative to the T=3/2 parent,

(2) their allowed spectroscopic amplitudes $\theta^{p(n)}$, and

(3) their isospin-mixing matrix element with the T=3/2 state.

Unfortunately, the exact location of these states relative to the T=3/2 parent and the allowed amplitudes $\theta^{p(n)}$ are uncertain both experimentally and theoretically. At present, these quantities have been determined experimentally for only one of the cases considered in this work [Iko 76], and this case will be discussed in detail in section 5.5. Unfortunately, there is no reliable way of estimating the uncertainty in theoretical values of the allowed spectroscopic amplitudes. On the other hand, theoretical estimates of excitation energies are generally uncertain by several hundred keV (for example, excitation energies obtained with the mass-dependent sd-shell Hamiltonian of Wildenthal are uncertain by at least 150 keV for low lying states [Wil 84]). In the present work, the effects of this uncertainty are studied by shifting the T=1/2 excitation energies relative to the T=3/2 state, and then, by evaluating eq.(5.2.3) estimate the theoretical uncertainty in $\theta_{INC}^{p(n)}$ due to the unknown location of the nearby T=1/2 states. As was mentioned in Chapter Two, there are two isovector interactions which can be applied in the 1s-0d shell. It was shown in Chapter Three, that for A=21, the isospin-mixing matrix elements obtained with these interactions differ

on the average by 8.5 keV. Therefore, it is also necessary to determine what effects these alternative interactions have on the final result. This is done by comparing values of $\theta_{INC}^{p(n)}$ obtained using both interactions for the case in which the most experimental information is known, and is presented in section 5.5.

5.3 Isospin-Mixing Matrix Elements

One method to evaluate the isospin-mixing matrix elements appearing in eq.(5.2.4) is that used to calculate the b- and c-coefficients in Chapter Two. The reduced many-body matrix element of V_{INC} is then

$$\langle\Psi_0(\Gamma_1,J,T_1,T_Z)||\ V_{INC}\ ||\Psi_0(\Gamma_2,J,T_2,T_Z)\rangle =$$

$$\sum_{\text{orbits}} OBTD(\rho,\rho')\ \langle core,\rho||\ V_{INC}\ ||core,\rho'\rangle +$$

$$\sum_{\text{orbits}} TBTD(\rho_1,\rho_2;\lambda_{12}:\rho_3,\rho_4;\lambda_{34})\langle\rho_1,\rho_2;\lambda_{12}||\ V_{INC}\ ||\rho_3,\rho_4;\lambda_{34}\rangle, \quad (5.3.1)$$

where again the one-body (OBTD) and two-body (TBTD) transition density matrices are given by eq.(2.2.7) (note that the matrix elements of the creation and annihilation operators are reduced only in angular momentum space and that $\sqrt{(2\lambda+1)} = \sqrt{(2J+1)}$).

The principal drawback of this procedure is that it involves the calculation of OBTD and TBTD matrices for each isospin-mixing amplitude appearing in eq.(5.2.3). This is a difficult and often time consuming process. Another, and perhaps easier, procedure is to evaluate the direct overlap $\langle\Psi_0(k)|\Psi(i)\rangle = a(i;k)$, and, by inverting eq.(5.2.4)

obtain the isospin-mixing matrix element. Care, however, must be exercised when applying eq.(5.2.4) to states in which $\Delta E(i;k) = E(i) - E(k)$ is small. This difficulty can be avoided by noting that the matrix element $V_{ik}=\langle\Psi_0(i)|\ V_{INC}\ |\Psi_0(k)\rangle$ is generally small relative to $\Delta E(i;k)$, and that the mixing between these two states can be approximated by a two-level mixing model.

In this two-level model the mixed states $\Psi(i)$ and $\Psi(k)$ are given by

$$\Psi(i) = N(i)\Psi_0(i) + a(i;k)\Psi_0(k),$$

$$\Psi(k) = a(k;i)\Psi_0(i) + N(k)\Psi_0(k), \qquad (5.3.2)$$

where $N(i) = N(k) = N$, and $a(i;k) = -a(k;i) = a = V_{ik}/[N(E(i) - E(k))]$. Noting that $N = [1 - a^2]^{1/2}$, we have

$$a(i;k) = \frac{1}{\sqrt{2}}\left[1 - \left\{1 - 4\left(V_{ik}/\Delta E(i;k)\right)^2\right\}^{1/2}\right]^{1/2} \qquad (5.3.3)$$

where the sign of $a(i;k)$ is the same as the ratio $V_{ik}/\Delta E(i;k)$.

One indication of the validity of applying the two-level model to determine V_{ik} is the condition $a(i;k) \approx -a(k;i)$. Shown in Table 5.1 are values of $a(i;k)$ obtained for the lowest ten $J^\pi=1/2^+$ states in ^{21}Na (these values are typical for all the nuclei studied in the present work). The shell-model configuration space used for this calculation was the 1s-0d shell, and the total Hamiltonian was obtained by adding isovector and isotensor interactions determined with the parameters given in Tables 2.4 and 2.14 onto the mass-dependent sd-shell Hamiltonian of Wildenthal. As can be seen from the table, the condition

Table 5.1

Mixing amplitudes $a(i;k) = \langle \Psi_0(k) | \Psi(i) \rangle$ for the ten lowest $J^\pi = 1/2^+$ states in ^{21}Na.

		k	1	2	3	4	5	6	7	8	9	10
i	E(i)	T	1/2	1/2	1/2	1/2	3/2	1/2	1/2	1/2	1/2	3/2
1	0.000		1.0000	0.0045	0.0024	0.0001	-0.0025	0.0017	0.0009	0.0001	0.0001	-0.0026
2	2.986		-0.0045	0.9999	-0.0059	-0.0018	-0.0040	-0.0060	0.0009	0.0010	0.0011	0.0005
3	4.191		-0.0024	0.0059	0.9999	-0.0039	0.0086	0.0037	0.0004	-0.0014	-0.0015	0.0016
4	6.074		0.0001	0.0021	0.0031	0.9951	0.0966	-0.0064	-0.0150	-0.0013	-0.0033	0.0043
5	6.141		0.0024	0.0038	-0.0090	-0.0960	0.9947	0.0138	0.0306	0.0040	-0.0036	-0.0008
6	6.666		-0.0018	0.0059	-0.0036	0.0077	-0.0132	0.9998	0.0001	0.0012	-0.0030	-0.0011
7	7.254		-0.0010	-0.0010	-0.0001	0.0178	-0.0289	-0.0006	0.9990	-0.0248	0.0019	-0.0041
8	7.795		-0.0001	-0.0010	0.0014	0.0021	-0.0046	-0.0013	0.0247	0.9995	0.0046	0.0082
9	9.558		0.0001	-0.0011	0.0015	0.0030	0.0040	0.0029	-0.0021	-0.0045	0.9996	-0.0137
10	9.725		0.0027	-0.0005	-0.0016	-0.0042	0.0003	0.0012	0.0040	-0.0084	0.0138	0.9997

Table 5.2

Comparison between isospin-mixing matrix elements V_{ik} evaluated with perturbation theory (eq.(5.3.1)) and the two-level model.

k	Perturbation Theory (keV)	Two-Level Model (keV)
1	15.0	14.8
2	12.6	12.0
3	-16.6	-17.5
4	-6.7	-6.4
5	-7.1	-7.2
6	-32.1	-34.0
7	-6.7	-6.6
8	13.4	12.3

$a(i;k) \approx -a(k;i)$ is generally satisfied. In addition, the average deviation of matrix elements V_{ik} and V_{ki} evaluated with $a(i;k)$ and $a(k;i)$, respectively, is only 0.6 keV.

An additional, and perhaps better indication of the validity of the two-level model is a comparison between values of V_{ik} obtained with eq.(5.3.1) and the two-level mixing approximation. Shown in Table 5.2 is such a comparison for the isospin-mixing matrix elements for the lowest $J^{\pi}=1/2^{+}$ T=3/2 state in ^{21}Na. The rms deviation between the two-level model and perturbation theory values is 0.8 keV. This, coupled with the results given above, indicates that the mixing due to V_{INC} can be approximated by the two-level mixing model without loss of accuracy.

5.4 Results for $\Theta^{p(n)}_{INC}$

In this section, the results of a calculation of the isospin-forbidden spectroscopic amplitudes $\Theta^{p(n)}_{INC}$ are presented and compared with experiment. $\Theta^{p(n)}_{INC}$ was evaluated using the perturbation expansion of eq.(5.2.3), where typically 20-30 states in both the parent and daughter nuclei were included in the sum. The wave functions $\Psi_0(i)$ and the allowed spectroscopic amplitudes $\Theta^{p(n)}$ were obtained with the Oxford-Buenos Aires-MSU shell-model code. The shell-model configuration space consisted of the $0d_{5/2}$, $1s_{1/2}$, and $0d_{3/2}$ orbits, and the total Hamiltonian was obtained by adding the isovector and isotensor interactions (determined with the parameters given in Tables 2.4 and 2.14) onto the mass-dependent sd-shell Hamiltonian of Wildenthal. In addition, the validity of the perturbation expansion was verified by comparing the values obtained with eq.(5.2.1) with those of eq.(5.2.3).

Due to the large number of basis states that occur in proton-neutron formalism for nuclei in the middle of the 1s-0d shell, some model-space truncations for A=25 and 29 were necessary. The truncations were made according to the monopole energy of the diagonal matrix elements, and were selected so that the calculations of the $J^{\pi}=5/2^{+}$ states were feasible (the number of $5/2^{+}$ states in A=29 were reduced from the full space value of 12878 to 2236). The excitation energies obtained with these truncations were found to deviate systematically from the full space values [Wil 84]. To account for these effects of the model-space truncations, the T=1/2 excitation energies used to evaluate the isospin-mixing amplitude (eq.(5.3.3)) were shifted relative to the ground state by the average deviation from the full-space values.

Shown in Table 5.3 are the results obtained for θ^{p}_{INC} for the decay of the lowest T=3/2 state in each nucleus. Tabulated are the individual contributions in eq.(5.2.3) due to the lowest T=1 and 2 daughter states, the lowest T=1/2 parent state, and those T=1/2 states which are within ±500 keV of the T=3/2 state (except for A=37, where the contribution due to the two closest T=1/2 states is given). The isospin-mixing amplitudes were obtained by first determining the matrix elements V_{ik} from the direct overlaps $\langle\Psi_0(k)|\Psi(i)\rangle$, and then evaluating eq.(5.3.3) using experimental T=3/2 excitation energies. Since experimental T=1/2 excitation energies are generally unknown, theoretical values for these states were used. The states shown in the table are the principal contributors to the total value; the remaining contributions are typically less than unity and tend to cancel with one another. In addition, note that contributions due to mixing in the daughter nucleus

Table 5.3

Contribution to θ^{p}_{INC} (×1000) for the lowest J^{π} T=3/2 state due to mixing with states in the parent (T=1/2) and daughter (T=1 and 2). For the T=3/2 state the experimental excitation energy E_x (MeV) is given, while theoretical excitation energies (in MeV) for the remaining states are given. The sum of contributions due to states listed is given, as well as the total which includes essentially all states in the parent and daughter nuclei.

	^{21}		^{25}		^{29}		^{33}		^{37}	
J^{π} E_x	$5/2^+$	8.970	$5/2^+$	7.898	$5/2^+$	8.384	$1/2^+$	5.548	$3/2^+$	5.052
T	E_x	θ_{INC}	E_x	θ_{INC}	E_x	θ_{INC}	E_x	θ_{INC}	E_x	θ_{INC}
1	13.61	0.0	12.84	-0.1	10.71	-0.7	7.32	2.3	10.87	3.6
2	16.57	-2.3	15.28	-2.4	15.23	-1.6	11.99	3.5	15.50	0.2
1/2	0.24	1.6	0.00	1.1	1.96	1.2	0.82	-4.4	0.00	-1.7
1/2	8.58	1.8	7.61	-0.1	7.71	0.0	5.60	8.4	5.06	-15.3
1/2	9.06	4.2	7.81	2.4	8.31	0.2	6.02	2.7	6.83	0.0
1/2	-	-	7.87	1.1	8.54	7.4	-	-	-	-
1/2	-	-	8.30	2.4	-	-	-	-	-	-
1/2	-	-	8.37	0.1	-	-	-	-	-	-
SUM		5.3		4.5		6.5		12.5		-13.2
TOTAL		5.3		5.8		7.0		12.1		-13.7

and the lowest T=1/2 state tend to cancel, thereby amplifying the importance of contributions due to nearby T=1/2 states.

As can be seen from Table 5.3, those states which lie within ±500 keV of the T=3/2 state contribute significantly to the total. As was mentioned in section 5.2, however, the exact location of these T=1/2 states relative to the T=3/2 state is uncertain both experimentally and theoretically. Therefore, it is necessary to determine how sensitive $\theta_{INC}^{p(n)}$ is to the uncertainty in the T=1/2 energy spectrum. This is done in the present work by shifting the T=1/2 energy spectrum by an amount $\delta\varepsilon$, and evaluating $\theta_{INC}^{p(n)}$ using eq.(5.2.3), giving $\theta_{INC}^{p(n)}(\delta\varepsilon)$. The "best" estimate of $\theta_{INC}^{p(n)}$ is then the unweighted average of the values $|\theta_{INC}^{p(n)}(\delta\varepsilon)|$ obtained within a total interval $\pm\Delta E$ (note that experiments are sensitive only to the absolute value of $\theta_{INC}^{p(n)}$). The uncertainty in the calculation of $\theta_{INC}^{p(n)}$ can then be estimated by evaluating the upper and lower rms deviations of the values obtained at each increment $\delta\varepsilon$ from the average value. In the present work ΔE was taken to be 500 keV, and sufficient accuracy was achieved by choosing the increment for $\delta\varepsilon$ to be 10 keV.

As an additional illustration of the importance of the location of nearby T=1/2 parent states, the value $|\theta_{INC}^{p}|$ is plotted as a function of $\delta\varepsilon$ in Figure 5.1 for the lowest $J^{\pi}=1/2^{+}$ T=3/2 state in ^{33}Cl. Here it is seen that as $\Delta E=(E(T=3/2) - E(k,T=1/2))$ becomes smaller, θ_{INC}^{p} gets larger, with the maximum value being approximately $\sqrt{(2)}\ \theta^{p}(k,T=1/2)$.

A comparison between experimental data and the calculated values is shown in Table 5.4 and Figure 5.2. The experimental results were determined from (n,n) [Wei 76 and Hin 84] and (p,p) [McD 69 and Wil 83]

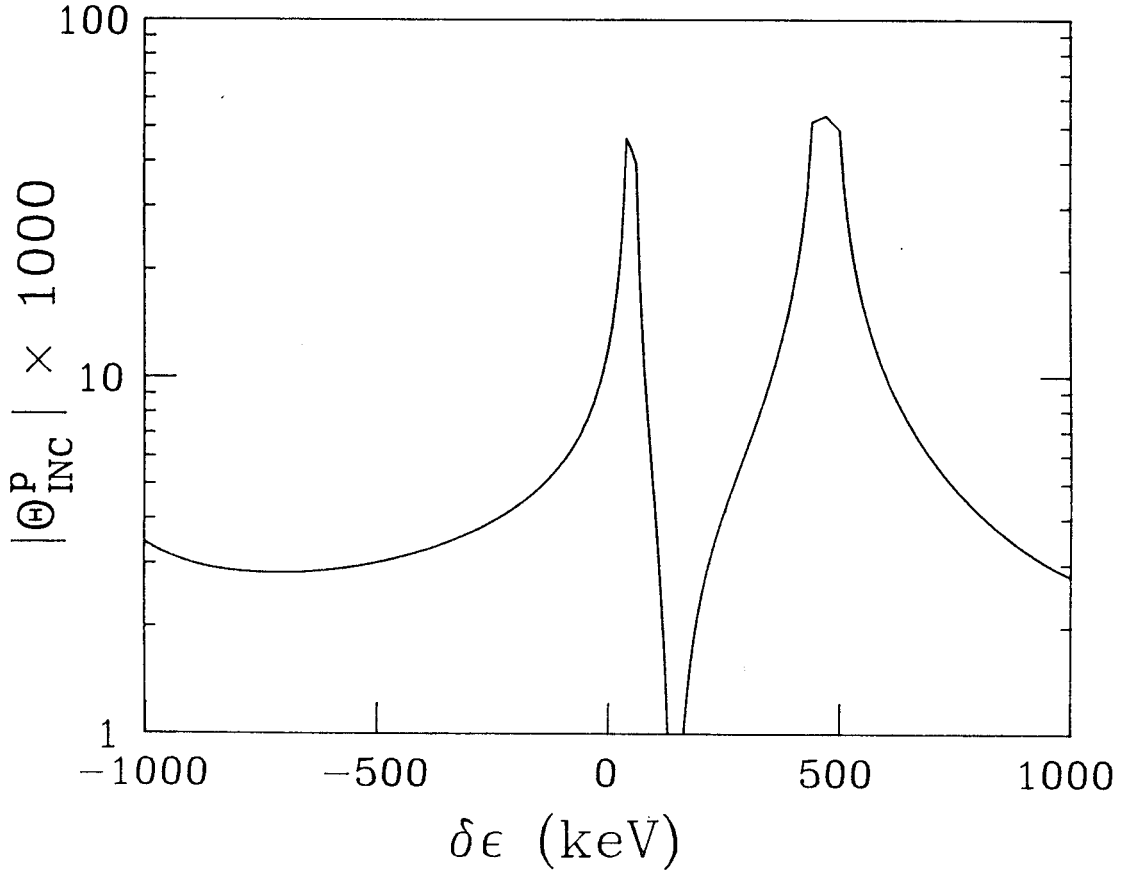

Figure 5.1 Plot of Θ^{p}_{INC} as a function of the T=1/2 excitation energy shift $\delta\epsilon$ for the decay of the lowest $J^{\pi}=1/2^{+}$, T=3/2 state in ^{33}Cl.

Table 5.4

Comparison between calculated and experimental values of $\theta_{INC}^{p(n)} \times 1000$ for the lowest T=3/2 state of each spin, 2J = 5, 1, and 3.

		Protons			Neutrons		
A	J^{π}	E_x(MeV)	Exp	Calculated	E_x(MeV)	Exp	Calculated
	$5/2^+$	8.970	$7.4^{+0.3}_{-1.6}$	$6.1^{+10.2}_{-3.5}$	8.860	11.5 ± 1.2	$4.9^{+10.5}_{-3.3}$
21	$1/2^+$	9.219	10.9 ± 1.5	$7.4^{+15.0}_{-4.6}$	9.140	22.3 ± 1.5	$10.7^{+14.1}_{-6.3}$
	$3/2^+$	10.825	-	$1.7^{+2.2}_{-1.0}$	10.726	7.8 ± 1.1	$1.4^{+1.9}_{-0.5}$
	$5/2^+$	7.898	3.1 ± 0.3	$6.4^{+10.9}_{-3.5}$	7.786	6.4 ± 0.4	$2.9^{+9.4}_{-1.9}$
25	$1/2^+$	8.858	-	$9.9^{+11.8}_{-5.9}$	8.810	-	$7.5^{+9.1}_{-3.3}$
	$3/2^+$	7.968	11.2 ± 0.3	$11.1^{+12.6}_{-8.8}$	7.867	-	$10.8^{+12.2}_{-5.4}$
	$5/2^+$	8.384	11.6 ± 0.1	$3.6^{+10.6}_{-2.6}$	8.331	-	$0.6^{+1.5}_{-0.5}$
29	$1/2^+$	9.659	18.2 ± 0.2	$5.7^{+15.7}_{-3.5}$	9.678	-	$7.0^{+13.0}_{-3.8}$
	$3/2^+$	10.480	5.3 ± 0.3	$4.1^{+8.8}_{-2.3}$	10.498	-	$3.6^{+6.3}_{-2.7}$
	$5/2^+$	7.390	9.6 ± 0.1	$2.9^{+4.3}_{-1.8}$	7.337	-	$3.0^{+4.5}_{-1.2}$
33	$1/2^+$	5.548	7.5 ± 0.3	$8.1^{+18.5}_{-4.3}$	5.475	-	$21.7^{+27.4}_{-9.7}$
	$3/2^+$	6.848	11.8 ± 1.8	$7.1^{+12.4}_{-5.0}$	6.903	-	$4.8^{+29.1}_{-3.7}$
	$5/2^+$	8.071	-	$0.2^{+1.3}_{-.01}$	8.066	-	$2.7^{+4.2}_{-1.5}$
37	$1/2^+$	6.692	12.9 ± 3.7	$0.7^{+0.2}_{-0.4}$	6.657	-	$1.0^{+1.2}_{-0.4}$
	$3/2^+$	5.052	16.8 ± 1.2	$2.1^{+4.0}_{-1.0}$	4.993	-	$4.0^{+9.1}_{-2.1}$

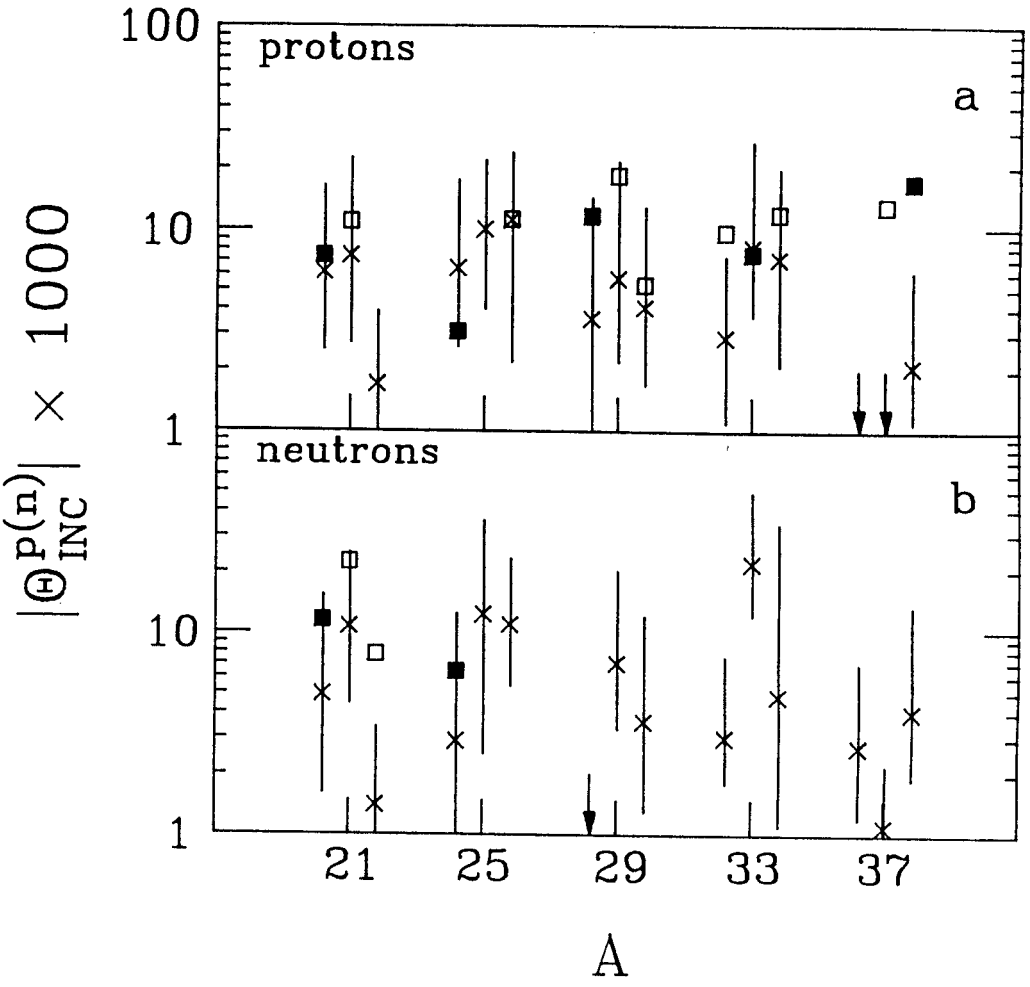

Figure 5.2: Comparison between experimental and theoretical spectroscopic amplitudes for the isospin-forbidden decay of the T=3/2 states by (a) proton emmision and (b) neutron emission. For each A, one value of each spin is given and is plotted in the order: 2J = 5, 1, 3. Experimental data are represented by squares (filled in for the lowest T=3/2 state for each A, and open for the remaining states). Crosses with error bars denote the "best" estimate and its upper and lower limits as described in the text.

resonance data. The conventional method of relating the spectroscopic amplitudes to the decay width Γ_μ, which is also used in previous works (eg. [Wil 83 and Hin 84]), is that θ^μ is given by

$$\theta^\mu = \frac{\Gamma_\mu}{2 P_C \gamma_{sp}^2}, \qquad (5.4.1)$$

where the penetration factor P_C removes the angular momentum and kinematic factors from the width Γ_μ and γ_{sp}^2 is the single-particle reduced width. In this work, as in that of Wilkerson et al., the value $\gamma_{sp}^2 = \hbar/MR^2$ was used, where $M = A/(A+1)$ and $R = 1.4A^{1/3}$fm. There is some uncertainty in this method, however, as 1.5 times this value has been used by Hinterberger et al. [Hin 84]. This uncertainty, however, should be systematic and tend to shift all experimental values by the same amount. Experimental errors are typically less than 10% and have been suppressed from the figure. Experimental excitation energies for the T=3/2 states were used to evaluate the isospin-mixing amplitudes given by eq.(5.3.3). In the absence of experimental values, excitation energies of the analog states in the neighboring $T_Z = -3/2$ (neutron rich) nuclei were used. The excitation energies of the T=3/2 states are given in Table 5.4.

In Figure 5.2, it is seen that there is generally good agreement between experimental and calculated values, with the noted exception of A=37. This disagreement, however, is most likely due to nearby T=1/2 0f-1p-shell configurations which are not included in the calculations. The results show that θ_{INC}^p is roughly constant as a function of A, with seemingly random fluctuations about this constant value. This is consistent with the known experimental data. Although the data for the

lowest T=3/2 states in each nucleus show an oscillation with period $\Delta A=8$, the data for the remaining T=3/2 states fail to show this feature. Our results indicate that the observed variations in θ^{p}_{INC} are due to the precise location of the nearby T=1/2 states, and that the oscillation in the lowest T=3/2 states is, in fact, part of these "random" variations.

Any difference between θ^{p}_{INC} and θ^{n}_{INC} that is not due to the different energy denominators used in eq.(5.3.3) is attributable to the charge-dependent (isotensor) part of the INC interaction, as the charge-asymmetric (isovector) part can only produce $\Delta T=1$ mixing, and would therefore give identical spectroscopic amplitudes for both proton and neutron emission. Although there is relatively little data available for neutron emission (see Figure 5.2b), some comparisons can still be made. First, the neutron amplitudes are on the order of 2 to 3 times greater than their proton counterparts. This is consistent with results obtained for $A \leq 17$ [McD 78]. The calculated values of $\theta^{p(n)}_{INC}$ do not show a systematic asymmetry between the proton and neutron spectroscopic amplitudes, although individual cases may differ significantly. A comparison between the calculated and experimental values for the neutron decays (see fig. 5.2b) indicates that the theoretical values of θ^{n}_{INC} are perhaps smaller than experiment. To fully determine this, however, more experimental data are necessary.

The forbidden amplitudes for higher excited states have also been evaluated and are shown in Table 5.5 and Figure 5.3. The calculations indicate that $\theta^{p(n)}_{INC}$ tends to decrease slightly as a function of excitation energy and fluctuates in the same manner as the lower states. This is in agreement with experiment [Wil 83]. Although the density of background states is higher, and the isospin-mixing matrix elements are

Table 5.5

Comparison between calculated and experimental values of $\theta_{INC}^{p(n)} \times 1000$ for the second T=3/2 state of each spin, 2J = 5, 1, and 3.

		Protons			Neutrons		
A	J^{π}	E_x(MeV)	Exp	Calculated	E_x(MeV)	Exp	Calculated
		12.633	-	$1.6^{+2.6}_{-0.9}$	12.549	-	$3.0^{+3.8}_{-2.2}$
21	$1/2^+$	12.804		$1.6^{+2.4}_{-0.6}$	12.737	-	$1.8^{+3.7}_{-0.9}$
		12.475	-	$3.6^{+7.3}_{-2.0}$	12.377	-	$3.3^{+4.1}_{-1.9}$
	$5/2^+$	10.777	-	$1.8^{+2.8}_{-1.3}$	10.772	-	$1.7^{+8.1}_{-1.1}$
25	$1/2^+$	11.976	-	$4.8^{+6.4}_{-2.7}$	11.934	-	$4.1^{+9.4}_{-2.1}$
	$3/2^+$	9.978	-	$8.5^{+14.7}_{-4.8}$	9.950	-	$7.5^{+17.3}_{-4.1}$
	$5/2^+$	11.356	5.0 ± 0.8	$2.3^{+3.8}_{-1.3}$	11.369	-	$3.5^{+3.7}_{-1.9}$
29	$1/2^+$	11.700	-	$3.6^{+8.6}_{-2.1}$	11.720	-	$6.0^{+8.4}_{-2.9}$
	$3/2^+$	11.346	-	$4.0^{+7.5}_{-2.3}$	11.371	-	$3.4^{+8.5}_{-2.2}$
	$5/2^+$	8.988	-	$1.2^{+2.1}_{-0.6}$	7.337	-	$1.3^{+2.6}_{-0.9}$
33	$1/2^+$	11.877	-	$0.8^{+1.5}_{-0.4}$	11.842	-	$3.7^{+6.4}_{-1.9}$
	$3/2^+$	8.100	-	$2.5^{+5.2}_{-1.3}$	8.107	-	$7.1^{+6.1}_{-2.9}$
	5/2	11.164	-	$0.5^{+2.3}_{-0.3}$	11.186	-	$0.5^{+1.3}_{-0.3}$
37	$1/2^+$	13.339	-	$0.01^{+0.005}_{-0.006}$	13.284	-	$0.5^{+0.01}_{-0.01}$
	$3/2^+$	9.183	-	$0.07^{+0.005}_{-0.005}$	9.114	-	$1.5^{+0.02}_{-0.04}$

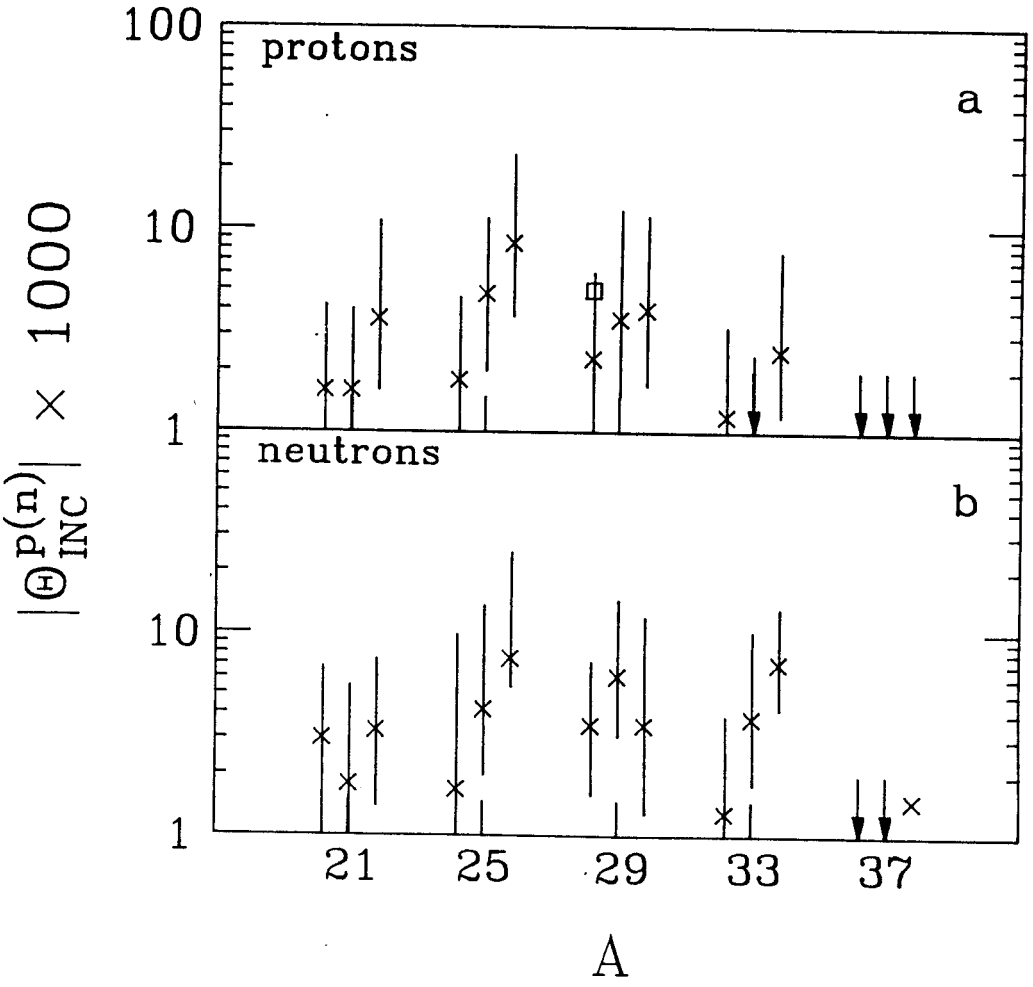

Figure 5.3: Same as Figure 5.2, except that the isospin-forbidden spectroscopic amplitudes for the second state of each J are plotted.

of the same order of magnitude as for lower states, the decrease in $\theta^{p(n)}_{INC}$ is due to a reduction in the allowed spectroscopic amplitudes which appear in eq.(5.2.3).

5.5 Detailed Analysis of ^{33}Cl

In this section, the isospin-forbidden spectroscopic amplitude for the decay of the first $J^{\pi}=1/2^{+}$, T=3/2 state in ^{33}Cl is discussed in detail. This is the only state under investigation in this work where both the excitation energies and the allowed spectroscopic amplitudes have been determined experimentally for the nearby T=1/2 states [Iko 76]. Shown in Table 5.6 are the theoretical values for the excitation energies, the isospin-mixing matrix elements, the allowed spectroscopic amplitudes for the lowest T=1/2 state and the two T=1/2 states (fourth and fifth states) which are within ±500 keV of the T=3/2 state, and the contributions to θ^{p}_{INC} due to these states. In addition, contributions due to mixing in the daughter nucleus and all other parent states are also given in the table.

The experimental excitation energies for the fourth and fifth T=1/2 states are E(4) = 5.451 MeV and E(5) = 5.740 MeV, respectively. The experimental decay widths for these states are $\Gamma_p(4) = 30 \pm 4$ keV and $\Gamma_p(5) = 40 \pm 5$ keV [Iko 76]. Using Coulomb penetrabilities tabulated by Marion and Young [Mar 68] and $\gamma^2_{sp} = 2.16$ MeV (see eq.(5.4.1)), we find $\theta^{p}_{exp}(4) = 0.135 \pm 0.009$ and $\theta^{p}_{exp}(5) = 0.143 \pm 0.008$. These differ somewhat from the theoretical values shown in Table 5.6. However, the sum of the squares of the experimental spectroscopic amplitudes (0.039) does not differ much from the sum of the squares of the corresponding theoretical values (0.045), indicating that perhaps the fourth and fifth states

Table 5.6

List of excitation energies, isospin-mixing matrix elements, and allowed spectroscopic amplitudes for the principal contributors to the lowest $J^{\pi}=1/2^{+}$ $T=3/2$ state in ^{33}Cl.

i	E(i) (MeV)	V_{ik} (keV)	$\theta^{p}(i)$ (× 1000)	θ^{p}_{INC} (× 1000)
1	0.815	43.7	-479.6	-4.4
4	5.598	-2.2	190.5	8.4
5	6.017	-13.7	91.8	2.7
All other states				5.5
Total				12.2

should be mixed. This mixing is not due to isospin-symmetry violation, but rather to a residual component of the isoscalar Hamiltonian. Recall that excitation energies of the mass-dependent sd-shell Hamiltonian are uncertain by at least 150 keV [Wil 84]. Therefore, it is not unreasonable to expect that some correction to the isoscalar interaction is necessary. We construct mixed states $\Psi'(4)$ and $\Psi'(5)$

$$\Psi'(4) = \alpha\Psi(4) + \beta\Psi(5) \qquad (5.5.1a)$$

$$\Psi'(5) = -\beta\Psi(4) + \alpha\Psi(5) \qquad (5.5.1b)$$

Requiring that $|\theta^p(4)'/\theta^p(5)'|^2 = |\theta^p_{exp}(4)/\theta^p_{exp}(5)|^2 = 0.891$, we find two solutions:

(I) $\alpha = 0.9339$ and $\beta = -0.3575$, and

(II) $\alpha = -0.3023$ and $\beta = -0.9532$.

The residual isoscalar-mixing matrix elements for solutions I and II are then -98.2 keV and 84.7 keV, respectively. Note, however, that the second solution actually produces a level crossing between these states. Shown in Table 5.7 are the isospin-mixing matrix elements for the states $\Psi'(4)$ and $\Psi'(5)$ using solutions I and II and the contribution to θ^p_{INC} due to these states. In addition to the allowed spectroscopic amplitudes for the fourth and fifth states, θ^p for the lowest T=1/2 level has also been measured experimentally, $\theta^p(1) = -0.7\pm0.2$ (this is an average of the values obtained by Bobrouska et al. [Bob 69 and Bob 70] and Mermaz et al. [Mer 71]). The new contribution to θ^p_{INC} due to this state is also

Table 5.7

Contributions to $\theta^{p(n)}_{INC}$ for the lowest $J^{\pi}=1/2^{+}$, T=3/2 state in ^{33}Cl due to the mixed states $\Psi(4)'$ and $\Psi(5)'$ and the lowest T=1/2 state.

i	$E_{exp}(i)$ (MeV)	$\theta^{p}_{exp}(i)$ (× 1000)	Solution I V_{ik} (keV)	Solution I θ^{p}_{INC} (× 1000)	Solution II V_{ik} (keV)	Solution II θ^{p}_{INC} (× 1000)
1	0.811	-700±180	43.7	-6.3±1.8	43.7	-6.3±1.8
4	5.451	135±9	2.8	3.9	13.7	-18.8
5	5.740	143±8	-13.6	9.8	-2.0	-1.4
All other states				5.5		5.5
Total				12.9±1.8		-21.0±1.8[a]

[a]Note that for solution II the sign of both the mixing matrix elements and the allowed spectroscopic amplitudes change.

given in Table 5.7. The total value of (θ^{p}_{INC} × 1000) is then 12.9±1.8 for solution I and -21.0±1.8 for solution II. Since the later solution gives a value for θ^{p}_{INC} which is three times the experimental value, and it requires a level crossing between the fourth and fifth T=1/2 states, it is perhaps not unreasonable to reject this possibility. On the other hand, for the first solution, we see that θ^{p}_{INC} is very sensitive to the small isospin-mixing matrix element of the fourth T=1/2 state (this is due to ΔE = 97 keV). In fact, the isoscalar mixing causes this matrix element to change sign, and therefore gives a larger value of θ^{p}_{INC}. With this in mind, it is important to consider the effects of the alternative isovector interaction discussed in Chapter Two.

With the INC interaction determined with the parameters given in the last row of Table 2.12 and $C^{(2)}$ = 0.93 and $A^{(2)} = -(5.5\pm0.2) \times 10^{-2}$, the isospin-mixing matrix elements for Ψ(4) and Ψ(5) are -6.1 and -10.1 keV, respectively. Using solution I, these matrix elements for the isoscalar-mixed states Ψ'(4) and Ψ'(5) are then -2.1 and -11.6 keV. The isospin-forbidden amplitude (θ^{p}_{INC} × 1000) is then 4.0±1.8 (for the second solution (θ^{p}_{INC} × 1000) = -23.0±1.8).

The results of this last calculation indicate that not only is it necessary to know the exact location and the allowed spectroscopic amplitudes for these nearby states, but it is also important that we know the isospin-mixing matrix elements for these states to within 5 keV! This, unfortunately, is quite difficult. Meaningful information has, however, been gained from this study. The calculations reported here are strong evidence that the amplitudes $\theta^{p(n)}_{INC}$ are greatly influenced by the nearby T=1/2 levels, and that, therefore, the observed

oscillation in these quantities is in fact due to details of the structure of the parent nucleus.

5.6 Relationship Between the Decay Width and the Spectroscopic Amplitude

Recently, a new procedure for determining the decay width Γ_μ from the spectroscopic amplitude has been developed by Bertsch [Ber 85]. In this section, this procedure is outlined briefly, and the application of this method to the isospin-forbidden decay of the lowest $J^\pi=1/2^+$, $T=3/2$ state in ^{33}Cl is discussed.

The partial decay width is given by [Mer 61]

$$\Gamma_\mu(\Gamma,J;\Gamma',0,j) = 2\pi \left|\langle\bar{\Psi}(\Gamma,J,T_Z+\mu)\right| V \left|\phi^c_{j\mu}\Psi(\Gamma',J'=0,T_Z)\rangle\right|^2 \frac{dn_c}{dE}, \quad (5.6.1)$$

where V is the potential which causes the particle emission, $\phi^c_{j\mu}$ is a continuum wave function normalized in a box of radius R (for $r >> 0$, $\phi^c_j = \sqrt{(2/R)}\sin(kr+\delta)/r$, where δ is the potential phase shift), $dn_c/dE = Rm/\pi\hbar^2k$ is the density of continuum states, and $\bar{\Psi}(\Gamma,J,T_Z+\mu)$ excludes the amplitude $\phi_{j\mu}\Psi(\Gamma',J'=0,T_Z)$, and, therefore is given by

$$\bar{\Psi}(\Gamma,J,T_Z+\mu) = \Psi(\Gamma,J,T_Z+\mu) - \Theta^\mu(\Gamma,J;\Gamma',J'=0;j)\ \phi_{j\mu}\Psi(\Gamma',J'=0,T_Z).$$

Here $\phi_{j\mu}$ denotes the normalized bound state wave function for the particle in the orbit j and $\Theta_\mu(\Gamma,J;\Gamma',J'=0;j)$ is given by eq.(5.2.1). The exact continuum wave functions $\phi^{exact}_{j\mu}$ are normalized for $r >> 0$ as $\sin(kr+\delta)/\sqrt{(k)}r$, and therefore, the decay width Γ_μ is given by

$$\Gamma_\mu(\Gamma,J;\Gamma',0,j) = \frac{4m}{\hbar^2} \left|\langle\bar{\Psi}(\Gamma,J,T_Z+\mu)\right| V \left|\phi_{j\mu}^{exact}\ \Psi(\Gamma',J'=0,T_Z)\rangle\right|^2. \quad (5.6.2)$$

For small distances, $r \leq R_n$ (R_n is the nuclear radius), we postulate that $\phi_{j\mu}^{exact} = b\ \phi_{j\mu}$. In addition, first-order perturbation theory gives

$$(\varepsilon_{j\mu}^c - \varepsilon_{j\mu})\theta^\mu(\Gamma,J;\Gamma',J'=0;j) = \langle\Psi(\Gamma,J,T_Z+\mu| V |\phi_{j\mu}^c\Psi(\gamma',J'=0,T_Z)\rangle,$$

where $\varepsilon_{j\mu}^c$ is the continuum energy and $\varepsilon_{j\mu}$ is the single-particle bound-state energy. The relationship between the spectroscopic amplitude θ^μ and the decay width Γ_μ is then

$$\Gamma_\mu(\Gamma,J;\Gamma',J'=0;j) = \frac{4m}{\hbar^2} (\varepsilon_{j\mu}^c - \varepsilon_{j\mu})^2\ b^2\ |\theta^\mu(\Gamma,J;\Gamma',J'=0,j)|^2. \quad (5.6.3)$$

Note that in this procedure the factor $(\varepsilon_{j\mu}^c - \varepsilon_{j\mu})^2\ b^2\ 4m/\hbar^2$ replaces the quantity $2P_C\gamma_{sp}^2$ given in eq.(5.4.1).

As an example, this method is applied to the decay of the $J^\pi=1/2^+$, T=3/2 state in ^{33}Cl, which was discussed in detail in section 5.5. The single particle wave functions $\phi_{j\mu}$ and $\phi_{j\mu}^{exact}$ were obtained using the standard Woods-Saxon procedure. The potential V(r) is

$$V(r) = -V_0\ f(r) - V_S\ g(r)\ \vec{\ell}\cdot\vec{\sigma} + V_C(r),$$

where

$$f(r) = \{1 + \exp((r - R_n)/a)\}^{-1},$$

$$g(r) = \left(\frac{\hbar}{m_\pi c}\right) \frac{1}{a_s r} \exp\left(\frac{r - R_s}{a_s}\right) \{1 + \exp((r - R_s)/a_s)\}^{-2},$$

$$V_C(r) = \begin{cases} Ze^2/r & \text{for } r \geq R_C \\ \frac{Ze^2}{2R_C}\left(3 - \frac{r^2}{R_C^2}\right) & \text{for } r \leq R_C. \end{cases}$$

For this case, the following parameters were used:

$$V_0 = 53.0 \text{ MeV}, \; V_s\left(\frac{\hbar}{m_\pi c}\right) = 15.65 \text{ MeV}$$

$$R_n = R_s = R_C = 1.25 \, A^{1/3} \text{ fm},$$

$$a = a_s = 0.65 \text{ fm},$$

$$A = 32, \text{ and } Z = 16.$$

The continuum energies were determined from the proton separation energies [Wap 82, Iko 77 and Wil 83]. The bound-state energy of the 1s orbit was found to be -5.998 MeV. The quantities b were obtained by minimizing the rms deviation between $\phi_{j\mu}^{\text{exact}}$ and $b\phi_{j\mu}$ over the range $0 \leq r \leq R_n$. Shown in Table 5.8 are the experimental excitation energies, the decay widths Γ_p (including the isospin-forbidden width for the T=3/2 state), $\varepsilon_{j\mu}^c$ (in the center-of-mass system), the coefficients b, and the extracted spectroscopic amplitudes for the fourth and fifth T=1/2 states and the lowest T=3/2 state, respectively. Note that the amplitudes presented in Table 5.8 differ from those in Tables 5.4 (experimental isospin-forbidden) and 5.7 (theoretical allowed). In addition, we now have $\left|\theta_{\text{exp}}^p(4)/\theta_{\text{exp}}^p(5)\right|^2 = 1.0$. Applying the isoscalar-mixing model of eq.(5.5.1), we find $\alpha = 0.9440$ and $\beta = -0.3329$. Using these mixed states

Table 5.8

Experimental excitation energies, experimental decay widths Γ_p, ε^c_{jp}, the coefficient b, and spectroscopic amplitudes for the lowest $J^\pi=1/2^+$, T=3/2 state and the fourth and fifth $J^\pi=1/2^+$, T=1/2 states in ^{33}Cl.

i	T	$E_{exp}(i)$ (MeV)	$\Gamma_p(i)$ (keV)	ε^c_{jp} (MeV)	b	$\theta^p_{exp}(i)$ (× 1000)
4	1/2	5.451	30±4	3.078	0.718	85±6
5	1/2	5.740	40±5	3.363	0.805	85±6
1	3/2	5.548	0.098±0.009	3.172	0.748	4.6±0.2

and the "new" experimental values for the allowed amplitudes, the isospin-forbidden amplitudes ($\theta^{p}_{INC} \times 1000$) are found to be 7.2±1.8 and 2.1±1.8 for the isovector interactions with and without the nuclear charge-asymmetric potentials, respectively. Again the experimental isospin-forbidden amplitude of ($\theta^{p}_{INC} \times 1000$) = 4.6±0.2 lies between the values obtained with the two isovector interactions.

Finally, it should be noted that the procedure given above has been developed recently, and that the dependence on the single-particle potential parameters has not yet been determined. With this in mind, this method should be studied extensively in order that a judgement as to whether it is better than the conventional procedure, given by eq.(5.4.1), can be made.

5.7 Suggestions For Future Work

This section concludes the fifth chapter by making some suggestions for future work in this field. As was pointed out in the section 5.5, when experimental excitation energies and allowed spectroscopic amplitudes are used in the perturbation expansion of eq.(5.2.3) for the decay of the lowest $J^{\pi}=1/2^{+}$, T=3/2 state in ^{33}Cl, the experimental value for θ^{p}_{INC} lies within the the limits set by the two alternative isovector interactions. Although these limits may be large in some cases, it would still be interesting if excitation energies and allowed spectroscopic amplitudes for nearby T=1/2 states could be determined experimentally for some of the other cases shown in Figure 5.2. From the standpoint of the calculations presented here, the most interesting cases would be those in which the density of background T=1/2 states is not too high. This is generally true for $J^{\pi}=1/2^{+}$ states, and not for $J^{\pi}=5/2^{+}$ and $3/2^{+}$

states. An additional feature of these $1/2^+$ states is that, since they have $\ell = 0$, it is experimentally easier to determine their spin assignments, as compared to $J^\pi=5/2^+$ and $3/2^+$ states which both have $\ell = 2$. In addition, in order to isolate the role of the isotensor part of the interaction, it would be necessary to measure the relative locations and allowed amplitudes for both proton and neutron background states for a few cases.

In section 5.5, it was indicated that in order to evaluate $\theta_{INC}^{p(n)}$ for T=3/2 states, it is necessary that the isospin-mixing matrix elements be known to within 5 keV. This type of precision may be impractical. However, another solution is to find isospin-forbidden decays which are not as sensitive to the mixing matrix element. Possible candidates are the decay of T=5/2 states in $T_Z=\pm1/2$ nuclei, and decay of $J^\pi=0^+$, T=2 states in $T_Z=0$ and -1 nuclei. An important feature of the first set of transitions is that although the density of background T=1/2 states is high, both the allowed spectroscopic amplitudes and the isospin-mixing matrix elements are quite small. In addition, these matrix elements sample only the isotensor interaction, which is perhaps better understood than the isovector part. Unfortunately, preliminary observations indicate that at least one nearby level may contribute significantly to the total forbidden amplitude. In the case of the decay of T=2 states, the density of nearby T=0 and 1 levels is not very high. For example, in the theoretical excitation energy spectrum for A=20, there is only one T=1 level and three T=0 levels within 2 MeV of the $J^\pi=0^+$, T=2 parent. Since the mixing with T=0 states is only isotensor, and the density of background T=1 states is low, it is quite possible

that the problems encountered with the T=3/2 states in the present work may not be as important for the decay of these $J^{\pi}=0^{+}$, T=2 states.

Chapter Six

6.1 Summary of Chapter Two

In Chapter Two, isospin-nonconserving Hamiltonians were determined empirically for the 0p, 1s-0d, $0d_{3/2}$-$0f_{7/2}$, and 0f-1p model spaces by requiring that these interactions reproduce experimental b- and c-coefficients of the isotopic mass multiplet equation. The empirical Hamiltonians reproduce the experimental data rather well, with rms deviations between theory and experiment being approximately 30 and 10 keV for the b- and c-coefficients, respectively.

A general feature of the fits to b-coefficients was that only the isovector single-particle energies and the Coulomb potential were necessary to reproduce the experimental quantities. However, when the contribution due to differences in proton and neutron radial wave functions for 1s-0d-shell nuclei were included, a nuclear charge-asymmetric interaction was needed. The effect of this interaction was to increase $v^{(nn)}$ by 1.5% relative to $v^{(pp)}$.

In order to reproduce experimental c-coefficients a nuclear charge-dependent interaction was necessary. It was found that this interaction can be accurately parameterized by increasing proton-neutron T=1 matrix elements by 2%.

6.2 Summary of Chapter Three

The subject of Chapter Three was the theoretical evaluation of corrections to the Fermi matrix element for superallowed β-decays. The procedure followed was essentially the same as that of previous works, except that many recent improvements in nuclear models were used. Among

these are: recently developed isoscalar Hamiltonians, radial wave functions obtained from a self-consistent Hartree-Fock calculation using a Skyrme-type interaction, and the empirical INC interactions determined in Chapter Two. Values of radial overlap (δ_{RO}) and isospin-mixing (δ_{IM}) corrections presented here are systematically smaller than those of previous studies. The reduction in δ_{IM} was found to be related to the selection of the isovector-single particle energies, while the reduction in the radial-overlap correction was found to be due to a previously neglected single-particle isovector potential which counteracts the effects of Coulomb repulsion. The purpose of this study was to apply the calculated corrections to experimental ft values, and then determine empirical values of the ratio of the effective vector coupling constants for nucleon and muon β-decay, G_V/G_μ. The calculated corrections presented here, like those of the previous studies, fail to yield constant values of G_V/G_μ. However, the suggestion is made that that perhaps the calculated corrections for 0f-1p-shell nuclei are too small because of configuration-space truncations, and that experimental spectroscopic amplitudes may be able to resolve the current discrepancy between values of G_V/G_μ determined from high- and low-Z transitions.

6.3 Summary of Chapter Four

Comparisons between experimental and predicted isospin-forbidden Fermi transitions are made in Chapter Four. It was found that the INC interactions developed in Chapter Two give isospin-mixing matrix elements and forbidden Fermi matrix elements which are comparable to experimentally observed quantities.

6.4 Summary of Chapter Five

In Chapter Five, calculated spectroscopic amplitudes $\theta_{INC}^{p(n)}$ for the decay of T=3/2 states in A=4n+1 nuclei ($21 \leq A \leq 37$) to $J^{\pi}=0^{+}$, T=0 states in A=4n nuclei by isospin-forbidden proton and neutron emission are presented and compared with experimental values. The forbidden amplitudes are given in terms of contributions due to isospin-mixing in both the parent and daughter nuclei. It was found that the calculations are sensitive to the properties of nearby T=1/2 parent states. These properties are the exact location of these states relative to the T=3/2 parent and the allowed spectroscopic amplitudes for these states. Unfortunately, these properties are uncertain both experimentally and theoretically. In order to perform a systematic study of the isospin-forbidden amplitudes across the entire 1s-0d shell, these uncertainties in the nearby T=1/2 states were estimated by shifting the T=1/2 energy spectrum relative to the T=3/2 parent by ±500 keV in small steps. The forbidden amplitudes were then evaluated at each step. The best estimate $\theta_{INC}^{p(n)}$ was taken to be the unweighted average of the values obtained at each step, and the uncertainty in the calculation was determined by evaluating the upper and lower rms deviations of the values obtained at each step from the average. Taking this uncertainty into account there is generally good agreement between theory and experiment. With this mind, it is proposed that the observed oscillation in the lowest T=3/2 states is not due to a global phenomenon, but rather to the specific properties of nearby T=1/2 levels. These properties include the excitation energies relative to the T=3/2 parent, the isospin-allowed spectroscopic amplitudes, and the isospin-mixing matrix elements, and are statistical rather than global in nature.

The decay of the lowest $J^{\pi}=1/2^{+}$, T=3/2 state in ^{33}Cl is the only case under investigation in this work where experimental data on the nearby T=1/2 states are available, and, was therefore examined in detail. In order to explain the experimental allowed spectroscopic amplitudes it was found that mixing between the fourth and fifth T=1/2 states, due to residual isoscalar components of the Hamiltonian, was necessary. With this, it was determined that θ^{p}_{INC} is very sensitive to the small isospin-mixing matrix element of the fourth T=1/2 state, indicating that even a 5 keV error in this quantity may be unacceptable. As a check, θ^{p}_{INC} was re-evaluated using the isovector interaction which includes a nuclear charge-asymmetric interaction. The experimental value for the forbidden amplitude was found to lie between the theoretical values obtained using the two alternative isovector interactions. This again supports the postulate that the experimentally observed values are due to the specific properties of the nearby T=1/2 states.

A recently developed procedure which relates the spectroscopic amplitudes and the observed decay width Γ_{μ} is also presented. The application of this procedure to the lowest $J^{\pi}=0^{+}$, T=3/2 state in ^{33}Cl is discussed.

Suggestions for future experimental and theoretical work were made. With perhaps the most promising of these being an investigation into the decay of $J^{\pi}=0^{+}$, T=2 states in $T_{Z}=0$ and -1 nuclei.

As a final remark, it is noted that the procedure used in this work to predict isospin-symmetry violation in light nuclei was generally successful. With this in mind, we are therefore encouraged to continue working on this problem with the hope that many of the unanswered questions of today may be resolved.

LIST OF REFERENCES

LIST OF REFERENCES

Abe 68 E. S. Abers, D. A. Dicus, R. E. Norton and H. R. Quinn, Phys. Rev. 167 (1968) 1461

Ade 64 M. Ademollo and R. Gatto, Phys. Rev. Lett. 13 (1964) 264

Ade 85 E. G. Adelberger, P. B. Fernandez, C. A. Gosset, J. L. Osborne, and V. J. Zeps, Phys. Rev Lett. 55 (1985) 2129

Adl 72 J. C. Adloff et al., Phys. Rev. C 5 (1972) 664

Ajz 80 F. Ajzenberg-Selove, Nucl. Phys. A336 (1980) 1

Ajz 81 F. Ajzenberg-Selove and C. L. Busch, Nucl. Phys. A360 (1981) 1

Ajz 82 F. Ajzenberg-Selove, Nucl. Phys. A375 (1982) 1

Ajz 83 F. Ajzenberg-Selove, Nucl. Phys. A413 (1982) 1

Alb 79 D. E. Alburger and E. K. Warburton, Phys. Rev. C 20 (1979) 793

Ari 71 A. Arima and S. Yoshida, Nucl. Phys. A161 (1971) 492

Arn 83 G. Arnison et al., Phys. Lett. 126B (1983) 398

Aue 71 N. Auerbach and A. Lev, Phys. Lett. 34B (1971) 13

Aue 83 N. Auerbach, Phys. Rpts. 98 (1983) 273

Bag 83 P. Bagnaia et al., Phys. Lett. 129B (1983) 130

Beg 69 M. A. Beg, J. Bernstein, and A. Sirlin, Phys. Rev. Lett 23 (1969) 270

Beh 60 R. E. Behrends and A. Sirlin, Phys. Rev. Lett. 4 (1960) 186

Bei 75 M. Beiner, H. Flocard, N. V. Giai, and P. Quentin, Nucl. Phys. A238 (1975) 29

Ben 79 W. Benenson and E. Kashy, Rev. Mod. Phys. 51 (1979) 527

Ber 85 G. F. Bertsch, private communication

Bli 67 R. J. Blin-Stoyle and S. K. Nair, Nucl. Phys. A105 (1967) 640

Bli 69 R. J. Blin-Stoyle, Isospin in Nuclear Physics, edited by D. H. Wilkinson (North Holland, Amsterdam, 1969) p. 115

Bli 70 R. J. Blin-Stoyle and J. M. Freeman, Nucl. Phys. A150 (1970) 369

Bob 69 Bobrouska et al., Contributions to Montreal Conference (University of Tronto Press, 1969) p. 283

Bob 70 Bobrouska et al., Acta Phys. Polonica B1 (1970) 201

Bro 80 B. A. Brown, W. Chung, and B. H. Wildenthal, Phys. Rev. C22 (1980) 774

Bro 82 B. A. Brown et al., Phys. Rev. C 26 (1982) 2247

Bro 83 B. A. Brown and B. H. Wildenthal, Phys. Rev. C 28 (1983) 2397

Bro 84 B. A. Brown, C. R. Bronk, and P. E. Hodgson, J. Phys. G: Nucl. Phys. 10 (1984) 1683

Bro 85 B. A. Brown and B. H. Wildenthal, to be published in Atomic and Nuclear Data Sheets, (1985)

Bru 77 P. J. Brussard and P. W. M. Glaudemans, Shell-Model Applications in Nuclear Spectroscopy, (North Holland, Amsterdam, 1977). {Note that the second and third lines of eq. 14.60 should be divided by $\sqrt{[(1 + \rho_1\rho_2)(1 + \rho_3\rho_4)]}$}

Cer 64 J. Cerny et al., Phys. Rev. Lett. 13 (1964) 726

Coh 65 S. Cohen and D. Kurath, Nucl. Phys. 73 (1965) 1

Dae 85 W. W. Daehnick and R. D. Rosa, Phys. Rev. C31 (1985) 1499

Dam 69 J. Damgaard, Nucl. Phys. A130 (1969) 233

Del 78 R. M. DelVecchio and W. W. Daehnick, Phys. Rev. C17 (1978) 1809

Dic 70 D. A. Dicus and R. E. Norton, Phys. Rev. D1 (1970) 1360

Dov 72 C. B. Dover and N. V. Giai, Nucl. Phys. A190 (1972) 373

Edm 60 A. R. Edmonds, Angular Momentum in Quantum Mechanics, (Princeton Universtiy Press, Princeton, 1960)

End 78 P. M. Endt and C. Van Der Leun, Nucl. Phys. A310 (1978) 1

Fay 71 S. A. Fayans, Phys. Lett 37B (1971) 155

Gab 81 B. Gabioud et al., Phys. Lett. 103B (1981) 9

Gio 84 K. L. Giovanetti et al., Phys. Rev. D29 (1984) 343

Hal 68 T. A. Halpern and B. Chern, Phys. Rev. 175 (1968) 1314

Har 75 J. C. Hardy and I. S. Towner, Nucl. Phys. A254 (1975) 221

Hei 32 W. Heisenberg, Zeits. f. Physik 77 (1932) 1

Hen 69 E. M. Henley, Isospin in Nuclear Physics, edited by D. H. Wilkinson (North Holland, Amsterdam, 1969) p. 17

Hen 72 E. M. Henley, in Proc. Int. Conf. on few particle problems in the nuclear interaction, Los Angeles 1972, edited by I. Slaus et al., (North-Holland, Amsterdam, 1973) p. 221

Hen 79 E. M. Henley and G. A. Miller, Mesons In Nuclei, edited by M. Rho and D. H. Wilkinson (North-Holland, Amsterdam, 1979) p.357

Hin 81 F. Hinterberger, et al., Nucl. Phys. A352 (1981) 93

Hin 84 F. Hinterberger, et al., Nucl. Phys. A424 (1984) 200

Hoy 83 C. D. Hoyle, E. C. Adelberger, J. S. Blair, K. A. Snover, H. E. Swanson, and R. D. Von Lintig, Phys. Rev. C 27 (1983) 27

Hsi 85 S. T. Hsieh, R. B. M. Mooy, and B. H. Wildenthal, Bull. of the American Physical Society 30 (1985) 731

Iko 76 P. G. Ikossi et al., Nucl. Phys. A274 (1976) 1

Ing 77 P. D. Ingalls, J. C. Overley, and H. S. Wilson, Nucl. Phys. A293 (1977) 117

Jau 70 W. Jaus and G. Rausche, Nucl. Phys. A143 (1970) 202

Jau 72 W. Jaus, Phys. Lett. 40B (1972) 616

Koo 77 J. E. Koops and P. W. M. Glaudemans, Zeits. f. Physik A280 (1977) 181

Kos 83 V. T. Koslowsky, Ph. D. thesis, Universtiy of Tronto (1983)

Kos 85 V. T. Koslowsky et al., AMCO-7 p.60

Lan 73 A. M. Lane and A. Z. Mekjian, Advances in Nuclear Physics, Vol. 7, ed. E. Vogt and M. Baranger (Plenum Press, New York, 1973) p. 97

Law 79 R. D. Lawson, Phys. Rev. C19 (1979)2359

Law 80 R. D. Lawson, Theory of the Nuclear Shell Model, (Clarendon Press, Oxford) 1980

Led 78 C. M. Lederer and V. S. Shirley, Table of Isotopes, seventh edition (Wiley, New York, 1978)

Lev 73 A. Lev and N. Auerbach, Nucl. Phys. A206 (1973) 563

Mar 68 J. B. Marion and F. C. Young, Nuclear Reaction Analysis, (Wiley, New York) 1968

Mat 65 J. H. E. Mattauch, W. Theile, and A. H. Wapstra, Nucl. Phys. 67 (1965) 1

McD 69 A. B. McDonald, J. R. Patterson, and H. Winkler, Nucl. Phys. A137 (1969) 545

McD 78 A. B. McDonald and E. G. Adelberger, Phys. Rev. Lett. 40 (1978) 1692

Mer 61 E. Merzbacher, Quantum Mechanics, second edition (Wiley, New York, 1961)

Mer 71 Mermaz et al. Phys. Rev. C4 (1971) 1778

Neg 71 J. W. Negele, Nucl. Phys. A165 (1971) 305

Nol 69 J. A. Nolen and J. P. Schiffer, Ann. Rev. Nucl. Sci. 19 (1969) 471

PDG 84 Review of particle properties, Rev. Mod. Phys. 56 (1984) S1

Rae 85 W. D. M. Rae, A. Etchegoyen, N. S. Godwin, and B. A. Brown, OXBASH, The Oxford-Buenos Aires Shell-Model Code, Michigan State University Cyclotron Laboratory report #524

Ray 82 A. Ray, C. D. Hoyle, and E. C. Adelberger, Nucl. Phys. A378 (1982) 29

Roo 74 M. Roos, Nucl. Phys. B77 (1974) 420

Sag 85 H. Sagawa, private communication

San 80 A. M. Sandorfi, C. J. Lister, D. E. Alburger, and E. K. Warburton, Phys. Rev. C 22 (1980) 2213

Sat 76 H. Sato, Nucl. Phys. A266 (1976) 269

She 85 B. M. Sherrill, Ph. D. thesis, Michigan State Universtiy (1985)

Shl 78 S. Shlomo, Repts. Prog. Phys. 41 (1978) 957

Sir 67 A. Sirlin, Phys. Rev. 164 (1967) 1767

Sir 74 A. Sirlin, Nucl. Phys. B71 (1974) 29

Sir 78 A. Sirlin, Rev. Mod. Phys. 50 (1978) 573

Sky 56 T. H. R. Skyrme, Phil. Mag. 1 (1956) 1043

Sky 59 T. H. R. Skyrme, Nucl. Phys. 9 (1959) 615

Tay 69 B. N. Taylor, W. H. Parker, and D. N. Langenberg, Rev. Mod. Phys. 41 (1969) 375

Tow 73 I. S. Towner and J. C. Hardy, Nucl. Phys. A205 (1973) 33

Tow 77 I. S. Towner, J. C. Hardy, and M. Harvey, Nucl. Phys. A284 (1977) 269

Tow 78 I. S. Towner and J. C. Hardy, Phys. Lett. 73B (1978) 20

Tow 84 I. S. Towner, private communication

Vau 72 D. Vautherin and D. M. Brink, Phys. Rev. C 5 (1972) 626

Van 81a A. G. M. van Hees and P. W. M. Glaudemans, Zeits. f. Physik A303 (1981) 267; The interaction is obtained by adding matrix elements of a modified surface delta interaction ($A_0 = 0.25$, $A_1 = 0.53$, $B_0 = -1.09$, $B_1 = 0.5$) to the matrix elements in the above reference, while all other matrix elements are taken from Koo 77.

Van 81b Nguyen Van Giai and H. Sagawa, Nucl. Phys. A371 (1981) 1

Van 81c Nguyen Van Giai and H. Sagawa, Phys. Lett. 106B (1981) 379

Wap 82 A. H. Wapstra and K. Bos, 1982 Atomic Mass Evaluation, Nuclear Data Center, Brookhaven National Laboratory (unpublished)

War 81 E. K. Warburton, C. J. Lister, D. E. Alburger, and J. W. Olness, Phys. Rev. C23 (1981) 1242

Wei 76 R. Weigmann, R. L. Macklin and J. A. Harvey, Phys. Rev. C 14 (1976) 1324

Wig 57 E. P. Wigner, Proceedings of the Robert A. Welch Conferences on Chemical Research (R. A. Welch Foundation, Houston, Texas, 1957) Vol. 1, p.67

Wil 73 D. H. Wilkinson, Nucl. Phys. A209 (1973) 209

Wil 74 D. H. Wilkinson and B. E. F. Macefield, Nucl. Phys. A232 (1974) 58

Wil 76 D. H. Wilkison, Phys. Lett. 65B (1976) 9

Wil 76a D. H. Wilkinson and D. E. Alburger, Phys. Rev. C13 (1976) 2517

Wil 77 D. H. Wilkinson, Phys. Lett. 67B (1977)13

Wil 82 D. H. Wilkinson, Nucl. Phys. A377 (1982) 474

Wil 83 J. F. Wilkerson, R. E. Anderson, T. B. Clegg, E. J. Ludwig, and W.J. Thompson, Phys. Rev. Lett. 51 (1983) 2269

Wil 84 B. H. Wildenthal, Progress in Particle and Nuclear Physics, edited by D. H. Wilkinson (Pergamon Press, Oxford, 1984) vol. 11, p.5.